chemical and Biophysical Research Communications 2002; **239**: 1364–1369.
11. Matsumoto M, Seya T. TLR3: interferon induction by double-stranded RNA including poly(I:C). *Advanced Drug Delivery Reviews* 2008; **60**: 805–812.
12. Weber F, Wagner V, Rasmussen SB, Hartmann R, Paludan SR. Double-stranded RNA is produced by positive-stranded RNA viruses and DNA viruses but not in detectable amounts by negative-stranded RNA viruses. *Journal of Virology* 2006; **80**: 5059–5064.
13. Hemmi H, Takeuchi O, Kawai T, *et al.* A Toll-like receptor recognizes bacterial DNA. *Nature* 2000; **408**: 740–745.
14. Heil F, Hemmi H, Hochrein H, *et al.* Species-specific recognition of single-stranded RNA via toll-like receptor 7 and 8. *Science* 2004; **303**: 1526–1529.
15. Diebold SS, Kaisho T, Hemmi H, Akira S, Sousa RC. Innate antiviral responses by means of TLR7-mediated recognition of single-stranded RNA. *Science* 2004; **303**: 1529–1531.
16. Lee HK, Lund JM, Ramanathan B, Mizushima N, Iwasaki A. Autophagy-dependent viral recognition by plasmacytoid dendritic cells. *Science* 2007; **315**: 1398–1401.
17. Hornung V, Ellegast J, Kim S, *et al.* 5′-Triphosphate RNA is ligand for RIG-I. *Science* 2006; **314**: 994–997.
18. Pichlmair A, Schulz O, Tan CP, *et al.* RIG-I-mediated anti-viral responses to single-stranded RNA bearing 5′-phosphates. *Science* 2006; **314**: 997–1001.
19. Schlee M, Roth A, Hornung V, *et al.* Recognition of 5′ triphosphate by RIG-I helicase requires short blunt double-stranded RNA as contained in panhandle of negative-strand virus. *Immunity* 2009; **31**: 25–34.
20. Schmidt A, Schwerd T, Hamm W, *et al.* 5′-triphosphate RNA requires base-paired structures to activate antiviral signaling via RIG-I. *Proceedings of the National Academy of Science of the United States of America* 2009; **106**: 12067–12072.
21. Rehwinkel J, Tan CP, Goubau D, *et al.* RIG-I detects viral genomic RNA during negative-strand RNA virus infection. *Cell* 2010; **140**: 397–408.
22. Kato H, Takeuchi O, Mikamo-Satoh E, *et al.* Length-dependent recognition of double-stranded ribonucleic acids by retinoic acid-inducible gene-I and melanoma differentiation-associated gene 5. *Journal of Experimental Medicine* 2008; **205**: 1601–1610.
23. Kato H, Sato S, Yoneyama M, *et al.* Cell type-specific involvement of RIG-I in antiviral response. *Immunity* 2005; **23**: 19–28.
24. Kato H, Takeuchi O, Sato S, *et al.* Differential roles of MDA5 and RIG-I helicases in the recognition of RNA viruses. *Nature* 2006; **441**: 101–105.
25. Gitlin L, Barchet W, Gilfillan S, *et al.* Essential role of mda-5 in type I IFN responses to polyriboinosinic:polyribocytidylic acid and encephalomyocarditis picornavirus. *Proceedings of the National Academy of Science of the United States of America* 2006; **103**: 8459–8464.
26. Saito T, Owen DM, Jiang F, Marcotrigiano J, Gale M Jr. Innate immunity induced by composition-dependent RIG-I recognition of hepatitis C virus RNA. *Nature* 2008; **454**: 523–527.
27. Rock FL, Hardiman G, Timans JC, Kastelein RA, Bazan JFA. A family of human receptors structurally related to *Drosophila* Toll. *Proceedings of the National Academy of Science of the United States of America* ; **95**: 588–593.
28. Prehaud C, Megret F, Lafage M, Lafon M. Virus infection switches TLR-3-positive human neurons to become strong producers of beta interferon. *Journal of Virology* 2005; **79**: 12893–12904.
29. Farina C, Krumbholz M, Giese T, Hartmann G, Aloisi F, Meinl E. Preferential expression and function of Toll-like receptor 3 in human astrocytes. *Journal of Neuroimmunology* 2005; **159**: 12–19.
30. Town T, Jeng D, Alexopoulou L, Tan J, Flavell RA. Microglia recognize double-stranded RNA via TLR3. *Journal of Immunology* 2006; **176**: 3804–3812.
31. Muzio M, Bosisio D, Polentarutti N, *et al.* Differential expression and regulation of Toll-like receptors (TLR) in human leukocytes: selective expression of TLR3 in dendritic cells. *Journal of Immunology* 2000; **64**: 5998–6004.
32. Visintin A, Mazzoni A, Spitzer JH, Wyllie DH, Dower SK, Segal DM. Regulation of Toll-like receptors in human monocytes and dendritic cells. *Journal of Immunology* 2001; **166**: 249–254.
33. Kadowaki M, Ho S, Antonenko S, *et al.* Subsets of human dendritic cell precursors express different Toll-like receptors and respond to different microbial antigens. *Journal of Experimental Medicine* 2001; **194**: 863–870.
34. Hornung V, Rothenfusser S, Britisch S, *et al.* Quantitative expression of Toll-like receptor 1-10 mRNA in cellular subsets of human peripheral blood mononuclear cells and sensitivity to CpG oligodeoxynucleotides. *Journal of Immunology* 2002; **168**: 4531–4537.
35. Matsumoto M, Funami K, Tanabe M, *et al.* Subcellular localization of Toll-like receptor 3 in human dendritic cells. *Journal of Immunology* 2003; **171**: 3154–3162.
36. Cario E, Podolsky DK. Differential alteration in intestinal epithelial cell expression of Toll-like receptor 3 (TLR3) and TLR4 in inflammatory bowel disease. *Infection and Immunity* 2000; **68**: 7010–7017.
37. Niimi K, Asano Y, Shiraishi T, *et al.* TLR3-mediated synthesis and release of eotaxin-1/CCL11 from human bronchial smooth muscle cells stimulated with double-stranded RNA. *Journal of Immunology* 2007; **178**: 489–495.
38. Nakamura M, Funami K, Komori A, *et al.* Increased expression of Toll-like receptor 3 in intrahepatic bilinary epithelial cells at sites of ductular reaction in diseased livers. *Hepatology International* 2008; **2**: 222–230.
39. Funami K, Sasai M, Ohba Y, Oshiumi H, Seya T, Matsumoto M. Spatiotemporal mobilization of Toll-IL-1 receptor domain-containing adaptor molecule 1 in response to dsRNA. *Journal of Immunology* 2007; **179**: 6867–6872.
40. Funami K, Matsumoto M, Oshiumi H, Akazawa T, Yamamoto A, Seya T. The cytoplasmic 'linker region' in Toll-like receptor 3 controls receptor localization and signaling. *International Immunology* 2004; **16**: 1143–1154.
41. Nishiya T, Kajita E, Miwa S, DeFranco A. TLR3 and TLR7 are targeted to the same intracellular compartments by distinct regulatory elements. *Journal of Biological Chemistry* 2005; **280**: 37107–37117.
42. Miettinen M, Sareneva T, Julkunen I, Matikainen S. IFNs activate toll-like receptor gene expression in viral infections. *Genes and Immunity* 2001; **2**: 349–355.
43. Heinz S, Haehnel V, Karaghiosoff M, *et al.* Species-specific regulation of Toll-like receptor 3 genes in men and mice. *Journal of Biological Chemistry* 2003; **24**: 21502–21509.
44. Tanabe M, Taniguchi M, Takeuchi K, *et al.* Mechanism of up-regulation of human Toll-like receptor (TLR) 3 secondary to infection of measles virus attenuated strains. *Biochemical and Biophysical Research Communications* 2003; **311**: 39–48.
45. Gay NJ, Gangloff M, Weber ANR. Toll-like receptors as molecular switches. *Nature Reviews. Immunology* 2006; **6**: 693–698.

46. Bell JK, Mullen GED, Leifer CA, Mazzoni A, Davies DR, Segal DM. Leucine-rich repeats and pathogen recognition in Toll-like receptors. *Trends in Immunology* 2003; **24**: 528–533.
47. Choe J, Kelker MS, Wilson IA. Crystal structure of human Toll-like receptor 3 (TLR3) ectodomain. *Science* 2005; **309**: 581–585.
48. Bell JK, Botos I, Hall PR, *et al.* The molecular structure of the Toll-like receptor 3 ligand-binding domain. *Proceedings of the National Academy of Science of the United States of America* 2005; **102**: 10976–10980.
49. Bell JK, Askins J, Hall PR, Davies DR, Segal DM. The dsRNA binding site of human Toll-like receptor 3. *Proceedings of the National Academy of Science of the United States of America* 2006; **103**: 8792–8797.
50. Fukuda K, Watanabe T, Tokisue T, *et al.* Modulation of double-stranded RNA recognition by the N-terminal histidine-rich region of the human Toll-like receptor 3. *Journal of Biological Chemistry* 2008; **283**: 22787–22794.
51. Pirher N, Ivicak K, Pohar J, Bencina M, Jerala R. A second binding site for double-stranded RNA in TLR3 and consequences for interferon activation. *Nature Structural and Molecular Biology* 2008; **15**: 761–763.
52. Leonard JN, Ghirlando R, Askins J, *et al.* The TLR3 signaling complex forms by cooperative receptor dimerization. *Proceedings of the National Academy of Science of the United States of America* 2008; **105**: 258–263.
53. Liu L, Botos I, Wang Y, *et al.* Structural basis of Toll-like receptor 3 signaling with double-stranded RNA. *Science* 2008; **320**: 379–381.
54. Rana TM. Illuminating the silence: understanding the structure and function of small RNAs. *Nature Reviews. Molecular Cell Biology* 2007; **8**: 23–36.
55. Oshiumi H, Matsumoto M, Funami K, Akazawa T, Seya T. TICAM-1, an adaptor molecule that participates in Toll-like receptor 3-mediated interferon-β induction. *Nature Immunology* 2003; **4**: 161–167.
56. Yamamoto M, Sato S, Hemmi H, *et al.* Role of adaptor TRIF in the MyD88-independent Toll-like receptor signaling pathway. *Science* 2003; **301**: 640–643.
57. Johnsen IB, Nguyen TT, Ringdal M, *et al.* Toll-like receptor 3 associates with c-Src tyrosine kinase on endosomes to initiate antiviral signaling. *EMBO Journal* 2006; **25**: 3335–3346.
58. Sarker SN, Peters K, Elco CP, Sakamoto S, Pal S, Sen GC. Novel roles of TLR3 tyrosine phosphorylation and PI3 kinase in double-stranded RNA signaling. *Nature Structural and Molecular Biology* 2004; **11**: 1060–1067.
59. Oshiumi H, Sasai M, Shida K, Fujita T, Matsumoto M, Seya T. TIR-containing adapter molecule (TICAM)-2, a bridging adapter recruiting to Toll-like receptor 4 TICAM-1 that induces interferon-β. *Journal of Biological Chemistry* 2003; **278**: 49751–49762.
60. Fitzgerald KA, Rowe DC, Barnes BJ, *et al.* LPS-TLR4 signaling to IRF-3/7 and NF-κB involves the toll adapters TRAM and TRIF. *Journal of Experimental Medicine* 2003; **198**: 1043–1055.
61. Funami K, Sasai M, Oshiumi H, Seya T, Matsumoto M. Homo-oligomerization is essential for Toll/IL-1 receptor domain-containing adaptor molecule-1 mediated NF-κB and IRF-3 activation. *Journal of Biological Chemistry* 2008; **283**: 18283–18291.
62. Sharma S, tenOever BR, Grandvaux N, Zhou GP, Lin R, Hiscott J. Triggering the interferon antiviral response through an IKK-related pathway. *Science* 2003; **300**: 1148–1151.
63. Fitzgerald KA, McWhirter SM, Faia KL, *et al.* IKKε and TBK1 are essential components of the IRF3 signaling pathway. *Nature Immunology* 2003; **4**: 491–496.
64. Sato S, Sugiyama M, Yamamoto M, *et al.* Toll/IL-1 receptor domain-containing adaptor-inducing IFN-β (TRIF) associates with TNFR-associated factor 6 and TANK-binding kinase 1, and activates two distinct transcription factors, NF-κB and IFN-regulatory factor 3, in the Toll-like receptor signaling. *Journal of Immunology* 2003; **171**: 4304–4310.
65. Sasai M, Tatematsu M, Oshiumi H, *et al.* Direct binding of TRAF2 and TRAF6 to TICAM-1/TRIF adaptor participates in activation of the Toll-like receptor 3/4 pathway. *Molecular Immunology* 2010; **47**: 1283–1291.
66. Hacker H, Redecke V, Blagoev B, *et al.* Specificity in Toll-like receptor signaling through distinct effector functions of TRAF3 and TRAF6. *Nature* 2006; **439**: 204–207.
67. Oganesyan G, Saha SK, Guo B, *et al.* Critical role of TRAF3 in the Toll-like receptor-dependent and –independent antiviral response. *Nature* 2006; **439**: 208–211.
68. Sasai M, Oshiumi H, Matsumoto M, *et al.* Cutting edge: NF-kappaB-activating kinase-associated protein 1 participates in TLR3/Toll-IL-1 homology domain- containing adapter molecule-1-mediated IFN regulatory factor 3 activation. *Journal of Immunology* 2005; **174**: 27–30.
69. Tatematsu M, Ishii A, Oshiumi H, *et al.* A molecular mechanism for Toll/IL-1 receptor domain-containing adaptor molecule-1-mediated IRF-3 activation. *Journal of Biological Chemistry* 2010; **285**: 20128–20136.
70. Meylan E, Burns K, Hofmann K, *et al.* RIP1 is an essential mediator of Toll-like receptor 3-induced NF-kappa B activation. *Nature Immunology* 2004; **5**: 503–507.
71. Han KJ, Su X, Xu LG, Bin LH, Zhang J, Shu HB. Mechanisms of the TRIF-induced interferon-stimulated response element and NF-kappaB activation and apoptosis pathways. *Journal of Biological Chemistry* 2004; **279**: 15652–15661.
72. Kaiser WJ, Offermann MK. Apoptosis induced by the Toll-like receptor adaptor TRIF is dependent on its receptor interacting protein homotypic interaction motif. *Journal of Immunology* 2005; **174**: 4942–4952.
73. Gohda J, Matsumura T, Inoue J. Cutting edge: TNFR-associated factor (TRAF) 6 is essential for MyD88-dependent pathway but not Toll/IL-1 receptor domain-containing adaptor-inducing IFN-β (TRIF)-dependent pathway in TLR signaling. *Journal of Immunology* 2004; **173**: 2913–2917.
74. Carty M, Goodbody R, Schroder M, Stack J, Moynagh PN, Bowie A. The human adaptor SARM negatively regulates adaptor protein TRIF-dependent Toll-like receptor signaling. *Nature Immunology* 2006; **7**: 1074–1081.
75. Kayagaki N, Phung Q, Chan S, *et al.* DUBA: a deubiquitinase that regulates type I interferon production. *Science* 2007; **318**: 1628–1632.
76. Boone DL, Turer EE, Lee EG, *et al.* The ubiquitin-modifying enzyme A20 is required for termination of Toll-like receptor responses. *Nature Immunology* 2004; **5**: 1052–1060.
77. Edelman KH, Richardson-Burns S, Alexopoulou L, Tyer KL, Flavell RA, Oldstone MBA. Does Toll-like receptor 3 play a biological role in virus infections? *Virology* 2004; **322**: 231–238.
78. Hardarson HS, Baker JS, Yang Z, *et al.* Toll-like receptor 3 is an essential component of the innate stress response in virus-induced cardiac injury. *American Journal of Physiology. Heart and Circulatory Physiology* 2007; **292**: 251–258.

79. Abe Y, Nagata N, Sata T, Takeuchi O, Akira S, Koike S. TLR3-TRIF pathway is important for type I IFN responses in poliovirus infection. *Proceedings of 57th Annual Meeting of the Japanese Society for Virology* 2009; 234.
80. Oshiumi H, Matsumoto M, Seya T. TICAM-1/TRIF, a TLR3 adaptor, is essential for protection against poliovirus infection. *International Immunology* 2010 **22**(Suppl. 1) i19. (abstract).
81. Racaniello VR. Picornaviridae: the viruses and their replication. In *Fields Virology*, 5th edn, Knipe DM, Howly PM (eds). Lippincott Williams & Wilkins: Philadelphia, 2007; 795–838.
82. Negishi H, Osawa T, Ogami K, *et al.* A critical link between Toll-like receptor 3 and type II interferon signaling pathways in antiviral innate immunity. *Proceedings of the National Academy of Science of the United States of America* 2008; **105**: 20446–20451.
83. Wang T, Town T, Alexopoulou L, Anderson JF, Fikrig E, Flavell RA. Toll-like receptor 3 mediates West Nile virus entry into the brain causing lethal encephalitis. *Nature Medicine* 2004; **10**: 1366–1373.
84. Daffis S, Samuel MA, Suthar MS, Gale M Jr, Diamond MS. Toll-like receptor 3 has a protective role against West Nile virus infection. *Journal of Virology* 2008; **82**: 10349–10358.
85. Guillot L, Goffic RL, Bloch S, *et al.* Involvement o Toll-like receptor 3 in the immune response of lung epithelial cells to double-stranded RNA and influenza A virus. *Journal of Biological Chemistry* 2005; **280**: 5571–5580.
86. Rudd BD, Burstein E, Duckett CS, Li X, Lukacs NW. Differential role for TLR3 in respiratory syncytial virus-induced chemokine expression. *Journal of Virology* 2005; **79**: 3350–3357.
87. Rudd BD, Smit JJ, Flavell RA, *et al.* Deletion of TLR3 alters the pulmonary immune environment and mucs production during respiratory syncytial virus infection. *Journal of Immunology* 2006; **176**: 1937–1942 .
88. Goffic RL, Baalloy V, Lagranderie M, *et al.* Detrimental contribution of the Toll-like receptor (TLR) 3 to influenza A virus-induced acute pneumonia. *PLoS Pathogens* 2006; **2**: 526–535.
89. Gowen BB, Hoopes JD, Wong M-H, *et al.* TLR3 deletion limits mortality and disease severity due to phlebovirus infection. *Journal of Immunology* 2006; **177**: 6301–6307.
90. Tabeta K, Georgel P, Janssen E, *et al.* Toll-like receptor 9 and 3 as essential components of innate immune defense against mouse cytomegalovirus infection. *Proceedings of the National Academy of Science of the United States of America* 2004; **101**: 3516–3521.
91. Heath WR, Belz GT, Behrens GM, *et al.* Cross-presentation, dendritic cell subsets, and the generation of immunity to cellular antigens. *Immunology Reviews* 2004; **199**: 9–26.
92. Shen L, Lock KL. Priming of T cells by exogenous antigen cross-presented on MHC class I molecules. *Current Opinion in Immunology* 2006; **18**: 85–91.
93. Edwards AD, Diebold SS, Slack EM, *et al.* Toll-like receptor expression in murine DC subsets: lack of CD8 α+ DC correlates with unresponsiveness to imidazoquinolines. *European Journal of Immunology* 2003; **33**: 827–833.
94. Jongbloed SL, Kassianos AJ, McDonald KJ, *et al.* Human CD141+ (BDCA-3)+ dendritic cells (DCs) represent a unique myeloid DC subset that cross-presents necrotic cell antigens. *Journal of Experimental Medicine* 2010; **207**: 1247–1260.
95. Poulin LF, Salio M, Griessinger E, *et al.* Characterization of human DNGR-1+ BDCA3+ leukocytes as putative equivalents of mouse CD8α+ dendritic cells. *Journal of Experimental Medicine* 2010; **207**: 1261–1271.
96. Bachem A, Güttler S, Hartung E, *et al.* Superior antigen cross-presentation and XCR1 expression define human CD11c+ CD141+ cells as homologues of mouse CD8+ dendritic cells. *Journal of Experimental Medicine* 2010; **207**: 1273–1281.
97. Crozat K, Guiton R, Contreras V, *et al.* The XC chemokine receptor 1 is a conserved selective marker of mammalian cells homologous to mouse CD8α+ dendritic cells. *Journal of Experimental Medicine* 2010; **207**: 1283–1292.
98. Schultz O, Diebold SS, Chen M, *et al.* Toll-like receptor 3 promotes cross-priming to virus-infected cells. *Nature* 2005; **433**: 887–892.
99. Bon AL, Etchart N, Rossmann C, *et al.* Cross-priming of CD8+ T cells stimulated by virus-induced type I interferon. *Nature Immunology* 2003; **4**: 1009–1015.
100. Ebihara T, Shingai M, Matsumoto M, Wakita T, Seya T. Hepatitis C virus (HCV)-infected apoptotic cells extrinsically modulate dendritic cell function to activate T cells and NK cells. *Hepatology* 2008; **48**: 48–58.
101. Zhang S-Y, Jouanguy E, Ugolini S, *et al.* TLR3 deficiency in patients with Herpes Simplex encephalitis. *Science* 2007; **317**: 1522–1527.
102. Lauterbach H, Bathke B, Gilles S, *et al.* Mouse CD8α+ DCs and human BDCA3+ DCs are major producers of IFN-λ in response to poly(I:C). *Journal of Experimental Medicine* 2010; **207**: 2703–2717.
103. Akazawa T, Ebihara T, Okuno M, *et al.* Antitumor NK activation induced by the TLR3–TICAM-1 (TRIF) pathway in myeloid dendritic cells. *Proceedings of the National Academy of Science of the United States of America* 2007; **104**: 252–257.
104. Ebihara T, Azuma M, Oshiumi H, *et al.* Identification of a polyI:C-inducible membrane protein that participates in dendritic cell-mediated natural killer cell activation. *Journal of Experimental Medicine* 2010; **207**: 2675–2687.
105. Miyake T, Kumagai Y, Kato H, *et al.* Poly I:C-induced activation of NK cells by CD8 alpha+ dendritic cells via the IPS-1 and TRIF-dependent pathways. *Journal of Immunology* 2009; **183**: 2522–2528.
106. McCartney S, Vermi W, Gilfillan S, *et al.* Distinct and complementary functions of MDA5 and TLR3 in poly(I:C)-mediated activation of mouse NK cells. *Journal of Experimental Medicine* 2009; **206**: 2967–2976.
107. Lee HKS, Dunzendorfer K, Soldau K, Tobias PS. 2006; Double-stranded RNA-mediated TLR3 activation is enhanced by CD14. *Immunity* **24**: 153–163.
108. Kim J-I, Lee CJ, Jin MS, *et al.* Crystal structure of CD14 and its implications for lipopolysaccharide signaling. *Journal of Biological Chemistry* 2005; **280**: 11347–11351.
109. Itoh K, Watanabe A, Funami K, Seya T, Matsumoto M. The clathrin-mediated endocytic pathway participates in dsRNA-induced IFN-β production. *Journal of Immunology* 2008; **181**: 5522–5529.
110. Okahira S, Nishikawa F, Nishikawa S, Akazawa T, Seya T, Matsumoto M. Interferon-β induction through Toll-like receptor 3 depends on double-stranded RNA structure. *DNA and Cell Biology* 2005; **24**: 614–623.
111. Gowen BB, Wong M-H, Jung K-H, *et al.* TLR3 is essential for induction of protective immunity against Punta Toro virus infection by the double-stranded RNA (dsRNA), poly(I:C12U), but not poly(I:C): differential recognition of synthetic dsRNA molecules. *Journal of Immunology* 2007; **178**: 5200–5208.

MOLECULAR AND CELLULAR BIOLOGY, Sept. 2011, p. 3802–3819 Vol. 31, No. 18
0270-7306/11/$12.00 doi:10.1128/MCB.01368-10

DDX60, a DEXD/H Box Helicase, Is a Novel Antiviral Factor Promoting RIG-I-Like Receptor-Mediated Signaling[▽]†

Moeko Miyashita,[1,2] Hiroyuki Oshiumi,[1]* Misako Matsumoto,[1] and Tsukasa Seya[1]

Department of Microbiology and Immunology, Graduate School of Medicine,[1] and Graduate School of Life Science,[2] Hokkaido University, Kita-15, Nishi-7, Kita-ku, Sapporo 060-8638, Japan

Received 30 November 2010/Returned for modification 27 December 2010/Accepted 12 July 2011

The cytoplasmic viral RNA sensors RIG-I and MDA5 are important for the production of type I interferon and other inflammatory cytokines. DDX60 is an uncharacterized DEXD/H box RNA helicase similar to *Saccharomyces cerevisiae* Ski2, a cofactor of RNA exosome, which is a protein complex required for the integrity of cytoplasmic RNA. Expression of DDX60 increases after viral infection, and the protein localizes at the cytoplasmic region. After viral infection, the DDX60 protein binds to endogenous RIG-I protein. The protein also binds to MDA5 and LGP2 but not to the downstream factors IPS-1 and IκB kinase ε (IKK-ε). Knockdown analysis shows that DDX60 is required for RIG-I- or MDA5-dependent type I interferon and interferon-inducible gene expression in response to viral infection. However, DDX60 is dispensable for TLR3-mediated signaling. Purified DDX60 helicase domains possess the activity to bind to viral RNA and DNA. Expression of DDX60 promotes the binding of RIG-I to double-stranded RNA. Taken together, our analyses indicate that DDX60 is a novel antiviral helicase promoting RIG-I-like receptor-mediated signaling.

RIG-I and MDA5 are cytoplasmic viral RNA sensors belonging to the group of RIG-I-like receptors (RLRs), which includes LGP2 (57–59). RIG-I recognizes RNAs from vesicular stomatitis virus (VSV), hepatitis C virus (HCV), Sendai virus (SeV), and influenza A virus (21, 36, 37), while MDA5 recognizes RNA from picornaviruses such as encephalomyocarditis virus and poliovirus (PV) (3, 19, 21). RLRs are also involved in the recognition of cytoplasmic B-DNA. RNA polymerase III transcribes cytoplasmic AT-rich double-stranded DNA (dsDNA), and the transcribed RNA is recognized by RIG-I (1, 6). In contrast, Choi et al. have reported that RIG-I associates with dsDNA (7).

When RIG-I or MDA5 is activated by viral infection, the N-terminal caspase recruitment domains (CARDs) associate with the adaptor protein IPS-1 (also called MAVS/Cardif/VISA) on the outer mitochondrial membrane (22, 26, 42, 55). After this association occurs, IPS-1 activates TBK1 and IκB kinase ε (IKK-ε) and signals interferon (IFN) regulatory factor 3 (IRF-3)- and NF-κB-responsive genes, such as those for type I IFNs or other inflammatory cytokines (22, 23, 26, 42, 44, 55).

Both the helicase and C-terminal domain (CTD) of RIG-I bind to RNA, but it is the CTD that is responsible for the recognition of the 5′ triphosphate double-stranded structure typical of viral RNA (16, 39, 40). Recently, Rehwinkel et al. showed that the physiological ligand of RIG-I during influenza A virus or SeV infection is the full-length viral genomic single-stranded RNA (ssRNA), which possesses base-paired regions or defective interfering (DI) genomes (35). In contrast to RIG-I, MDA5 recognizes long viral double-stranded RNA (dsRNA) (21). The RNA binding activity of the MDA5 CTD is relatively weak compared with that of the RIG-I CTD, because the basic surface of the MDA5 CTD has a more extensive flat region than the RIG-I CTD (8, 45, 46). Although the RNA binding activity of the MDA5 CTD is weak, this protein plays a pivotal role in the recognition of picornavirus RNA (20, 21).

For the efficient recognition of viral RNA, RIG-I and MDA5 require protein modification and association with upstream factors. LGP2 is one of the upstream factors. LGP2 lacks an N-terminal CARD; thus, LGP2 itself cannot transmit the signal in the absence of RIG-I or MDA5 (36, 38, 49). The CTD of LGP2, which binds to the terminal region of viral double-stranded RNA, is more similar to the CTD of RIG-I than to that of MDA5 (24, 33, 45). LGP2 knockout studies have revealed that LGP2 is essential for type I IFN production by MDA5 but plays only a minor role in type I IFN production by RIG-I (38, 49). RIG-I requires modification of K63-linked polyubiquitination by TRIM25 and Riplet/REUL ubiquitin ligases for its full activation (11, 13, 30, 31). High-mobility-group box (HMGB) proteins also act as upstream factors of RLRs. Recently, Yanai and colleagues reported that HMGB1, HMGB2, and HMGB3 serve as sentinels for the nucleic acids required for both RIG-I and MDA5 recognition of viral RNA (56). Hayakawa and colleagues reported that ZAPS associates with RIG-I to promote oligomerization and ATPase activity of RIG-I (15). Another factor interacting with RLRs is DDX3, a DEXD/H box RNA helicase, which is similar to LGP2 in that it does not contain a CARD but promotes signaling by forming a complex with either RIG-I or MDA5 (32). DDX3 also plays important roles in TBK-1- and IKK-ε-mediated IRF activation, and Schröder et al. and Soulat et al. were the first to describe results showing that DDX3 is a non-RLR helicase involved in innate immune responses (41, 43).

DDX60, a DEXD/H box helicase, was annotated in a genome project, and the protein function is unknown. The protein is weakly similar to SKIV2L and SKIV2L2 and is the

* Corresponding author. Mailing address: Department of Microbiology and Immunology, Graduate School of Medicine, Hokkaido University, Kita-15, Nishi-7, Kita-ku, Sapporo 060-8638, Japan. Phone: 81-11-706-5056. Fax: 81-11-706-7866. E-mail: oshiumi@med.hokudai.ac.jp.

† Supplemental material for this article may be found at http://mcb.asm.org/.

▽ Published ahead of print on 2 May 2011.

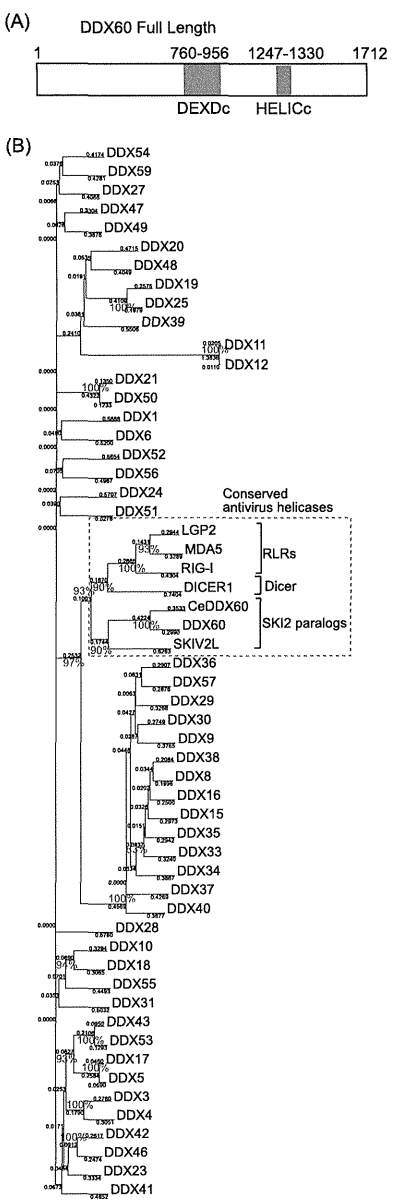

human homolog of *Saccharomyces cerevisiae* (budding yeast) Ski2, a cofactor of the RNA exosome (9, 18). The RNA exosome is a macromolecular protein complex that includes ribonucleases and helicases and controls the quality of host RNA molecules in both the nucleus and cytoplasm (17). It is composed of nine core components and several cofactor proteins (18). In budding yeast, the RNA exosome and Ski2 together exhibit antiviral activity (53, 54); similarly, the mammalian RNA exosome, together with its cofactors, shows antiviral activity against Moloney leukemia virus and Sindbis virus (5, 14). Our microarray analysis has shown that DDX60 is upregulated in human dendritic cells during infection with measles virus (MV) (our unpublished results). Thus, we expected DDX60 to be a novel antiviral protein and found that DDX60 is involved in RIG-I-like receptor-dependent antiviral pathways.

Here, we show that DDX60 is induced during viral infection and suppresses viral replication. DDX60 was found to form a complex with RLRs, promoting signaling; the results of knockdown experiments indicated that DDX60 is involved in RLR-dependent pathways. Moreover, the DDX60 helicase domain was observed to bind to viral RNA and DNA. Furthermore, DDX60 is required for type I IFN expression after DNA virus infection. These data indicate that DDX60 is a novel antiviral helicase involved in RLR-dependent pathways.

MATERIALS AND METHODS

Cell cultures. HEK293 and Vero cells were cultured in Dulbecco's modified Eagle's medium with 10% heat-inactivated fetal calf serum (Invitrogen), and HeLa cells were cultured in minimum Eagle's medium with 2 mM L-glutamine and 10% heat-inactivated fetal calf serum (JRH Biosciences). HEK293FT cells were maintained in Dulbecco's modified Eagle's high-glucose medium containing 10% heat-inactivated fetal calf serum (Invitrogen). RAW 264.7 cells were cultured in RPMI 1640 medium with 10% heat-inactivated fetal calf serum (Invitrogen). Mouse bone marrow-derived dendritic cells (BM-DCs) were induced as described in reference 2. PV receptor (PVR)-transgenic mice were provided by S. Koike (Tokyo Metropolitan Institute for Neuroscience).

Plasmids. Full-length human DDX60 cDNA was obtained from HeLa cell total RNA by reverse transcription-PCR (RT-PCR). The obtained cDNA fragments were sequenced, and we confirmed by PCR that the obtained cDNA clones do not contain nucleotide mutations. The DDX60 cDNA clone was cloned into XhoI and NotI restriction sites of pEF-BOS, and a hemagglutinin (HA) tag sequence was inserted just before the stop codon. EXOSC1, EXOSC4, or EXOSC5 was amplified by RT-PCR from HeLa cell total RNA. The obtained cDNA fragment was cloned into XhoI and NotI restriction sites of pEF-BOS vector, and the FLAG tag was fused at the C-terminal end. The DDX6 cDNA carrying a full-length open reading frame (ORF) was amplified by RT-PCR using *primers* DDX6-F (GGC CGC TCG AGC CAC CAT GAG CAC GGC CAG AAC AGA G) and DDX6-R (GGC GGG GTA CCC CAG GTT TCT CAT CTT CTA CAG). The fragment was cloned into XhoI and NotI sites of pEF-BOS vector. For *in vitro* viral RNA synthesis, we amplified VSV-G region cDNA by PCR using primers VSV-G-F and VSV-G-R. The obtained cDNA fragment was cloned into pGEM-T Easy vector. The primer sequences are as follows: for VSV-G-F, ACAGGAGAATGGGTTGATTC; and for VSV-G-R, ATGCAAA GATGGATACCAAC. Vectors expressing full RIG-I or RIG-I fragments were described before (30). The plasmids expressing TLR3 or TICAM-1 are described in reference 29. The p125luc reporter plasmid was a gift from T. Taniguchi (University of Tokyo, Tokyo, Japan). Mutant DDX60 expression constructs were amplified using primers for DDX60 (amino acids [aa] 1 to 169), (aa 169 to 334), (aa 334 to 490), (aa 478 to 656), (aa 657 to 857), (aa 857 to 1054), (aa 1049 to 1256), (aa 1256 to 1409), (aa 1407 to 1543), and (aa 1543 to 1712). The primer sequences are shown in Table S1 in the supplemental material.

Phylogenetic analysis. The amino acid sequences of the DEXD/H box domain were aligned using ClustalW software on the NIG server. The phylogenetic tree was drawn using the neighbor-joining method and GENETYX-MAC software (version 13.0.3).

Northern blotting. A human DDX60 644-bp cDNA fragment (from the region at bp 3978 to 4621) was used for the probe for Northern blotting. The Northern blot membranes (human 12-lane multiple-tissue Northern [MTN] blot and MTN blot III) were purchased from Clontech. The probe was labeled using

FIG. 1. The phylogenetic tree of DEXD/H box RNA helicase. (A) Schematic diagram of DDX60. DDX60 encodes a peptide of 1,712 amino acids (aa) that contains a DEXD/H box (DEXDc; aa 760 to 956) and HELICc (aa 1247 to 1330). (B) The phylogenetic tree of DEXD/H box RNA heliases. Ce, *C. elegans*. The bootstrap probabilities and genetic distances are shown in red and black, respectively.

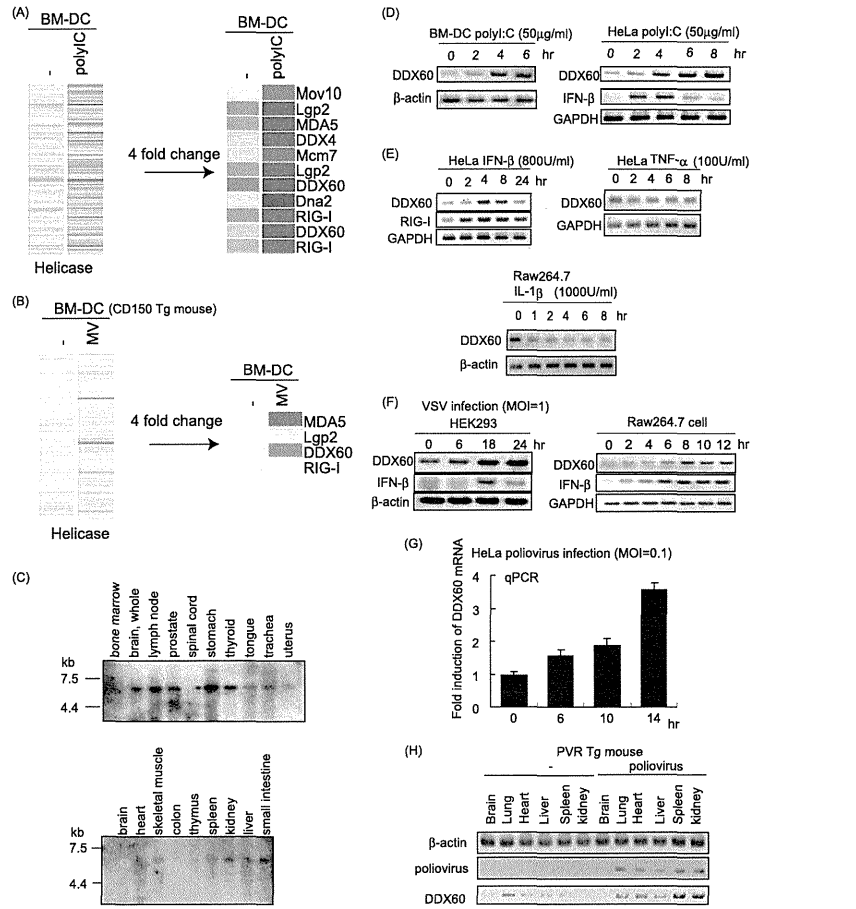

FIG. 2. Expression of DDX60 mRNA. (A and B) Mouse BM-DCs were stimulated with poly(I · C) (A) or infected with MV in the presence of anti-IFN-AR antibody (B). Total RNA was extracted from the cells, and microarray analysis was performed. The heat maps in the left column show the expression profiles of the genes encoding the helicase domain. The heat maps in the right column show the genes encoding the helicase domain whose expression levels changed more than 4-fold. (C) Northern blot of human DDX60 mRNAs in specified tissues. Northern blots of human tissues were probed with DDX60 cDNA. (D and E) Mouse BM-DCs, HeLa cells, or RAW 264.7 cells were stimulated with 50 μg of poly(I · C)/ml (D), 800 U of IFN-β/ml (E), 100 U of TNF-α/ml (E), or 1,000 U of IL-1β/ml (E). Expression of DDX60, RIG-I, GAPDH (glyceraldehyde-3-phosphate dehydrogenase), and β-actin mRNA was examined by RT-PCR. (F and G) HEK293 cells, RAW 264.7 cells, or HeLa cells were infected with VSV at an MOI of 1 (F) or PV at an MOI of 0.1 (G). Expression of DDX60, IFN-β, β-actin, and/or GAPDH was examined by RT-PCR (F) or RT-qPCR (G). (H) PV was injected intraperitoneally (i.p.) into PVR-transgenic mice susceptible to PV. Tissue RNA extraction was performed before or 3 days after infection, and RT-PCR was carried out on these samples.

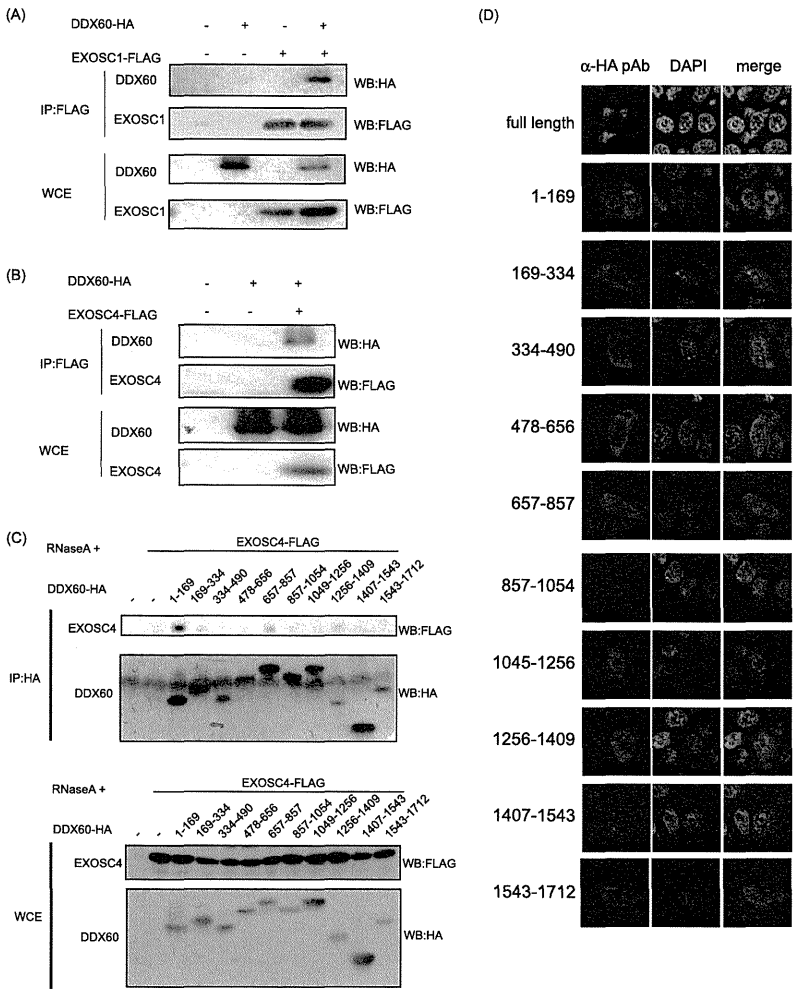

FIG. 3. Interactions between DDX60 and RNA exosome components. (A and B) HA-tagged DDX60 and FLAG-tagged EXOSC1 (A) and EXOSC4 (B) expression vector was transfected into HEK293FT cells. After 24 h, cell lysates were prepared and immunoprecipitation (IP) was performed with anti-FLAG antibody. The samples were analyzed by SDS-PAGE and detected by Western blotting (WB) using anti-HA or anti-FLAG antibodies. WCE, whole-cell extract (WCE). (C) HA-tagged DDX60 partial fragments and/or FLAG-tagged EXOSC4 expression vectors were transfected into HEK293FT cells, and immunoprecipitation was carried out as described for panel A in the presence of RNase A. (D) HA-tagged DDX60 fragment-expressing vectors were transfected into HeLa cells. The cells were stained with anti-HA antibody and DAPI and then observed by confocal microscopy.

[α-^{32}P]dCTP and a Rediprime II random prime labeling system (GE Healthcare). The labeled probe was hybridized to the membrane by the use of ExpressHyb hybridization solution (Clontech) at 68°C for 1 h. The membrane was washed with washing solution I (2× SSC [1× SSC is 0.15 M NaCl plus 0.015 M sodium citrate], 0.05% sodium dodecyl sulfate [SDS]) for 40 min and then washed with washing solution II (0.1× SSC, 0.1% SDS) for 40 min. DDX60 mRNA bands were detected with X-ray film.

RT-PCR and real-time PCR. Total RNA was extracted with TRIzol reagent (Invitrogen), and then the samples were treated with DNase I to remove the DNA contamination. The reverse transcription reaction was carried out using a

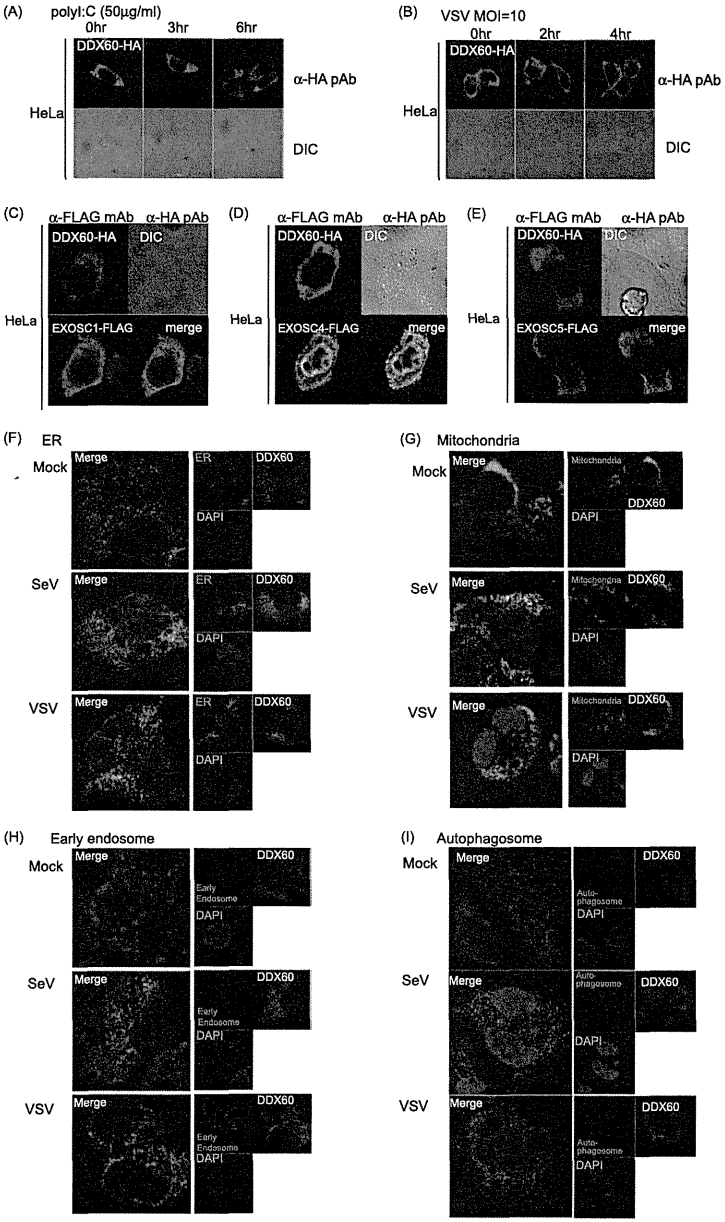

high-capacity cDNA reverse transcription kit (ABI). Quantitative PCR (qPCR) analysis was performed using Step One software version 2.0 (ABI) and SYBR Green Master Mix (ABI). The primer sequences for qPCR and PCR are described in Table S2 and S3 in the supplemental material, respectively.

Microarray analysis. Mouse bone marrow-derived dendritic cells were stimulated with poly(I · C) or infected with MV with anti-IFN-AR antibody (Ab) (see Fig. 2A). Total RNA was extracted from the cells, and we performed microarray analysis using Affimetrix GeneChip Mouse 430.2 software (10). The data were analyzed by GeneSpring GX 11 software.

RNA interference. RNA interference (RNAi) vectors were constructed by the insertion of oligonucleotides into the XbaI and PstI site of the pH 1 vector. The target sequence for DDX60 is 5′-CTTTACCACTTTCCTACGA-3′, the target sequence for EXOSC4 is 5′-TATAGTTCAGCGACCTT-3′, and the target sequence for EXOSC5 is 5′-GGATCCTACATCCAAGCAA-3′. HeLa cells or HEK293 cells were transfected with RNAi vector (0.5 μg) by the use of 24-well plates and FuGENE HD (Roche). After incubation for 24 h, cells were recovered and suspended in 12 ml of medium and then seeded to a 24-well plate. At 24 h after incubation, puromycin (1.0 μg/ml) was added. The medium containing puromycin was changed every 5 days, puromycin-resistant colonies were recovered, and the mRNAs of endogenous DDX60 or EXOSC4 and EXOSC5 were checked by RT-PCR. The sequences of the primers used for RT-PCR are described in Table S3 in the supplemental material. Small interfering RNA (siRNA) for DDX60 was purchased from Ambion and was transfected with Lipofectamine 2000 reagent (Invitrogen). The target sequence was 5′-GGC TAA CAA ACT TCG AAA A-3′.

Immunoprecipitation. HEK293FT cells were transfected in 6-well plates with plasmids encoding FLAG-tagged RIG-I, MDA5, EXOSC1, EXOSC4, EXOSC5, LGP2, IKK-ε, and Ubc13- and/or HA-tagged DDX60. The plasmid amounts were normalized by the addition of empty plasmid. At 24 h after transfection, cells were lysed with lysis buffer (20 mM Tris-HCl [pH 7.5], 150 mM NaCl, 1 mM EDTA, 10% glycerol, 1% Nonidet P-40, 30 mM NaF, 5 mM Na_3VO_4, 20 mM iodoacetamide, 2 mM phenylmethylsulfonyl fluoride), and then proteins were immunoprecipitated with rabbit anti-HA polyclonal antibody (Sigma) or anti-FLAG M2 monoclonal antibody (Sigma). The precipitates were analyzed by SDS-polyacrylamide gel electrophoresis (SDS-PAGE) and stained with anti-HA polyclonal or anti-FLAG M2 monoclonal antibody or monoclonal antibody to RIG-I (Alme-1) (Alexis Biochemicals).

Confocal microscopy. HeLa and HEK293 cells were plated onto Micro Cover glass sheets (Matsunami) and poly-L-lysin-coated cover glass sheets (eBioscience), respectively, in a 24-well plate. The following day, cells were transfected with the indicated plasmids. At 24 h after transfection, cells were infected with VSV or transfected with poly(I · C) by the use of 0.5 μg/ml DEAE-dextran for 4 h and then fixed using 3% formaldehyde-phosphate-buffered saline (PBS) for 30 min and permeabilized with 0.2% Triton X-100 for 15 min. Fixed cells were blocked in 1% bovine serum albumin (BSA)–PBS for 10 min and labeled with the indicated primary Abs (5 μg/ml) for 60 min at room temperature. Alexa-conjugated secondary Abs (1:400) were used to visualize staining of the primary Abs for 30 min at room temperature, and the mixture was mounted onto glass slides by the use of PBS containing 2.3% 1,4-diazabicyclo[2.2.2]octane and 50% glycerol or Prolong Gold antifade reagent with DAPI (4′,6′diamidino-2-phenylindole; Invitrogen). Cells were visualized at a magnification of ×63 with an LSM510 Meta microscope (Zeiss). To stain the mitochondria, endoplasmic reticulum (ER), early endosome, and autophagosome, we used Mitotracker (Invitrogen), anti-calnexin polyclonal antibody (Stressgen), anti-EEA1 polyclonal antibody (ABR), and anti-LC3 polyclonal antibody (MBL), respectively.

Reporter gene analysis. HEK293 cells were transiently transfected using 24-well plates and FuGENE HD (Roche) with expression vectors, reporter plasmids, and an internal control plasmid coding *Renilla* luciferase. The total amounts of plasmids were normalized with empty vector. For poly(I · C) stimulation, at 24 h after transfection, cells were stimulated with medium containing poly(I · C) (50 μg/ml) and DEAE-dextran (0.5 μg/ml) for 1 h, and then the medium was replaced with normal medium and incubation was performed for an additional 3 h. dsRNA was transfected using Lipofectamine 2000 (Invitrogen). Cells were lysed with lysis buffer (Promega) and luciferase, and *Renilla* luciferase activities were measured using a dual-luciferase assay kit (Promega). Relative luciferase activities were calculated by normalizing luciferase activity by control experiments in which only empty vector and reporter and internal control plasmids were transfected.

Viruses. VSV (Indiana strain), poliovirus (Mahoney strain), herpes simplex virus 1 (HSV-1) (K strain), and SeV (HVJ strain) were amplified using Vero cells. To determine the virus titer, we performed plaque assays using Vero cells. To observe the cytopathic effect (CPE), virus-infected cells were fixed at indicated times using 10% formaldehyde–PBS for 10 min and then stained using 1% crystal violet–PBS for 5 min at room temperature.

DDX60 helicase recombinant protein. The DDX60 helicase domain (bp 2254 to 4047) was amplified by PCR using primers DDX60 helicase-F and DDX60 helicase-R. The obtained cDNA fragment was cloned into KpnI and SalI restriction sites of pCold II DNA vector. The primer sequences were as follows: for DDX60 helicase-F, CGGGGTACCATGAGAAAAGACCCAG ATCCCAG; and for DDX60 helicase-R, GACGCGTCGACTTTTCCTATT TTGGGGAATG. The DDX6 helicase domain (aa 114 to 429) was amplified by RT-PCR using primers F (*GGC GGG GTA CCA TGG GCT GGG AAA AGC* CAT C) and R (GGA CGC GTC GAC ACC AAA GCG ACC TGA TCT TC). The cDNA fragment was cloned into the KpnI and SalI sites of pCold II DNA vector. Expression vectors were introduced into *Escherichia coli* BL21-competent cells and cultured in 10 ml of LB medium with ampicillin added for 12 h at 37°C and then added to 250 ml of LB medium and cultured for 3 h at 37°C. The cells were incubated at 15°C for 30 min, and protein expression was induced by the addition of 1 mM IPTG (isopropyl-β-D-thiogalactopyranoside). The cells were then cultured at 15°C for 24 h. The culture fluid was centrifuged for 10 min at 10,000 rpm and 4°C, and the *E. coli* cells were recovered. The cells were suspended in 5 ml of Tag binding buffer (20 mM Tris-HCl [pH 7.4], 0.5 M NaCl, 20 mM imidazol, 10% glycerol), 5 mg of lysozyme was added for 30 min on ice, and the mixture was subjected to shaking for 10 min; 500 μl of 10% Triton X-100 was then added, and the mixture was incubated for 10 min and centrifuged for 30 min at 5,000 rpm. The reaction was conducted at 4°C. The supernatant was subjected to filtration using a 0.45-μm-pore-size filter. The protein was purified using a HisTrap HP column (GE Healthcare) in accordance with the manufacturer's protocol. The protein was eluted with elution buffer (20 mM Tris-HCl [pH 7.4], 0.5 mM NaCl, 200 mM imidazol, 10% glycerol). We then collected the nonabsorbed fraction (that sample that had dropped out after the mixture was applied to the column), the wash fraction (the sample that dropped out after washing using the binding buffer was performed), and 500 μl each of elute fractions 1 to 10. The obtained samples were checked for purification by SDS-PAGE and detected by Coomassie brilliant blue (CBB) staining.

RNA synthesis. VSV-G RNA was synthesized from plasmids by using Riboprobe combination system SP6/T7 RNA polymerase (Promega) in accordance with the manufacturer's protocol. VSV RNA was produced from PCR products by the use of VSV G-pGEM-T Easy for its template and amplified by using a 5′ primer containing the T7 promoter (TAATACGACTCACTATAGGG) and a 3′ primer containing the SP6 promoter (GATTTAGGTGACACTATAG). The dsRNA was made by mixing equal amounts of positive strand (SP6) and negative strand (T7). The obtained ssRNA or dsRNA was added to 10 U of DNase I (Promega) at 37°C for 30 min and purified by phenol-chloroform treatment.

Gel shift assay. The components and final concentrations of the reaction solution were BSA (0.02 mg/ml), $MgCl_2$ (10 mM), dithiothreitol (DTT; 0.1 mM), glycerol (20%), NaCl (200 mM), Tris-HCl (20 mM), and ssRNA (0.6 μg), dsRNA (0.24 μg), or dsDNA (0.1 μg); we then added DDX60 or DDX6 helicase recombinant protein. The total volume was adjusted to 20 μl by adding water. The reaction solution was incubated at 30°C for 30 min; 1% agarose gel electrophoresis was then performed at 4°C for 90 min, and we observed the RNA results by the use of ethidium bromide (EtBr).

Pulldown assay. The RNA used for the assay was purchased from JBioS. The RNA sequences were as follows: for the sense strand, AAA CUG AAA GGG

FIG. 4. Intracellular localization of DDX60. (A and B) HA-tagged DDX60 expression vector was transfected into HeLa cells, and transfected cells were stimulated with 50 μg/ml poly(I · C) (A) or infected with VSV at an MOI of 10 (B). The cells were fixed and stained with anti-HA antibodies and observed using confocal microscopy. DIC, differential interference contrast; pAb, polyclonal antibody. (C to E) HA-tagged DDX60 was transfected into HeLa cells together with FLAG-tagged EXOSC1 (C), EXOSC4 (D), or EXOSC5 (E). Transfected cells were fixed and stained with anti-HA and anti-FLAG antibodies and observed using confocal microscopy. mAb, monoclonal antibody. (F to I) HEK293 cells stably expressing DDX60-HA were infected with VSV or SeV. DDX60-HA was stained with anti-HA antibody. The ER, mitochondria, early endosome, and autophagosome were stained with calnexin (F), Mitotracker Red (G), anti-EEA1 antibody (H), and anti-LC3 antibody (I).

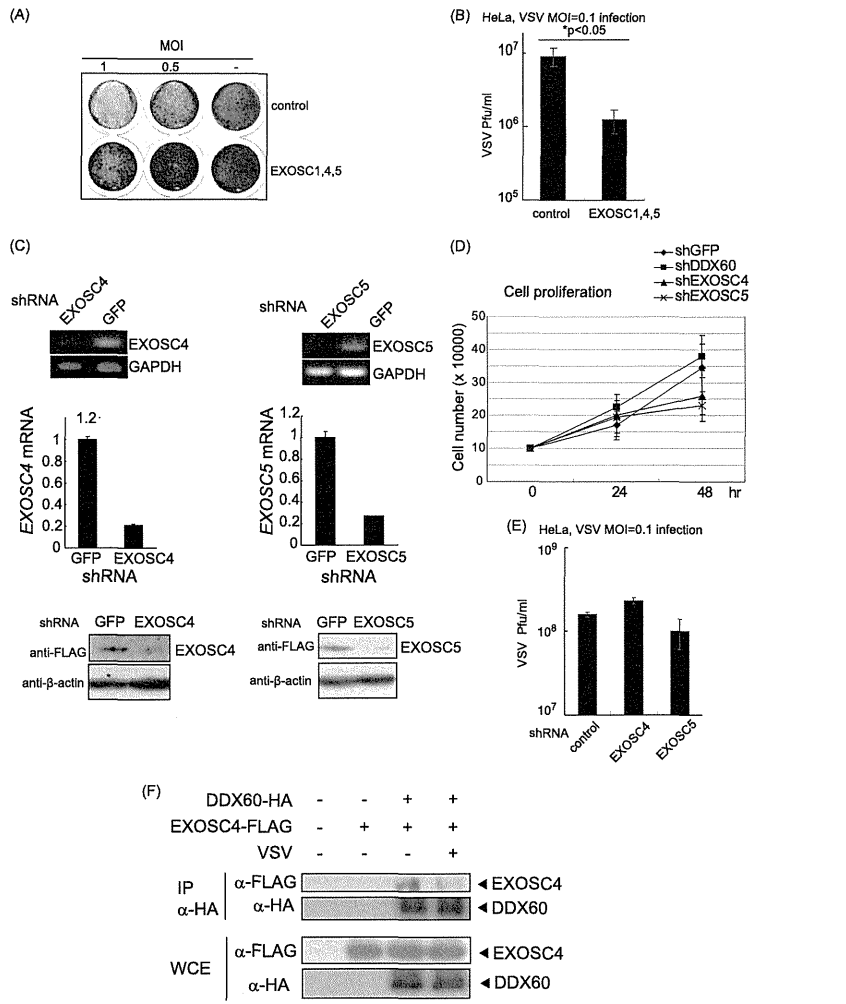

FIG. 5. Antiviral activity of RNA exosome. (A and B) HeLa cells were transfected with expression vectors containing EXOSC1, EXOSC4, and EXOSC5, and 24 h later, the transfected cells were infected with VSV at an MOI of 1 or 0.5. One day after infection, the cells were fixed and stained with crystal violet (A). Viral titers of culture media after 76 h were measured by a plaque assay (B). (C) Expression of EXOSC4 and EXOSC5 in stable HeLa clones, which express shRNA for EXOSC4, EXOSC5, or GFP, was examined by RT-PCR (upper panel), RT-qPCR (middle panel), and Western blotting (lower panel). The amounts of EXOSC4 and EXOSC5 cDNA in each sample were normalized by dividing by the amount of GAPDH. (D and E) Cell growth rates of stable HeLa clones, which express shRNA for EXOSC4, EXOSC5, DDX60, or GFP, were determined (D). The cells were infected with VSV at an MOI of 0.1 for 48 h, and viral titers of culture media were determined by a plaque assay (E). (F) FLAG-tagged EXOSC4- and HA-tagged DDX60-expressing vectors were transfected into HEK293FT cells. After VSV or mock infection, the immunoprecipitation was performed with anti-HA antibody.

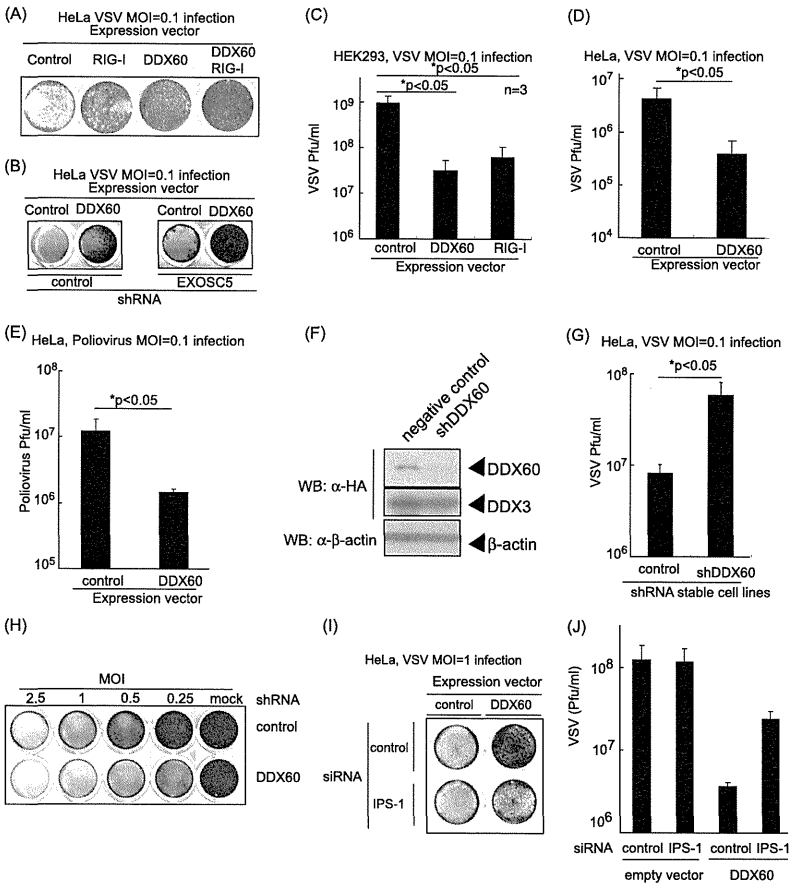

FIG. 6. Antiviral activity of DDX60. (A and B) HeLa cells (A) or the cells stably expressing shRNA for EXOSC5 or GFP (B) were transiently transfected with empty, DDX60-expressing, and/or RIG-I-expressing vectors. After 24 h, cells were infected with VSV at an MOI of 0.1 for 30 h. Cells were fixed and stained with crystal violet. (C and D) HEK293 clones stably expressing DDX60 or RIG-I (C) and HeLa cells subjected to mock treatment or transiently expressing DDX60 (D) were infected with VSV at an MOI of 0.1 for 24 h (C) or 48 h (D). Viral titers of culture media were measured by plaque assay. (E) Empty or DDX60-expressing vectors were transfected into HeLa cells, and 24 h after transfection, cells were infected with PV at an MOI of 0.1 for 26 h. Viral titers of culture media were measured by a plaque assay. (F) DDX60-expressing vector was transfected into HeLa clones stably expressing shRNA for GFP or DDX60, and the protein results were observed by Western blotting. (G) Control or DDX60 knockdown cells were infected with VSV at an MOI of 0.1 for 12 h, and viral titers of the culture media were measured by a plaque assay. (H) Control and DDX60 knockdown cells were infected with VSV at the indicated MOI for 12 h. The cells were fixed and stained with crystal violet. (I and J) Empty or DDX60-expressing vectors were transfected into HeLa cells with negative-control siRNA or siRNA for IPS-1. The cells were infected with VSV at an MOI of 1. After 24 h, cells were stained with crystal violet (I), and the viral titers of culture media were determined by a plaque assay (J).

AGA AGU GAA AGU G; and for the antisense strand, CAC UUU CAC UUC UCC CUU UCA GUU U. The biotin is conjugated at the U residue at the 3′ end of antisense strand (underlined). Biotinylated dsRNAs were phosphorylated by the use of T4 polynucleotide kinase (Takara). dsRNA was incubated for 1 h at 25°C with 10 μg of protein from the cytoplasmic fractions of cells that were transfected with FLAG-tagged RIG-I and/or HA-tagged DDX60-expressing vectors. The mixture was transferred into 400 μl of lysis buffer (20 mM Tris-HCl [pH 7.5], 150 mM NaCl, 1 mM EDTA, 10% glycerol, 1% NP-40, 30 mM NaF, 5 mM Na_3VO_4, 20 mM iodoacetamide, 2 mM phenylmethylsulfonyl fluoride [PMSF]) containing 25 μl of streptavidin Sepharose beads, rocked at 4°C for 2 h, collected by centrifugation, washed three times with lysis buffer, and resuspended in SDS sample buffer.

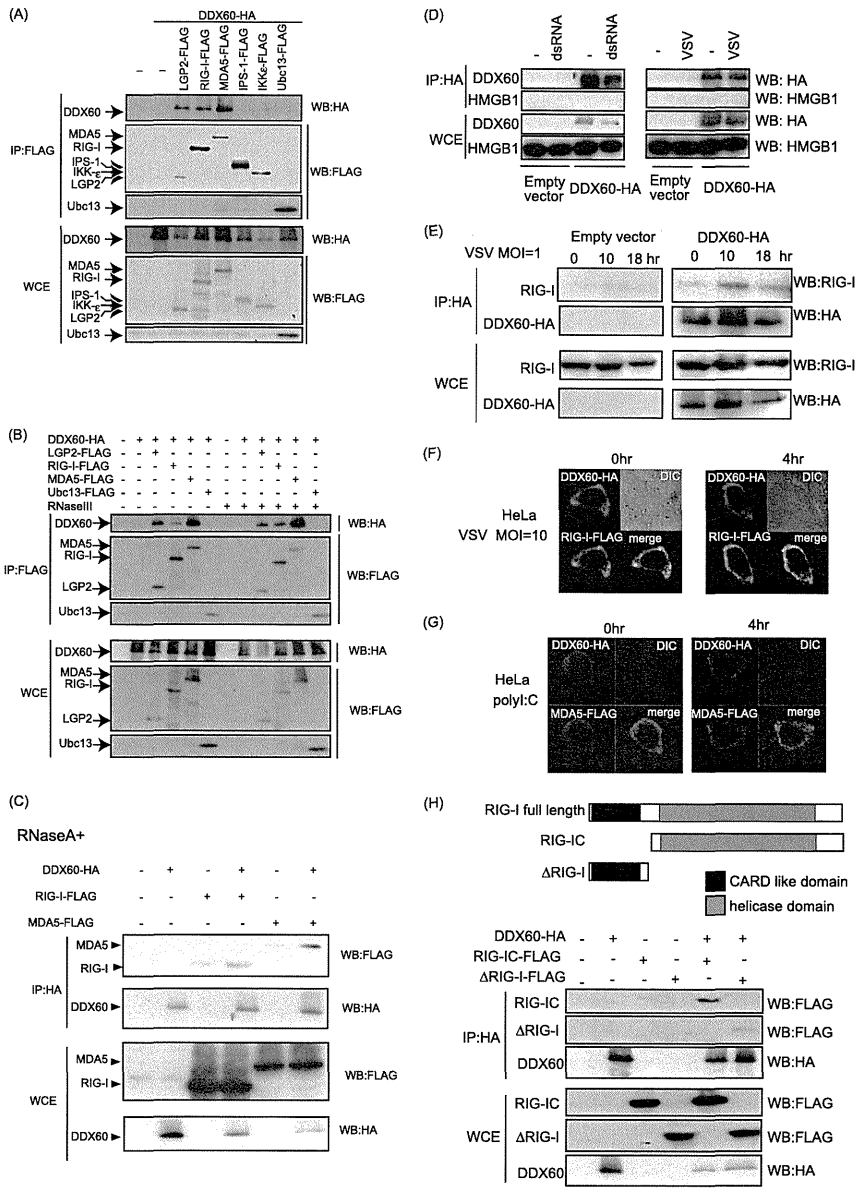

RESULTS

Phylogenetic analysis of the DEXD/H box domain of DDX60. The DDX60 protein contains a DEXD/H box RNA helicase domain and long N- and C-terminal regions with no typical domains or motifs (Fig. 1A). The DEXD/H box domain is common in the human genome. Phylogenetic analysis using amino acid sequences from this domain revealed that DDX60 is clustered within a group that includes RIG-I, MDA5, DICER1, and SKIV2L (bootstrap probability, 93%) and is most closely related to SKIV2L (bootstrap probability, 90%) (Fig. 1B). The functions of RIG-I and MDA5 have been described above. Dicer is an evolutionarily conserved protein required for RNAi and is known to perform antiviral functions in *Drosophila melanogaster* (12, 48, 51). SKIV2L is a homolog of *S. cerevisiae* Ski2, an antiviral protein that acts against dsRNA virus. Thus, the DDX60 DEXD/H box domain is found to cluster into a group composed of evolutionarily conserved antiviral helicases.

Expression of DDX60 mRNA. We carried out the microarray analysis using mouse bone marrow-derived dendritic cells (BM-DCs) and found that RLRs and DDX60 were included in the helicases whose expression had increased over 4-fold in response to viral infection (Fig. 2A and B). We investigated the expression profile of human DDX60 mRNA by Northern blot analysis and detected a single mRNA band at approximately 5.5 kb in the human brain, lymph node, prostate, stomach, thyroid, tongue, trachea, uterus, skeletal muscle, spleen, kidney, liver, and small intestine (Fig. 2C). Next, we examined the regulation of DDX60 expression. DDX60 mRNA was detected in unstimulated cells such as mouse BM-DCs, HeLa cells, HEK293 cells, and RAW 264.7 cells (Fig. 2D to F). DDX60 expression was upregulated by stimulation with poly(I · C) (Fig. 2D) or IFN-β (Fig. 2E). However, DDX60 expression was not increased by tumor necrosis factor alpha (TNF-α) or interleukin-1β (IL-1β) stimulation (Fig. 2E). Interestingly, DDX60 mRNA levels were increased by infection with VSV (Fig. 2F) or PV (Fig. 2G and H). Thus, DDX60 is an interferon-inducible gene and is upregulated during VSV or PV infection.

DDX60 associates with the components of the RNA exosome. Since the sequence of DDX60 is similar to that of RNA exosome cofactor SKIV2L, we examined whether the DDX60 protein associates with the RNA exosome core components in the same manner as the cofactor proteins. The RNA exosome core components form a tight protein complex (18); thus, it is expected that one of the core components would be coimmunoprecipitated with other core components and cofactors of the RNA exosome. These core components include EXOSC1 and EXOSC4. DDX60 protein was observed to coimmunoprecipitate with EXOSC1 and EXOSC4 (Fig. 3A and B), indicating the physical interaction of DDX60 with EXOSC1 and EXOSC4. We used partial DDX60 fragments to identify the region of DDX60 that binds to the RNA exosome. EXOSC4 was coimmunoprecipitated with the N-terminal 169-aa fragment of DDX60, indicating that the RNA exosome binds to the N-terminal region of DDX60 (Fig. 3C). All fragments were localized in the cytoplasmic region (Fig. 3D).

Intracellular localization of DDX60. Next, we studied the intracellular localization of the DDX60 protein by the use of confocal microscopy. In resting cells, DDX60 was localized in the cytoplasmic region but not in the nucleus before and after poly(I · C) stimulation or viral infection (Fig. 4A and B). EXOSC1, EXOSC4, and EXOSC5 were localized at both the cytoplasm and nucleus. The DDX60 protein was partially colocalized with the RNA exosome components at cytoplasmic region (Fig. 4C to E). To observe the intracellular localization of DDX60 after viral infection, we used HEK293 cell clones stably expressing HA-tagged DDX60. Most DDX60 staining was not colocalized with mitochondria, the endoplasmic reticulum (ER), LC3 (autophagosome marker), and endosome markers (EEA1) (Fig. 4F to I). However, the DDX60-HA protein was partially colocalized with the ER after VSV infection (Fig. 4F) and with the mitochondria after SeV infection (Fig. 4G).

Antiviral activity of DDX60 is independent of the RNA exosome. DDX60 expression was found to increase after viral infection, and the RNA exosome plays an antiviral role in lower eukaryotes such as budding yeast. Therefore, we assessed the antiviral activity of both DDX60 and the RNA exosome. Under our experimental conditions, 70% to 90% of cells expressed the proteins encoded by the transfected plasmids. Overexpression of three core components (EXOSC1, EXOSC4, and EXOSC5) suppressed the cytopathic effect (CPE) (Fig. 5A) and reduced the viral titer in the case of a low (0.1) multiplicity of infection (MOI) (Fig. 5B). Next, we performed a short hairpin RNA (shRNA) knockdown assay. We used shRNAs for EXOSC4 and EXOSC5, which were previously described as efficiently reducing expression of the target mRNA (4). We confirmed that shRNAs for EXOSC4 and EXOSC5 effectively reduced expression of their target mRNAs and the proteins (Fig. 5C). A partial decrease in levels of EXOSC4 in knockdown assays is known to reduce cell growth (47). We observed that the presence of shRNA for EXOSC4 and EXOSC5 reduced cell growth (Fig. 5D); however, knockdown of EXOSC4 or EXOSC5 showed a marginal effect on VSV replication (Fig. 5E), at least under our experimental conditions. We do not exclude the possibility that knockdown of EXOSC4 or EXOSC5 is not an efficient method by which to reduce the antivirus role of the RNA exosome. Unexpectedly, the physical interaction between EXOSC4 and DDX60 was reduced after VSV infection (Fig. 5F).

We next examined the antiviral activity of DDX60. Interestingly, DDX60 overexpression suppressed the CPE induced by VSV infection and reduced VSV replication in HEK293 and HeLa cells (Fig. 6A to D). The suppression induced by DDX60 overexpression was observed even in EXOSC5 knockdown cells (Fig. 6B). PV replication was also suppressed by overexpression of DDX60 (Fig. 6E). Next, we performed a knockdown assay using shRNA for DDX60, which reduced expression of DDX60 mRNA and protein (Fig. 6F) (see also Fig. 11 and 12). Unlike the results seen with EXOSC4 and EXOSC5, knockdown of DDX60 increased VSV replication and enhanced CPE and did not inhibit cell growth (Fig. 5D and Fig. 6G and H). Because the interaction between DDX60 and the RNA exosome core component was reduced after viral infection, we examined the molecular mechanism by which DDX60 suppresses viral replication.

DDX60 associates with RIG-I-like receptors. To identify the antiviral pathway in which DDX60 is involved, we used immunoprecipitation assays to search for the protein that binds to DDX60. Because the RLR-dependent pathway plays an important role in the antiviral activity of the host cell, we examined the binding of DDX60 to proteins involved in this pathway. Interestingly, DDX60 was coimmunoprecipitated with RIG-I, MDA5, and LGP2 but not with IPS-1 or IKK-ε, which are downstream factors of RIG-I and MDA5 (Fig. 7A). RNase A or RNase III treatment did not abolish the interaction between DDX60 and RIG-I or MDA5 (Fig. 7B and C), indicating that these associations are not mediated via RNA. DDX60 did not bind to HMGB1 before or after dsRNA stimulation or VSV infection (Fig. 7D). To further confirm the binding of DDX60 to RIG-I, we examined the interaction of DDX60 with endogenous RIG-I by the use of anti-RIG-I monoclonal antibody. RIG-I mRNA levels are known to increase after viral infection (59). We observed an increase in RIG-I protein levels after poly(I · C) stimulation (data not shown). However, the protein level in HEK293FT cells was not increased after VSV infection in our experiment for unknown reasons (Fig. 7E). Endogenous RIG-I was found to interact with DDX60 after VSV infection but not in its absence (Fig. 7E), indicating that interaction between DDX60 and endogenous RIG-I is dependent on viral infection, although the interaction between overexpressed RIG-I and DDX60 was independent of viral infection.

Next, we used confocal microscopy to examine the intracellular colocalization of DDX60 with RIG-I and MDA5. Consistent with the immunoprecipitation assay, confocal microscopic analysis showed that DDX60 was partially colocalized with overexpressed RIG-I and MDA5 before and after VSV infection or poly(I · C) stimulation (Fig. 7F and G). We tried to observe endogenous RIG-I by confocal microscopy; however, we could not detect endogenous RIG-I in our tests for technical reasons. We also used RIG-I partial fragments to identify the region of RIG-I that binds to DDX60 (Fig. 7H). RIG-IC, which includes a helicase domain and CTD, was coimmunoprecipitated with DDX60, while the N-terminal CARD of RIG-I was not (Fig. 7H). These data indicate that DDX60 binds to the RIG-IC fragment.

The DDX60 helicase domain binds to viral RNA. In light of the binding of DDX60 to viral RNA sensors RIG-I and MDA5, we hypothesized that the RNA helicase domain of DDX60 binds to viral RNA. To test this hypothesis, we expressed a histidine-tagged DDX60 RNA helicase domain (aa 752 to 1337) in *E. coli* (Fig. 8A). The protein was purified using nickel-nitrilotriacetic acid (Ni-NTA) resin, analyzed by SDS-PAGE, and stained with CBB. Protein purity was found to be greater than 90% (Fig. 8B). VSV single- and double-stranded RNA was synthesized *in vitro*. Binding of the DDX60 helicase domain to *in vitro*-synthesized viral RNA was examined using gel-shift assays. Single- or double-stranded VSV RNA mobility was found to decrease as a result of the addition of DDX60 helicase (Fig. 8C and D). DDX60 was also found to bind to dsRNA treated with alkaline phosphatase, suggesting that the presence of 5′ triphosphate is nonessential for this binding (Fig. 8E). The mobility shift of ssRNA was different from that of dsRNA; this difference might have been a result of the stoichiometry assays. Interestingly, dsDNA was also shifted in the presence of DDX60 protein (Fig. 8F). As a control we used DDX6, a DEXD/H box RNA helicase distantly related to DDX60. DDX6 also bound to ssRNA (Fig. 8C); however, DDX6 only minimally reduced the mobility of dsRNA and dsDNA compared to DDX60 (Fig. 8D and F).

DDX60 promotes RIG-I- or MDA5-dependent expression of type I IFN. Next, we examined whether DDX60 is involved in RIG-I- or MDA5-mediated signaling. The prepared poly(I · C) solution contains various lengths of poly(I · C), both shorter and longer than 1 kbp (data not shown), in a mixture known to activate both RIG-I and MDA5 (20). Both RIG-I-mediated and MDA5-mediated IFN-β promoter activation by poly(I · C) transfection were enhanced by DDX60 expression (Fig. 9A and B). As a control we used DDX6, a helicase distantly related to DDX60. Expression of DDX6 produced neither a positive nor a negative effect on the RIG-I-dependent IFN-β promoter activation (Fig. 9C). To address the function of the DDX60 helicase domain, we introduced the mutation (K791A) on the Walker type ATP binding site, which is essential for ATPase activity of RNA helicase (50). The mutation reduced the enhancement of RIG-I-mediated IFN-β promoter activation by DDX60 (Fig. 9C). Knockdown analysis using shRNA for DDX60 showed that IFN-β promoter activation by viral dsRNA was reduced in DDX60 knockdown cells compared with control cells (Fig. 9D). To exclude the off-target effect, we also used siRNA for DDX60, whose target sequence is different from that of shRNA for DDX60. Expression of DDX60 was efficiently reduced by siRNA for DDX60, and the siRNA for DDX60 efficiently reduced IFN-β mRNA expression by poly(I · C) stimulation (Fig. 9E to G). These knockdown results are consistent with the overexpression results described above, providing further evidence that DDX60 promotes RLR-mediated IFN-β expression.

In contrast, TICAM-1- and TLR3-mediated IFN-β promoter activation was not increased by overexpression of DDX60 (Fig. 9H and I). In addition, poly(I · C) stimulation of TLR3 without transfection resulted in normal expression

FIG. 7. Association of DDX60 with RLRs. (A to C) Vectors expressing HA-tagged DDX60 were transfected into HEK293FT cells with FLAG-tagged LGP2, RIG-I, MDA5, IPS-1, IKK-ε, and/or Ubc13, and cell lysates were prepared. The lysates were treated with RNase III (B) or RNase A (C). Immunoprecipitation was carried out with anti-FLAG antibody, and the precipitates (IP) and 10% of whole-cell extract (WCE) were analyzed using SDS-PAGE. Proteins were stained by Western blotting using anti-HA or anti-FLAG antibody. (D and E) HEK293FT cells were transfected with empty or HA-tagged DDX60-expressing vectors, and cells were stimulated with dsRNA or infected with VSV. Cell lysates were prepared at the indicated times, and immunoprecipitation was performed with anti-HA antibody. The precipitates were analyzed using SDS-PAGE, and Western blotting was carried out using anti-HA and anti-HMGB1 (D) or anti-RIG-I (E) antibodies. (F and G) Vectors expressing HA-tagged DDX60 and FLAG-tagged RIG-I (F) or MDA5 (G) were transfected into HeLa cells. After 24 h, cells were fixed and stained with anti-HA or anti-FLAG antibody and then observed using confocal microscopy. (H) The upper panel shows a schematic diagram of RIG-I partial fragments. The lower panel shows results of an immunoprecipitation assay performed as described for panel A. DDX60 was found to bind to the RIG-IC region.

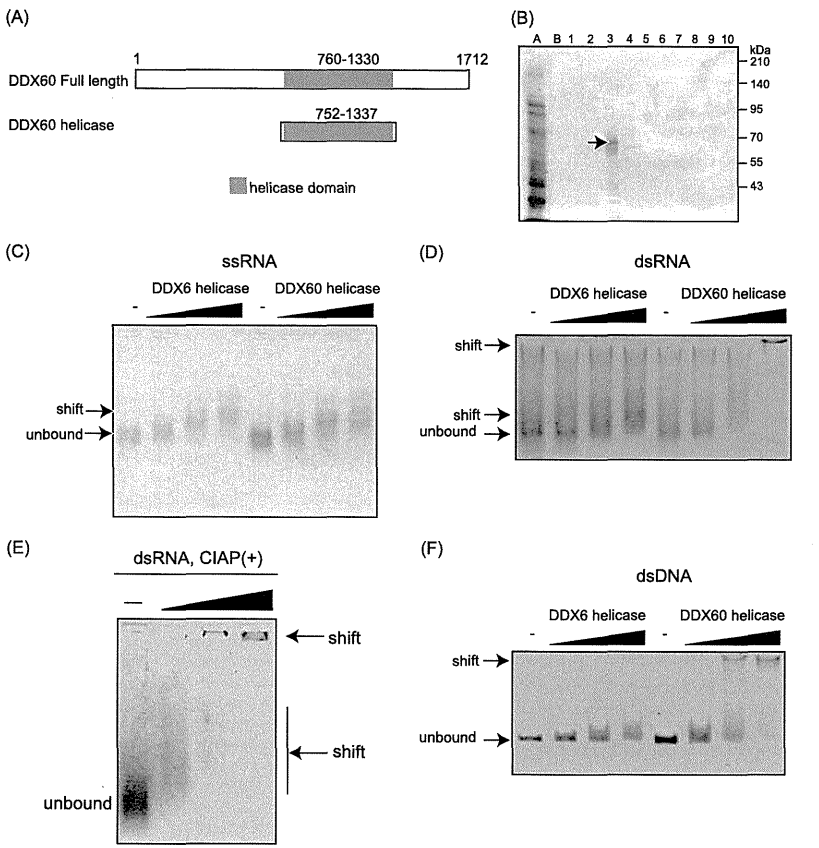

FIG. 8. Binding of the DDX60 helicase domain to viral RNA. (A) Schematic diagram showing the helicase region of DDX60 used for the following gel shift assay. (B) A His-tagged DDX60 helicase fragment was expressed in *E. coli* and purified using Ni-NTA resin. Purified products were analyzed by SDS-PAGE and stained with CBB. Lane A represents the nonabsorbed fraction, lane B represents the wash fraction, and lanes 1 to 10 represent the eluted fractions. The lane 3 fraction contains DDX60 protein. (C to F) Purified DDX60 and DDX6 fragments were incubated with *in vitro*-synthesized VSV ssRNA (C), dsRNA (D), dsRNA treated with calf intestinal alkaline phosphatase (CIAP) (E), or dsDNA (F), and the products were analyzed using agarose gel. The gel was stained with ethidium bromide.

of IFN-β in DDX60 knockdown cells (Fig. 9J). These data suggest that DDX60 is specific to the RLR pathway. Because the knockdown of EXOSC4 or EXOSC5 did not reduce the promoter activation resulting from VSV infection or dsRNA transfection (Fig. 9K and L), the data suggest that these proteins do not play a major role in DDX60-mediated enhancement of RIG-I or MDA5 signaling, at least under our experimental conditions. We also assessed the effect of DDX60 knockdown on IFN-β promoter activation by overexpressing TBK1, IPS-1, RIG-I CARDs, or MDA5 to discover the step at which DDX60 plays a role in RIG-I-mediated signaling. All of these procedures led to autoactivation, inducing transcription from the IFN-β promoter in the absence of RIG-I or MDA5 ligands (22). Although DDX60 knockdown reduces the IFN-β promoter activation induced by dsRNA transfection, it was not found to affect this autoactivation (Fig. 9M and N). These data suggest that shRNA suppression of DDX60 occurs upstream of RIG-I and MDA5 (Fig. 9O).

To examine the effect of DDX60 on the binding of RIG-I to dsRNA, we performed pulldown assays. The proteins were exogenously expressed in HEK293FT cells, and the proteins were recovered from cell lysates by the use of biotin-conjugated dsRNA and streptavidin Sepharose. RIG-I or DDX60 protein was recovered from cell extracts, suggesting the bind-

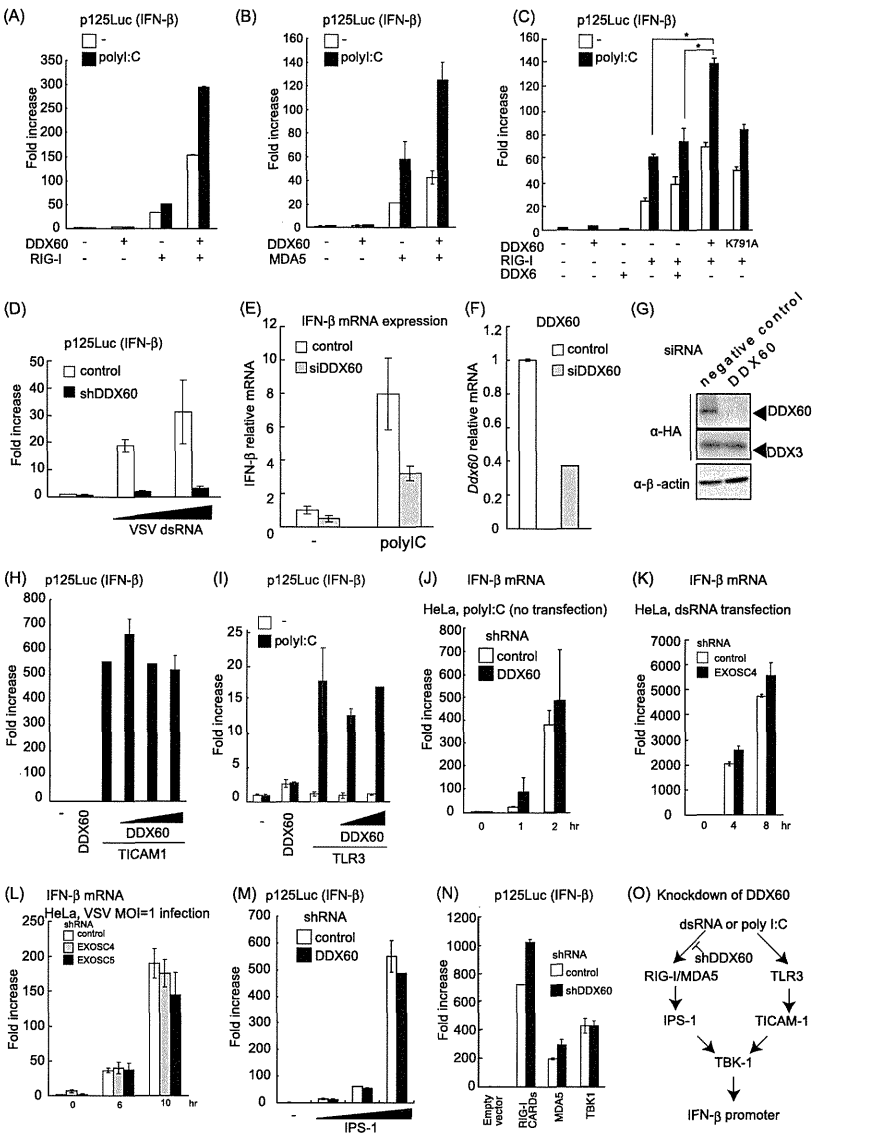

FIG. 9. DDX60 promotes RIG-I- or MDA5-mediated signaling. (A to C) Activation of the IFN-β promoter was examined using a reporter gene assay and p125luc plasmid. Vectors expressing RIG-I (A), MDA5 (B), DDX6 (C), and the wild type (WT) or DDX60-K791A (C) were transfected into HEK293 cells together with the reporter plasmid and *Renilla* luciferase plasmid (internal control). After 24 h, the cells were left unstimulated or stimulated with poly(I · C) by the use of DEAE-dextran for 4 h. Cell lysates were prepared, and luciferase activity was measured. (D) Control or DDX60 knockdown HEK293 cells were transfected with the p125luc reporter, *Renilla* luciferase plasmid, and/or *in vitro*-synthesized VSV

ing of RIG-I or DDX60 to dsRNA. Because both RIG-I and DDX60 can bind to dsRNA, the data do not imply an interaction between RIG-I and DDX60. Interestingly, coexpression of both proteins increased the levels of proteins recovered from the cell lysate (Fig. 10).

DDX60 is important for expression of type I IFN and IFN-inducible genes during viral infection. We next tested whether DDX60 is involved in cytokine expression during viral infection. RIG-I recognizes VSV and SeV, and MDA5 recognizes PV (3, 21). Interestingly, knockdown of DDX60 reduced IFN-β expression in HeLa cells after VSV, PV, and SeV infection. IFIT-1 and IP10 expression after VSV and SeV infection was also reduced by DDX60 knockdown (Fig. 11). Knockdown of DDX60 caused a marginal effect on expression of IFIT1 and IP10 in response to PV infection. Some of the IFN-α gene expression induced by other sensor molecules might have been responsible for the difference. Unlike viral infection, knockdown of DDX60 did not reduce expression of IFIT1 after IFN-β stimulation (Fig. 12A). Reduction of type I IFN expression was also observed after VSV infection in HEK293 cells (Fig. 12B and C). In addition, DDX60 knockdown reduced IRF-3 dimerization after VSV infection (Fig. 12D). These data indicate that DDX60 is required for RIG-I- and MDA5-dependent type I IFN and IFN-inducible gene expression during viral infection. We also observed that suppression of CPE and viral titers in culture medium induced by DDX60 overexpression can be reduced by IPS-1 knockdown (Fig. 6I and J), confirming that the antiviral activity of DDX60 is dependent on the presence of RLRs. Because the DDX60 helicase domain was found to bind to dsDNA, we examined whether DDX60 is involved in type I IFN expression after infection with HSV-1, a DNA virus. In this case, knockdown of DDX60 reduced expression of IFN-β and IP10 after HSV-1 infection (Fig. 12E and F).

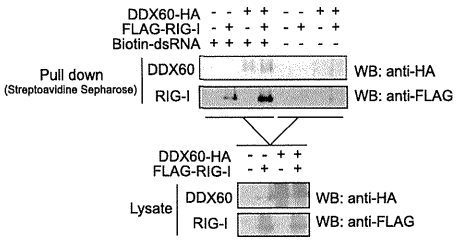

FIG. 10. DDX60 increases the association of RIG-I to short synthetic dsRNA. DDX60- and RIG-I-expressing vectors were transfected into HEK293FT cells. At 24 h later, cell lysate was prepared. The lysate was incubated with or without biotin-conjugated dsRNA, and the dsRNA was recovered using streptavidin Sepharose beads. The recovered fraction was analyzed by Western blotting.

DISCUSSION

Here, we report that DDX60 is a novel antiviral factor in human cells. The amino acid sequence of DDX60 is similar to that of Ski2 homologs, which are cofactors of the RNA exosome. DDX60 interacts with core components of the RNA exosome. After viral infection, the DDX60 protein binds to endogenous RIG-I protein and is involved in RIG-I-dependent pathway. The protein also binds to MDA5 and LGP2. The DDX60 helicase domain binds to viral RNA and DNA, and coexpression of RIG-I with DDX60 increases the binding of RIG-I and DDX60 to dsRNA. Knockdown of DDX60 reduces expression of type I IFN and IFN-inducible genes after VSV, PV, SeV, and HSV-1 infections. Therefore, we concluded that DDX60 is a novel antiviral helicase involved in RLR-dependent pathways.

Schröder et al. and Soulat et al. first reported that the non-RLR helicase DDX3 plays pivotal roles in RLR-dependent pathways (41, 43). DDX3 is ubiquitously expressed in a variety of cells and exerts its positive effect as a part of TBK-1- and/or IKK-ε-containing complexes that activate IRF-3 (41). DDX3 also binds to RIG-I and IPS-1 and promotes the activation of those proteins (28, 32). Our study showed that another non-RLR helicase, DDX60, is also involved in RLR-dependent pathways. Thus, our reports and previous studies demonstrate the important roles of non-RLR helicases in RLR-mediated signaling and antiviral response.

Because DDX60 protein does not contain CARDs, which are required for the interaction with IPS-1, it seems unlikely that DDX60 directly activates IPS-1 without RLRs. The results of knockdown studies suggest that DDX60 is an upstream factor of IPS-1, and the immunoprecipitation assay results suggest that DDX60 binds to the RLR upstream factors. On the basis of these findings, we expected that DDX60 would

dsRNA. After 24 h, cell lysates were prepared and luciferase activity was measured. (E and F) siRNA for DDX60 or control siRNA was transfected into HEK293 cells. The cells were left unstimulated or stimulated with poly(I · C), and expression of IFN-β and DDX60 mRNA was measured by RT-qPCR. Expression values were normalized using GAPDH. (G) siRNA for DDX60 or the control was transfected into HEK293 cells together with DDX60-expressing vector. The DDX60 protein was observed by Western blotting. (H) Vectors expressing TICAM-1 and/or DDX60 were transfected into HEK293 cells together with the p125luc reporter and *Renilla* luciferase plasmids. After 24 h, the cell lysates were prepared and luciferase activities were measured. (I) Vectors expressing TLR3 and/or DDX60 were transfected into HEK293 cells together with the p125luc reporter and *Renilla* luciferase plasmids. After 24 h, the cells were left unstimulated or stimulated with poly(I · C) for 4 h, the cell lysates were prepared, and luciferase activity was measured. (J and K) HeLa cells expressing shRNA for DDX60 (J) or EXOSC4 (K) were stimulated with 50 μg/ml of poly(I · C) (no transfection) (J) or dsRNA (transfection) (K). RT-qPCR was performed to measure IFN-β mRNA expression. (L) HeLa cells expressing shRNA for GFP, EXOSC4, or EXOSC5 were infected with VSV at an MOI of 1. Levels of induction of IFN-β mRNA were calculated as described for panel J. (M and N) Empty or IPS-1-expressing vector (M) and RIG-I CARD-, MDA5-, or TBK1-expressing vector (N) were transfected into control or DDX60 knockdown HEK293 cells together with p125luc reporter and *Renilla* luciferase plasmids. After 24 h, cell lysates were prepared and luciferase activity was measured. (O) shRNA for DDX60 did not inhibit the signaling from TLR3 (H to J). Although DDX60 promotes RLR-dependent signaling (A to E), shRNA for DDX60 did not reduce the signaling induced by RIG-I CARD, MDA5, IPS-1, or TBK1 overexpression (M and N). These data suggest that shRNA suppresses signaling upstream of RIG-I and MDA5.

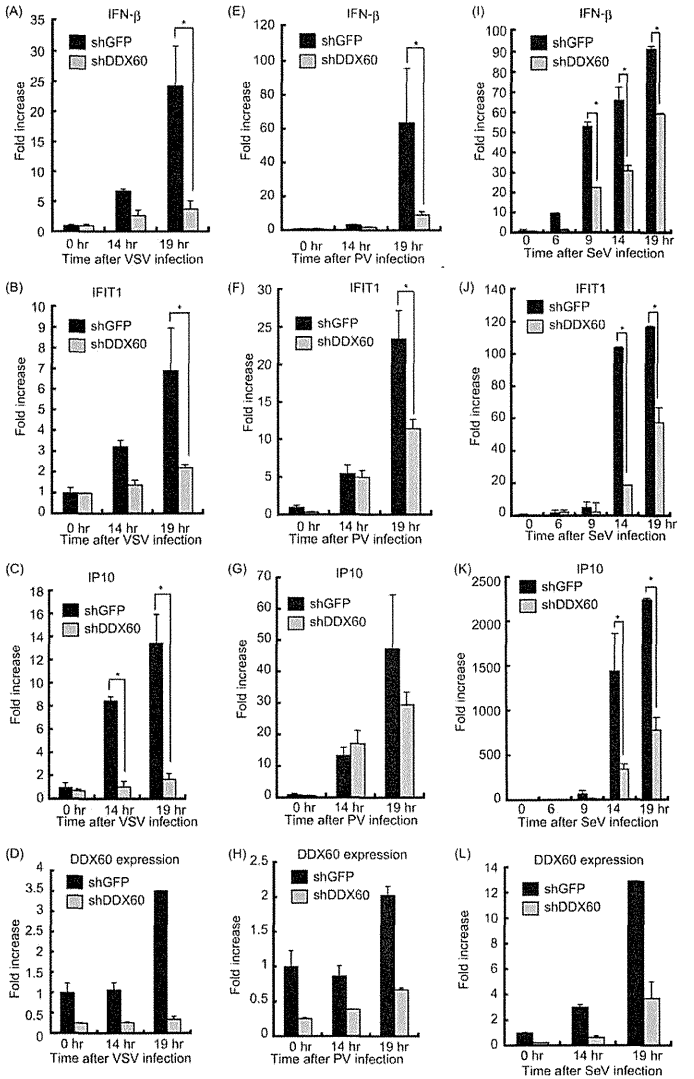

FIG. 11. Knockdown of DDX60 decreases expression of type I IFN during viral infection in HeLa cells. (A to L) Control cells or HeLa cells from a stable cell line expressing shRNA for DDX60 were infected with VSV (A to D), PV (E to H), or SeV (I to L). Total RNA was extracted at the indicated times. RT-qPCR was performed to measure expression of IFN-β (A, E, and I), IFIT1 (B, F, and J), IP10 (C, G, and K), and DDX60 (D, H, and L). The expression level of each sample was normalized to GAPDH expression.

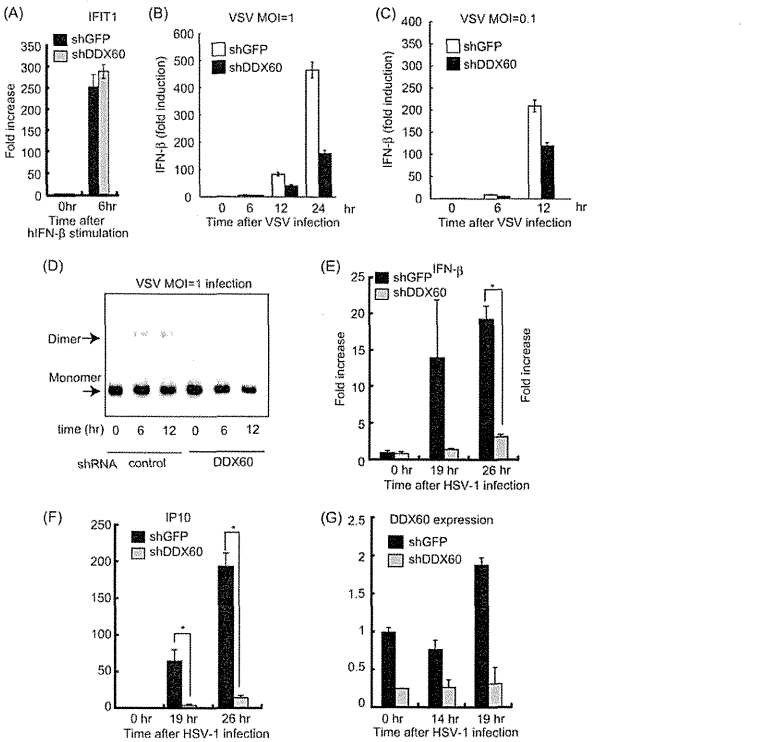

FIG. 12. Effects of DDX60 knockdown on antiviral responses. (A to C) Control or DDX60 knockdown cells were stimulated with human IFN-β (A) or infected with VSV at an MOI of 1 (B) or 0.1 (C), and expression of IFIT1 (A) and IFN-β (B and C) mRNA was examined by RT-qPCR. (D) Control or DDX60 knockdown HEK293 cells were infected with VSV at an MOI of 1, and cell lysates were prepared at the indicated times. Lysates were analyzed by native PAGE, and Western blot analysis was performed with anti-IRF-3 antibody. (E to G) Control or DDX60 knockdown HeLa cells were infected with HSV-1, and total RNA was extracted at the indicated times. RT-qPCR was performed to examine expression of IFN-β (E), IP10 (F), and DDX60 (G).

bind to viral RNA. The gel shift assay showed that DDX60 helicase can bind to dsRNA, and the pulldown assay showed that coexpression of DDX60 with RIG-I increased the binding of RIG-I to dsRNA. Thus, we speculate that DDX60 binds to viral dsRNA and associates with RLRs during viral infection. Further study is required to reveal the precise molecular mechanism by which DDX60 activates the RLR-dependent pathway.

The DDX60 helicase domain binds to dsDNA *in vitro*, and DDX60 was required for type I IFN expression during infection with HSV-1, a DNA virus. In human cells, RIG-I is involved in the pathway activated by cytoplasmic B-DNA or DNA virus infection (1, 6, 7). AT-rich dsDNA is transcribed by RNA polymerase III, and these transcripts are recognized by RIG-I (1, 6). In contrast, Choi et al. reported that the RIG-I protein associates with B-DNA and activates the signaling (7). Previously, Takahasi et al. reported that purified RIG-I protein does not itself bind to dsDNA (46). Therefore, RIG-I seems to associate with B-DNA via another protein that directly binds to dsDNA. HSV-1 was reported to produce considerable amounts of dsRNA and to activate RIG-I and MDA5 (25, 34, 52). Thus, we do not exclude the possibility that DDX60 is involved in recognition not of dsDNA but of dsRNA derived from HSV-1. Although RIG-I and MDA5 are involved in the signaling induced by cytoplasmic B-DNA, IPS-1 is dispensable for the signaling (23). Further study is required to reveal the molecular mechanism by which DDX60 plays an important role in the signaling induced by cytoplasmic B-DNA.

In addition to the *DDX60* gene, the human genome includes the closely related *DDX60L* gene, which is located 5′ upstream of *DDX60* on chromosome IV. However, the mouse genome encodes only one DDX60 protein. Our phylogenetic analysis indicated that the mouse gene is a shared ancestor of human *DDX60* and *DDX60L* genes, and a pilot study has revealed that

DDX60L is expressed after viral infection (unpublished results). Therefore, DDX60L is also expected to be an antiviral protein. Considering that knockdown of DDX60 severely reduced type I IFN expression after viral infection, there seem to be functional differences between DDX60 and 60L. Further study is required to reveal the functional differences between DDX60 and 60L.

The amino acid sequence of DDX60 is weakly similar to those of the exosome cofactors SKIV2L and SKIV2L2. In immunoprecipitation experiments, DDX60 protein was found to coimmunoprecipitate with core components of the RNA exosome. However, we could not determine the physiological role of the interaction between DDX60 and RNA exosome by knockdown analysis. We examined whether or not knockdown of DDX60 and the RNA exosome delays degradation of viral genomic RNA. We found that knockdown of DDX60 or RNA exosome components does not substantially delay degradation of transfected viral RNA (unpublished results). This observation is consistent with our results showing that knockdown of the RNA exosome does not increase viral titers. However, we do not exclude the possibility that the RNA exosome is involved in antiviral responses. There exist several antiviral nucleases, such as RNase L and ISG20. Thus, it is possible that those antiviral nucleases compensate for the defect of the RNA exosome. This possibility is not surprising, because there are several redundant pathways in the innate immune system. For example, poly(I · C) is a ligand common to TLR3 and MDA5; thus, not single but double knockout is required to abolish poly(I · C)-dependent NK cell cytotoxicity (27). Type I IFNs are produced from various kinds of cells, such as fibroblasts, dendritic cells, and macrophages; thus, we do not exclude the possibility that the RNA exosome performs some roles in DDX60 antiviral activity in other cells. The RNA exosome is required to maintain the integrity of host RNA and to disrupt RNA that lacks a 5′ catabolite gene activator protein (CAP) or 3′ poly(A) tail. Thus, it is also possible that DDX60 is involved in host RNA integrity. Further study is required to reveal the physiological role of the association of DDX60 with the RNA exosome.

In single-cell organisms such as budding yeast (*S. cerevisiae*), Ski2 plays a major role in the antiviral response to dsRNA virus. DDX60, a homolog of Ski2, is conserved among eukaryotes. For example, DDX60 is also encoded by the *Caenorhabditis elegans* genome. In a pilot study, we found nematode DDX60 expression to be increased after viral infection (unpublished results), leading us to predict that DDX60 possesses antiviral activity in this species as well. Phylogenetic tree analysis has shown that antiviral helicases such as DDX60, RLRs, and Dicer are clustered into one node. Considering that budding yeast uses Ski2 helicase for its antiviral activity, Ski2-DDX60 protein might represent the most primitive antiviral helicase, which has since diverged into several distinct but similar proteins, such as Dicer and RLRs.

ACKNOWLEDGMENTS

This work was supported in part by grants-in-aid from the Ministry of Education, Science and Culture of Japan, the Ministry of Health, Labor, and Welfare of Japan, Mitsubushi Foundation, and Akiyama Foundation.

We thank K. Matsumoto, H. Saito (National Research Institute for Child Health and Development), and H. Takaki for microarray data.

REFERENCES

1. **Ablasser, A., et al.** 2009. RIG-I-dependent sensing of poly(dA:dT) through the induction of an RNA polymerase III-transcribed RNA intermediate. Nat. Immunol. **10:**1065–1072.
2. **Akazawa, T., et al.** 2007. Antitumor NK activation induced by the Toll-like receptor 3-TICAM-1 (TRIF) pathway in myeloid dendritic cells. Proc. Natl. Acad. Sci. U. S. A. **104:**252–257.
3. **Barral, P. M., et al.** 2007. MDA-5 is cleaved in poliovirus-infected cells. J. Virol. **81:**3677–3684.
4. **Brouwer, R., et al.** 2001. Three novel components of the human exosome. J. Biol. Chem. **276:**6177–6184.
5. **Chen, G., X. Guo, F. Lv, Y. Xu, and G. Gao.** 2008. p72 DEAD box RNA helicase is required for optimal function of the zinc-finger antiviral protein. Proc. Natl. Acad. Sci. U. S. A. **105:**4352–4357.
6. **Chiu, Y. H., J. B. Macmillan, and Z. J. Chen.** 2009. RNA polymerase III detects cytosolic DNA and induces type I interferons through the RIG-I pathway. Cell **138:**576–591.
7. **Choi, M. K., et al.** 2009. A selective contribution of the RIG-I-like receptor pathway to type I interferon responses activated by cytosolic DNA. Proc. Natl. Acad. Sci. U. S. A. **106:**17870–17875.
8. **Cui, S., et al.** 2008. The C-terminal regulatory domain is the RNA 5′-triphosphate sensor of RIG-I. Mol. Cell **29:**169–179.
9. **Dangel, A. W., L. Shen, A. R. Mendoza, L. C. Wu, and C. Y. Yu.** 1995. Human helicase gene SKI2W in the HLA class III region exhibits striking structural similarities to the yeast antiviral gene SKI2 and to the human gene KIAA0052: emergence of a new gene family. Nucleic Acids Res. **23:**2120–2126.
10. **Ebihara, T., et al.** 2010. Identification of a polyI:C-inducible membrane protein that participates in dendritic cell-mediated natural killer cell activation. J. Exp. Med. **207:**2675–2687.
11. **Gack, M. U., et al.** 2007. TRIM25 RING-finger E3 ubiquitin ligase is essential for RIG-I-mediated antiviral activity. Nature **446:**916–920.
12. **Galiana-Arnoux, D., C. Dostert, A. Schneemann, J. A. Hoffmann, and J. L. Imler.** 2006. Essential function in vivo for Dicer-2 in host defense against RNA viruses in drosophila. Nat. Immunol. **7:**590–597.
13. **Gao, D., et al.** 2009. REUL is a novel E3 ubiquitin ligase and stimulator of retinoic-acid-inducible gene-I. PLoS One **4:**e5760.
14. **Guo, X., J. Ma, J. Sun, and G. Gao.** 2007. The zinc-finger antiviral protein recruits the RNA processing exosome to degrade the target mRNA. Proc. Natl. Acad. Sci. U. S. A. **104:**151–156.
15. **Hayakawa, S., et al.** 2011. ZAPS is a potent stimulator of signaling mediated by the RNA helicase RIG-I during antiviral responses. Nat. Immunol. **12:**37–44.
16. **Hornung, V., et al.** 2006. 5′-Triphosphate RNA is the ligand for RIG-I. Science **314:**994–997.
17. **Houseley, J., J. LaCava, and D. Tollervey.** 2006. RNA-quality control by the exosome. Nat. Rev. Mol. Cell Biol. **7:**529–539.
18. **Houseley, J., and D. Tollervey.** 2009. The many pathways of RNA degradation. Cell **136:**763–776.
19. **Kato, H., et al.** 2005. Cell type-specific involvement of RIG-I in antiviral response. Immunity **23:**19–28.
20. **Kato, H., et al.** 2008. Length-dependent recognition of double-stranded ribonucleic acids by retinoic acid-inducible gene-I and melanoma differentiation-associated gene 5. J. Exp. Med. **205:**1601–1610.
21. **Kato, H., et al.** 2006. Differential roles of MDA5 and RIG-I helicases in the recognition of RNA viruses. Nature **441:**101–105.
22. **Kawai, T., et al.** 2005. IPS-1, an adaptor triggering RIG-I- and Mda5-mediated type I interferon induction. Nat. Immunol. **6:**981–988.
23. **Kumar, H., et al.** 2006. Essential role of IPS-1 in innate immune responses against RNA viruses. J. Exp. Med. **203:**1795–1803.
24. **Li, X., et al.** 2009. The RIG-I-like receptor LGP2 recognizes the termini of double-stranded RNA. J. Biol. Chem. **284:**13881–13891.
25. **Melchjorsen, J., et al.** 2010. Early innate recognition of herpes simplex virus in human primary macrophages is mediated via the MDA5/MAVS-dependent and MDA5/MAVS/RNA polymerase III-independent pathways. J. Virol. **84:**11350–11358.
26. **Meylan, E., et al.** 2005. Cardif is an adaptor protein in the RIG-I antiviral pathway and is targeted by hepatitis C virus. Nature **437:**1167–1172.
27. **Miyake, T., et al.** 2009. Poly I:C-induced activation of NK cells by CD8 alpha+ dendritic cells via the IPS-1 and TRIF-dependent pathways. J. Immunol. **183:**2522–2528.
28. **Oshiumi, H., et al.** 2010. Hepatitis C virus core protein abrogates the DDX3 function that enhances IPS-1-mediated IFN-beta induction. PLoS One **5:**e14258.
29. **Oshiumi, H., M. Matsumoto, K. Funami, T. Akazawa, and T. Seya.** 2003. TICAM-1, an adaptor molecule that participates in Toll-like receptor 3-mediated interferon-beta induction. Nat. Immunol. **4:**161–167.
30. **Oshiumi, H., M. Matsumoto, S. Hatakeyama, and T. Seya.** 2009. Riplet/RNF135, a RING finger protein, ubiquitinates RIG-I to promote interferon-beta induction during the early phase of viral infection. J. Biol. Chem. **284:**807–817.

31. **Oshiumi, H., et al.** 2010. The ubiquitin ligase Riplet is essential for RIG-I-dependent innate immune responses to RNA virus infection. Cell Host Microbe **8:**496–509.
32. **Oshiumi, H., K. Sakai, M. Matsumoto, and T. Seya.** 1 February 2010, posting date. DEAD/H BOX 3 (DDX3) helicase binds the RIG-I adaptor IPS-1 to up-regulate IFN-beta inducing potential. Eur. J. Immunol. doi:10.1002/eji.200940203.
33. **Pippig, D. A., et al.** 2009. The regulatory domain of the RIG-I family ATPase LGP2 senses double-stranded RNA. Nucleic Acids Res. **37:**2014–2025.
34. **Rasmussen, S. B., et al.** 2009. Herpes simplex virus infection is sensed by both Toll-like receptors and retinoic acid-inducible gene-like receptors, which synergize to induce type I interferon production. J. Gen. Virol. **90:**74–78.
35. **Rehwinkel, J., et al.** 2010. RIG-I detects viral genomic RNA during negative-strand RNA virus infection. Cell **140:**397–408.
36. **Saito, T., et al.** 2007. Regulation of innate antiviral defenses through a shared repressor domain in RIG-I and LGP2. Proc. Natl. Acad. Sci. U. S. A. **104:**582–587.
37. **Saito, T., D. M. Owen, F. Jiang, J. Marcotrigiano, and M. Gale, Jr.** 2008. Innate immunity induced by composition-dependent RIG-I recognition of hepatitis C virus RNA. Nature **454:**523–527.
38. **Satoh, T., et al.** 26 January 2010, posting date. LGP2 is a positive regulator of RIG-I- and MDA5-mediated antiviral responses. Proc. Natl. Acad. Sci. U. S. A. doi:10.1073/pnas.0912986107.
39. **Schlee, M., et al.** 2009. Recognition of 5′ triphosphate by RIG-I helicase requires short blunt double-stranded RNA as contained in panhandle of negative-strand virus. Immunity **31:**25–34.
40. **Schmidt, A., et al.** 2009. 5′-Triphosphate RNA requires base-paired structures to activate antiviral signaling via RIG-I. Proc. Natl. Acad. Sci. U. S. A. **106:**12067–12072.
41. **Schröder, M., M. Baran, and A. G. Bowie.** 2008. Viral targeting of DEAD box protein 3 reveals its role in TBK1/IKKepsilon-mediated IRF activation. EMBO J. **27:**2147–2157.
42. **Seth, R. B., L. Sun, C. K. Ea, and Z. J. Chen.** 2005. Identification and characterization of MAVS, a mitochondrial antiviral signaling protein that activates NF-kappaB and IRF 3. Cell **122:**669–682.
43. **Soulat, D., et al.** 2008. The DEAD-box helicase DDX3X is a critical component of the TANK-binding kinase 1-dependent innate immune response. EMBO J. **27:**2135–2146.
44. **Sun, Q., et al.** 2006. The specific and essential role of MAVS in antiviral innate immune responses. Immunity **24:**633–642.
45. **Takahasi, K., et al.** 2009. Solution structures of cytosolic RNA sensor MDA5 and LGP2 C-terminal domains: identification of the RNA recognition loop in RIG-I-like receptors. J. Biol. Chem. **284:**17465–17474.
46. **Takahasi, K., et al.** 2008. Nonself RNA-sensing mechanism of RIG-I helicase and activation of antiviral immune responses. Mol. Cell **29:**428–440.
47. **van Dijk, E. L., G. Schilders, and G. J. Pruijn.** 2007. Human cell growth requires a functional cytoplasmic exosome, which is involved in various mRNA decay pathways. RNA **13:**1027–1035.
48. **van Rij, R. P., et al.** 2006. The RNA silencing endonuclease Argonaute 2 mediates specific antiviral immunity in Drosophila melanogaster. Genes Dev. **20:**2985–2995.
49. **Venkataraman, T., et al.** 2007. Loss of DExD/H box RNA helicase LGP2 manifests disparate antiviral responses. J. Immunol. **178:**6444–6455.
50. **Walker, J. E., M. Saraste, M. J. Runswick, and N. J. Gay.** 1982. Distantly related sequences in the alpha- and beta-subunits of ATP synthase, myosin, kinases and other ATP-requiring enzymes and a common nucleotide binding fold. EMBO J. **1:**945–951.
51. **Wang, X. H., et al.** 2006. RNA interference directs innate immunity against viruses in adult Drosophila. Science **312:**452–454.
52. **Weber, F., V. Wagner, S. B. Rasmussen, R. Hartmann, and S. R. Paludan.** 2006. Double-stranded RNA is produced by positive-strand RNA viruses and DNA viruses but not in detectable amounts by negative-strand RNA viruses. J. Virol. **80:**5059–5064.
53. **Wickner, R. B.** 1996. Double-stranded RNA viruses of Saccharomyces cerevisiae. Microbiol. Rev. **60:**250–265.
54. **Widner, W. R., and R. B. Wickner.** 1993. Evidence that the SKI antiviral system of Saccharomyces cerevisiae acts by blocking expression of viral mRNA. Mol. Cell. Biol. **13:**4331–4341.
55. **Xu, L. G., et al.** 2005. VISA is an adapter protein required for virus-triggered IFN-beta signaling. Mol. Cell **19:**727–740.
56. **Yanai, H., et al.** 2009. HMGB proteins function as universal sentinels for nucleic-acid-mediated innate immune responses. Nature **462:**99–103.
57. **Yoneyama, M., and T. Fujita.** 2007. RIG-I family RNA helicases: cytoplasmic sensor for antiviral innate immunity. Cytokine Growth Factor Rev. **18:**545–551.
58. **Yoneyama, M., et al.** 2005. Shared and unique functions of the DExD/H-box helicases RIG-I, MDA5, and LGP2 in antiviral innate immunity. J. Immunol. **175:**2851–2858.
59. **Yoneyama, M., et al.** 2004. The RNA helicase RIG-I has an essential function in double-stranded RNA-induced innate antiviral responses. Nat. Immunol. **5:**730–737.

J. Biochem. 2012;151(1):5–11 doi:10.1093/jb/mvr111

JB THE JOURNAL OF BIOCHEMISTRY

JB Review

Ubiquitin-mediated modulation of the cytoplasmic viral RNA sensor RIG-I

Received July 11, 2011; accepted August 17, 2011; published online September 2, 2011

Hiroyuki Oshiumi*, Misako Matsumoto and Tsukasa Seya

Department of Microbiology and Immunology, Graduate School of Medicine, Hokkaido University, Kita-15, Nishi-7, Kita-ku Sapporo 060-8638, Japan

*To whom correspondence should be addressed.
Tel: +81-11-706-5056, Fax: +81-11-706-7866,
E-mail: oshiumi@med.hokudai.ac.jp

RIG-I-like receptors, including RIG-I, MDA5 and LGP2, recognize cytoplasmic viral RNA. The RIG-I protein consists of N-terminal CARDs, central RNA helicase and C-terminal domains. RIG-I activation is regulated by ubiquitination. Three ubiquitin ligases target the RIG-I protein. TRIM25 and Riplet ubiquitin ligases are positive regulators of RIG-I and deliver the K63-linked polyubiquitin moiety to RIG-I CARDs and the C-terminal domain. RNF125, another ubiquitin ligase, is a negative regulator of RIG-I and mediates K48-linked polyubiquitination of RIG-I, leading to the degradation of the RIG-I protein by proteasomes. The K63-linked polyubiquitin chains of RIG-I are removed by a deubiquitin enzyme, CYLD. Thus, CYLD is a negative regulator of RIG-I. Furthermore, TRIM25 itself is regulated by ubiquitination. HOIP and HOIL proteins are ubiquitin ligases and are also known as linear ubiquitin assembly complexes (LUBACs). The TRIM25 protein is ubiquitinated by LUBAC and then degraded by proteasomes. The splice variant of RIG-I encodes a protein that lacks the first CARD of RIG-I, and the variant RIG-I protein is not ubiquitinated by TRIM25. Therefore, ubiquitin is the key regulator of the cytoplasmic viral RNA sensor RIG-I.

Keywords: RIG-I/type I interferon/ubiquitin/virus.

Abbreviations: CARD, caspase activation and recruitment domain; CTD, C-terminal domain; dsRNA, double-stranded RNA; RLR, RIG-I-like receptor; pDC, plasmacytoid dendritic cell; cDC, conventional dendritic cell; MEF, mouse embryonic fibroblast cell; BM, bone-marrow; Mf, macrophage; IFN, interferon; ISG, interferon-stimulated gene; TRIM, tripartite motif; RNF, RING finger.

Recognition of viral RNA

Type I interferons (IFNs) are inflammatory cytokines that possess strong anti-viral activity. During viral infection, type I IFNs are produced from dendritic cells (DC), macrophages (Mf) and fibroblast cells (Fig. 1A). Viral RNA is mainly recognized by Toll-like receptors (TLRs) and RIG-I-like receptors (RLRs). TLRs are type I transmembrane proteins. TLR3, 7 and 8, which are members of the TLR family, are localized to endosomes, and are responsible for the recognition of viral RNA (*1*). RLRs are DExD/H box RNA helicases and recognize viral RNA in the cytoplasmic region (Fig. 1B). There are three members of the RLR family: RIG-I, MDA5 and LGP2. RIG-I has the ability to recognize various types of viruses, and MDA5 mainly recognizes picornaviruses (*2*). LGP2 promotes RIG-I and MDA5-mediated signalling (*3*).

A cytoplasmic sensor for the detection of viral RNA

RIG-I, a cytoplasmic sensor for viral RNA, is induced by viral infection, polyIC and type I IFN stimulation (*4*). This protein is composed of two N-terminal caspase recruitment domains (CARDs), a central DExD/H box helicase/ATPase domain and a C-terminal regulatory domain (CTD) (Fig. 2). N-terminal CARDs are responsible for the binding to the adaptor molecule IPS-1/MAVS/VISA/Cardif, which is located on the outer membrane of the mitochondria (*5–8*). In the absence of viral RNA, RIG-I CTD represses the interaction between RIG-I CARDs and IPS-1 CARD (*9*). RIG-I CTD recognizes the 5′ triphosphate of short double-stranded RNA, leading to multimerization of RIG-I and IPS-1 (*10–13*). IPS-1 triggers signaling to induce type I IFN and other inflammatory cytokines through STING (also called MITA) protein, which is localized to the endoplasmic reticulum or the mitochondria (*14–17*). STING then activates transcription factors, such as IRF-3, IRF-7 and NF-κB (*15, 18*).

Knockout of RIG-I abrogates the production of type I IFNs and inflammatory cytokines from mouse embryonic fibroblasts (MEFs), conventional DC and Mfs in response to viral infections, including infections caused by vesicular stomatitis virus (VSV), Sendai virus (SeV), influenza A virus, Newcastle disease virus, hepatitis C virus and Japanese encephalitis virus (*2, 19*). However, RIG-I is not necessary for the production of type I IFNs by plasmacytoid dendritic cells (pDCs), which are strong inducers of type I IFNs *in vivo* (*19*). In pDCs, TLR7 is responsible for the detection of viral RNA (*20*). In addition, knockout of IPS-1 and STING inhibits the production of type I IFNs from MEFs, Mfs and cDCs, but not from pDCs (*15–18*). Once type I IFNs are produced from these cells, IFN production is secondly amplified via the IFNAR (*21*). The deficiency of the RIG-I-dependent pathway causes a reduction in early type I IFN production *in vivo* but shows only a marginal effect on late type I IFN production (*15–18*). Knockout of RIG-I increases the

Featured Article

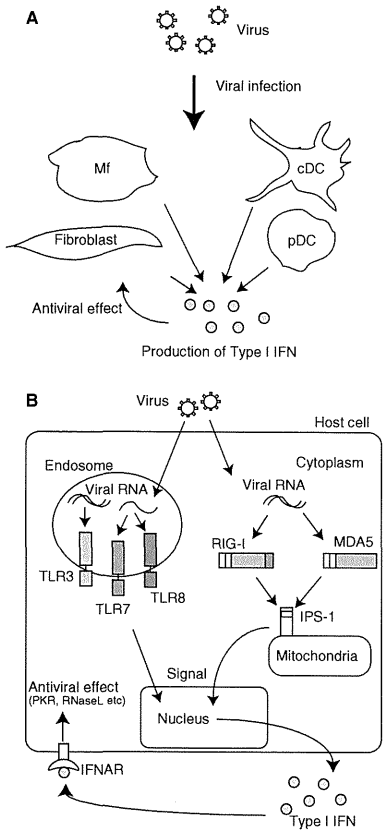

Fig. 1 Production of type I IFN in response to viral infection. (A) Type I IFN is a cytokine that possesses strong anti-viral activity. Type I IFN is produced from fibroblast cells, cDC, pDC and Mf in response to viral infection. (B) TLR3, 7 and 8 are localized to endosomes and are responsible for the recognition of viral RNA. Viral RNA in the cytoplasmic region is recognized by RIG-I and MDA5, leading to the activation of the adaptor molecule IPS-1. IPS-1 triggers the signal to induce type I IFNs. Type I IFNs binds to an IFN receptor, IFNAR, leading to the activation of anti-viral factors, such as PKR and RNaseL.

mortality due to viral infections (*2*, *19*). Thus, RIG-I-dependent pathways are necessary for efficient early type I IFN production and are required for protection against viral infections (*18*).

TRIM25 ubiquitin ligase is a positive factor for the RIG-I activation

During viral infection, the RIG-I protein has a modified form of ubiquitin. TRIM25 (also called Efp) is a ubiquitin ligase (*22*, *23*), and its domain structure is described in Fig. 2. This protein interacts with the first CARD of RIG-I (*22*, *24*). T55I mutation of the first CARD of RIG-I is found in RIG-I-deficient HuH7.5 cells. T55 of RIG-I is critical for the interaction between TRIM25 and RIG-I (*9*, *24*, *25*). Gack et al. detected the polyubiquitination of the K99, K169, K172, K181, K190 and K193 residues of RIG-I CARDs by mass spectrometry analysis (*22*), and the K172R mutation alone causes a near-complete loss of the polyubiquitination of RIG-I CARDs (*22*). TRIM25 delivers the K63-linked polyubiquitin moiety to the K172 residue of the second CARD of RIG-I, leading to efficient interaction with IPS-1/MAVS/VISA/Cardif (*22*, *24*). On the other hand, Zeng *et al.* reported another mechanism of the activation of RIG-I by ubiquitin. They reconstituted RIG-I pathway *in vitro* and showed that RIG-I CARDs sense unanchored polyubiquitin chains mediated by TRIM25, and the binding of RIG-I CARDs to the unanchored polyubiquitin chains leads to the activation of RIG-I (*26*). Knockout of TRIM25 abrogates IFN-β production from MEF in response to viral infection (*22*). Thus, ubiquitination or polyubiquitin binding is essential for the activation of RIG-I (Fig. 2).

The expression of a splice variant of RIG-I mRNA is robustly up-regulated upon viral infection (*24*). This splice variant encodes a protein that lacks the first 36–80 amino acid region within the first CARD of RIG-I; therefore, the RIG-I splice variant (RIG-I SV) protein loses TRIM25 binding, CARD ubiquitination and downstream signalling ability (Fig. 3) (*24*). RIG-I SV inhibits the multimerization of the wild-type RIG-I protein and IPS-1 interaction and shows a dominant negative effect on the RIG-I-mediated anti-viral IFN response (*24*). Thus, RIG-I SV acts as the off switch regulator of its own signalling pathway (*24*).

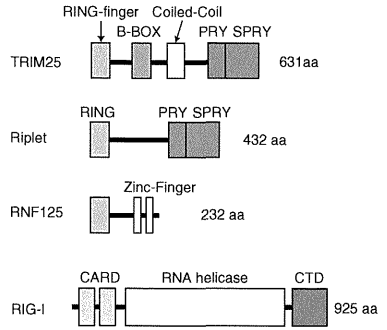

Fig. 2 Domain structures of TRIM25, Riplet, RNF125 and RIG-I. TRIM25 consists of RING finger, B-box, coiled-coil, PRY and SPRY domains. Riplet is similar to TRIM25 and consists of RING-finger, PRY and SPRY domains. RNF125 consists of RING-finger and two zinc-finger domains. Three proteins mediate the polyubiquitination of RIG-I. RIG-I consists of two N-terminal CARDs, central RNA helicase and CTDs.

In addition to the IPS-1 adaptor molecule, RIG-I also binds to the inflammasome adaptor apoptosis-associated speck-like protein containing a CARD domain (ASC), also known as Pycard, in response to viral infection (*27*). ASC activates caspase-1, leading to the proteolytic processing of pro-IL-1β into mature, bioactive IL-1β (*28*). TRIM25 activity is dispensable for caspase-1 activation through ASC (*27*). Thus, RIG-I polyubiquitination by TRIM25 is dispensable for ASC inflammasome adaptor activation (*27*).

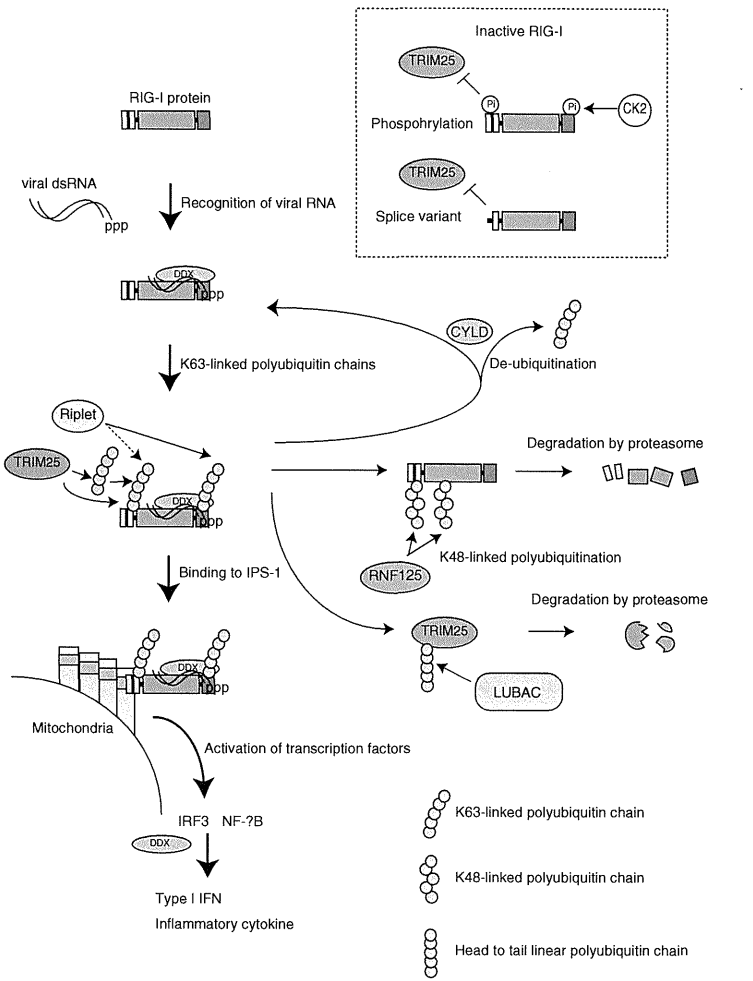

Fig. 3 Regulation of RIG-I by the ubiquitin chain. RIG-I binds to viral RNA together with other cofactors, such as DDX3. After the recognition of viral RNA, RIG-I changes its conformation and harbours K63-linked polyubiquitination by TRIM25 and Riplet. Polyubiquitination causes the activation of IPS-1, leading to the production of type I IFN. CYLD, a deubiquitin enzyme, removes the polyubiquitin chain of RIG-I. CK2 and other unknown kinase phosphorylate RIG-I, and the phosphorylated RIG-I protein is not polyubiquitinated by TRIM25. In addition, splice variant RIG-I (SV RIG-I) is not polyubiquitinated by TRIM25, and the SV RIG-I protein acts as a dominant negative form. RNF125 mediates the K48-linked polyubiquitinatioin of RIG-I, which causes the degradation of RIG-I by proteasomes. The LUBAC protein complex suppresses TRIM25 function by mediating the head-to-tail polyubiquitination of TRIM25.

Downloaded from http://jb.oxfordjournals.org/ at (D) Hokkaido U Med on March 9, 2012

However, RIG-I polyubiquitination is essential for NF-κB activation by RIG-I, which is required for IL-1β mRNA expression; thus, knockout of TRIM25 reduces the production of mature IL-1β (*4*, *19*, *27*).

Riplet ubiquitin ligase is essential for the activation of RIG-I

Riplet (also called Reul or RNF135) was isolated by yeast two-hybrid screening to isolate RIG-I CTD binding proteins (*29*). The Riplet protein is composed of N-terminal RING finger, C-terminal SPRY and PRY domains, and is similar to TRIM25 (Fig. 2). However, this protein lacks B-box, which is a typical feature of TRIM family proteins. Thus, the protein does not belong to the TRIM family. Riplet expression is observed in various tissues and cells such as DC, Mfs and MEF (*29*, *30*). Hu *et al.* (*31*) detected endogenous Riplet protein in human DC lysates. Riplet expression is induced in mouse bone marrow-derived DCs (BM-DCs) by polyIC stimulation, which is a double-stranded RNA analog; however, its expression is not changed in human fibroblast and HeLa cells (*29*).

The Riplet protein physically interacts with RIG-I CTD, and in some experimental conditions, it binds to RIG-I CARDs (*29*, *32*). The Riplet C-terminal region is responsible for this binding. Riplet mediates K63-linked polyubiquitination of RIG-I CTD, leading to the activation of RIG-I (Fig. 3) (*29*). The five CTD lysine residues at 849, 851, 888, 907 and 909 are important for the polyubiquitination and activation of RIG-I (*29*, *30*). In contrast, Gao *et al.* (*32*) reported that Riplet mediates K63-linked polyubiquitination of K154, K164 and K172 of RIG-I CARDs in their experimental conditions (Fig. 3).

In some strain backgrounds, RIG-I-deficient mice are embryonic lethal, but Riplet knockout mice are born at expected Mendelian ratios from Riplet$^{+/-}$ mice (*19*, *30*, *33*). Moreover, the development of DCs and Mfs is also normal in Riplet-deficient mice (*30*). Douglas *et al.* (*30*, *34*) reported that Riplet/RNF135 haploinsufficiency causes an overgrowth syndrome and learning disabilities in human: however, knockout of the Riplet gene in mice does not cause any apparent defects with regard to development. Knockout of Riplet severely reduces the production of type I IFN and abrogates the activation of RIG-I and RIG-I CTD polyubiquitination (*30*). Riplet knockout mice are more susceptible to VSV infection than wild-type mice. As IPS-1 and STING, Riplet is necessary for efficient, early type I IFN production *in vivo*, but it is dispensable for late type I IFN productions (*30*). This indicates the essential role that Riplet plays in the RIG-I-dependent innate immune response against RNA virus infection. Genetic evidence shows that knockout of either Riplet or TRIM25 destroyed the RIG-I-dependent innate immune response; therefore, both ubiquitin ligases are required for the activation of RIG-I in response to RNA virus infection (*22*, *30*). RLR pathways contribute to type I IFN expression in response to cytoplasmic DNA (*35–37*). However, Riplet-independent type I IFN expression pathway in response to cytoplasmic DNA exists in MEF (*30*).

Ubiquitin ligases target several proteins. For example, TRIM25 targets the proteolysis of 14-3-3 σ, a negative cell cycle regulator that causes G2 arrest, and thus, promotes breast tumour growth (*23*). Proteome analysis reveals that Riplet binds to the TRK-fused gene (TFG), which is a target of chromosome translocation in lymphoma (*38–40*). Pasmant *et al.* (*41*) reported that the Riplet/RNF135 gene is down-regulated in tumour Schwann cells from malignant peripheral nerve sheath tumours, and their study suggested the involvement of Riplet/RNF135 in an increased risk of malignancy observed in NF1 microdeletion patients. Thus, it is possible that Riplet targets not only RIG-I but also other proteins.

Negative regulators of RIG-I

The RNF125 (also called TRAC1) protein possesses a RING finger domain and functions as a ubiquitin ligase (*42*). Arimoto *et al.* (*43*) isolated RNF125 by yeast two-hybrid screening to obtain the protein that binds to UbcH8, which is an E2 ubiquitin-conjugating enzyme, and found that RNF125 also binds to RIG-I. Unlike Riplet and TRIM25, RNF125 ubiquitin ligase mediates K48-, but not K63-linked polyubiquitination of RIG-I, leading to the degradation of RIG-I by proteasomes (Fig. 3) (*43*). UbcH5c is possibly an E2 enzyme, which cooperates with RNF125, and UbcH8 acts as a negative factor in the RNF125-mediated polyubiquitination of RIG-I (*43*, *44*). Furthermore, RNF125 ubiquitinates MDA5, a member of RLRs, and the expression of RNF125 impairs MDA5-mediated signalling (*43*). RNF125 expression is induced by type I IFN and polyIC treatment. The increase in RNF125 mRNA expression correlates temporally with the decrease in RIG-I expression (*43*). Knockdown of RNF125 increases the type I IFN expression in response to viral infection (*43*). Since RNF125 is enhanced by type I IFN, the function of RNF125 constitutes a negative regulatory loop circuit for type I IFN production.

CYLD is a deubiquitinase that cleaves the K63-linked polyubiquitin chain. This protein acts as a negative regulator of NF-κB and Jun N-terminal kinase signalling pathways by cleaving the K63-linked polyubiquitin chains of NEMO, TRAF2 and BCL3 (*45–48*). Friedman *et al.* (*49*) performed a microarray analysis and found that the expression profile of RIG-I is correlated with that of CYLD. Moreover, they found that the CYLD protein physically interacts with RIG-I, TBK1 and IKKε, and deubiquitinates these proteins. CYLD inhibits SeV-induced type I IFN production. Thus, it is expected that CYLD attenuates the establishment of an anti-viral state (Fig. 3).

There are host and viral negative regulators for TRIM25. HOIL-1L and HOIP are members of the RING-IBR-RING (RBR) E3 ubiquitin ligase family and form complexes (*50*). HOIL-1L and HOIP form ubiquitin polymers through the linkage between the C- and N-termini of the ubiquitin molecules in order to assemble a head-to-tail linear polyubiquitin chain; thus, the protein complex is designated as LUBAC (linear ubiquitin assembly complex) (*50*). LUBAC has the ability to induce polyubiquitination of TRIM25; it specifically suppresses TRIM25-mediated RIG-I ubiquitination by inducing TRIM25 degradation and inhibiting TRIM25 interaction with RIG-I (Fig. 3) (*51*). Excessive production of IFNs or inflammatory cytokines is destructive rather than protective; thus, an absolute regulation of the immune signalling pathway is essential for a successful immune response against viral infections. HOIL-1L- and HOIP-mediated suppression of TRIM25 would be important for the absolute regulation of an immune response (*51*).

Viruses have evolved sophisticated mechanisms to evade the host IFN system. There are several virus-encoded IFN antagonists that inhibit host innate anti-viral responses. NS1 of the influenza A virus is one of the IFN antagonists (*52*, *53*). It sequestrates viral dsRNA from cellular sensors including RIG-I (*52*). In addition, it interacts with the coiled-coil region of TRIM25 and blocks TRIM25 multimerization and RIG-I CARD polyubiquitination (*54*).

Perspectives

Several ubiquitin-like proteins (UBLs) exist. ISG15 is a UBL and is induced in response to viral infection (*55*). Several anti-viral proteins are modified by ISG15, including RIG-I (*44*, *55*). UbcH8 is an E2 enzyme that promotes ISG15 conjugation to RIG-I (*44*). However, ISG15 knockout mice do not either reduce immunological functions or decrease anti-viral activity (*56*). Thus, the physiological role of ISG15 conjugation to RIG-I remains unknown.

In addition, the RIG-I protein is modified by phosphorylation. The T170 residue of RIG-I is phosphorylated under normal conditions, and phosphorylation is reduced after SeV infection (*24*). Phosphorylation of RIG-I CARDs inhibits the TRIM25-mediated polyubiquitination (Fig. 3). Thus, Gack *et al.* suggested that dephosphorylation of RIG-I permits the TRIM25 binding and TRIM25-mediated polyubiquitination of RIG-I, allowing RIG-I to form a stable complex with IPS-1 in order to trigger an IFN-mediated anti-viral innate immune response. However, the kinase and phosphatase that target RIG-I N-terminal CARDs are still unknown. In addition to RIG-I CARDs, RIG-I CTD is regulated by phosphorylation. In resting cells, casein kinase II (CK2) phosphorylates T770, and S854 and S855 (*57*). The phosphorylation of RIG-I CTD suppresses the RIG-I-mediated signalling (Fig. 3) (*57*). Following viral infection, phosphatases cause dephosphorylation of the RIG-I CTD, leading to the activation of RIG-I-mediated signalling (*57*).

RIG-I requires several cofactors. High mobility group box proteins are required for the RIG-I to recognize viral RNA (*58*). DDX3 and DDX60 are non-RLR helicases that are involved in RLR signallings, and play pivotal roles in RIG-I-mediated signalling (Fig. 3) (*59–62*). It remains to be determined whether the post-translational modification of RIG-I affects the interaction with those co-factors.

Riplet ubiquitinates RIG-I CTD. The molecular mechanism of how the Riplet-dependent polyubiquitination of RIG-I CTD triggers the downstream signalling remains to be determined yet. RIG-I CTD has two functions. In the absence of viral RNA, RIG-I CTD suppresses the activation of RIG-I CARDs. Following viral infection, RIG-I CTD binds to viral RNA, leading to the conformational changes and ultimately removal of the suppression. It is possible that CTD polyubiquitination affects both functions of RIG-I CTD.

Funding
Grants-in-Aid from the Ministry of Education, Science, and Culture and the Ministry of Health, Labor and Welfare of Japan.

Conflict of Interest
None declared.

References

1. Takeuchi, O. and Akira, S. (2010) Pattern recognition receptors and inflammation. *Cell* **140**, 805–820
2. Kato, H., Takeuchi, O., Sato, S., Yoneyama, M., Yamamoto, M., Matsui, K., Uematsu, S., Jung, A., Kawai, T., Ishii, K.J., Yamaguchi, O., Otsu, K., Tsujimura, T., Koh, C. S., Reis e Sousa, C., Matsuura, Y., Fujita, T., and Akira, S. (2006) Differential roles of MDA5 and RIG-I helicases in the recognition of RNA viruses. *Nature* **441**, 101–105
3. Satoh, T., Kato, H., Kumagai, Y., Yoneyama, M., Sato, S., Matsushita, K., Tsujimura, T., Fujita, T., Akira, S., and Takeuchi, O. (2010) LGP2 is a positive regulator of RIG-I- and MDA5-mediated antiviral responses. *Proc. Natl Acad. Sci. USA* **107**, 1512–1517
4. Yoneyama, M., Kikuchi, M., Natsukawa, T., Shinobu, N., Imaizumi, T., Miyagishi, M., Taira, K., Akira, S., and Fujita, T. (2004) The RNA helicase RIG-I has an essential function in double-stranded RNA-induced innate antiviral responses. *Nat. Immunol.* **5**, 730–737
5. Xu, L.G., Wang, Y.Y., Han, K.J., Li, L.Y., Zhai, Z., and Shu, H.B. (2005) VISA is an adapter protein required for virus-triggered IFN-beta signaling. *Mol Cell* **19**, 727–740
6. Seth, R.B., Sun, L., Ea, C.K., and Chen, Z.J. (2005) Identification and characterization of MAVS, a mitochondrial antiviral signaling protein that activates NF-kappaB and IRF 3. *Cell* **122**, 669–682
7. Meylan, E., Curran, J., Hofmann, K., Moradpour, D., Binder, M., Bartenschlager, R., and Tschopp, J. (2005) Cardif is an adaptor protein in the RIG-I antiviral pathway and is targeted by hepatitis C virus. *Nature* **437**, 1167–1172
8. Kawai, T., Takahashi, K., Sato, S., Coban, C., Kumar, H., Kato, H., Ishii, K.J., Takeuchi, O., and Akira, S. (2005) IPS-1, an adaptor triggering RIG-I- and Mda5-mediated type I interferon induction. *Nat. Immunol.* **6**, 981–988
9. Saito, T., Hirai, R., Loo, Y.M., Owen, D., Johnson, C.L., Sinha, S.C., Akira, S., Fujita, T., and Gale, M. Jr (2007) Regulation of innate antiviral defenses through a shared repressor domain in RIG-I and LGP2. *Proc. Natl. Acad. Sci. USA* **104**, 582–587
10. Schmidt, A., Schwerd, T., Hamm, W., Hellmuth, J.C., Cui, S., Wenzel, M., Hoffmann, F.S., Michallet, M.C., Besch, R., Hopfner, K.P., Endres, S., and Rothenfusser,

S. (2009) 5′-triphosphate RNA requires base-paired structures to activate antiviral signaling via RIG-I. *Proc. Natl. Acad. Sci. USA* **106**, 12067–12072
11. Myong, S., Cui, S., Cornish, P.V., Kirchhofer, A., Gack, M.U., Jung, J.U., Hopfner, K.P., and Ha, T. (2009) Cytosolic viral sensor RIG-I is a 5′-triphosphate-dependent translocase on double-stranded RNA. *Science* **323**, 1070–1074
12. Pichlmair, A., Schulz, O., Tan, C.P., Naslund, T.I., Liljestrom, P., Weber, F., and Reis e Sousa, C. (2006) RIG-I-mediated antiviral responses to single-stranded RNA bearing 5′-phosphates. *Science* **314**, 997–1001
13. Hornung, V., Ellegast, J., Kim, S., Brzozka, K., Jung, A., Kato, H., Poeck, H., Akira, S., Conzelmann, K.K., Schlee, M., Endres, S., and Hartmann, G. (2006) 5′-Triphosphate RNA is the ligand for RIG-I. *Science* **314**, 994–997
14. Zhong, B., Yang, Y., Li, S., Wang, Y.Y., Li, Y., Diao, F., Lei, C., He, X., Zhang, L., Tien, P., and Shu, H.B. (2008) The adaptor protein MITA links virus-sensing receptors to IRF3 transcription factor activation. *Immunity* **29**, 538–550
15. Ishikawa, H. and Barber, G.N. (2008) STING is an endoplasmic reticulum adaptor that facilitates innate immune signalling. *Nature* **455**, 674–678
16. Sun, Q., Sun, L., Liu, H.H., Chen, X., Seth, R.B., Forman, J., and Chen, Z.J. (2006) The specific and essential role of MAVS in antiviral innate immune responses. *Immunity* **24**, 633–642
17. Kumar, H., Kawai, T., Kato, H., Sato, S., Takahashi, K., Coban, C., Yamamoto, M., Uematsu, S., Ishii, K.J., Takeuchi, O., and Akira, S. (2006) Essential role of IPS-1 in innate immune responses against RNA viruses. *J. Exp. Med.* **203**, 1795–1803
18. Ishikawa, H., Ma, Z., and Barber, G.N. (2009) STING regulates intracellular DNA-mediated, type I interferon-dependent innate immunity. *Nature* **461**, 788–792
19. Kato, H., Sato, S., Yoneyama, M., Yamamoto, M., Uematsu, S., Matsui, K., Tsujimura, T., Takeda, K., Fujita, T., Takeuchi, O., and Akira, S. (2005) Cell type-specific involvement of RIG-I in antiviral response. *Immunity* **23**, 19–28
20. Diebold, S.S., Kaisho, T., Hemmi, H., Akira, S., and Reis e Sousa, C. (2004) Innate antiviral responses by means of TLR7-mediated recognition of single-stranded RNA. *Science* **303**, 1529–1531
21. Honda, K., Takaoka, A., and Taniguchi, T. (2006) Type I interferon [corrected] gene induction by the interferon regulatory factor family of transcription factors. *Immunity* **25**, 349–360
22. Gack, M.U., Shin, Y.C., Joo, C.H., Urano, T., Liang, C., Sun, L., Takeuchi, O., Akira, S., Chen, Z., Inoue, S., and Jung, J.U. (2007) TRIM25 RING-finger E3 ubiquitin ligase is essential for RIG-I-mediated antiviral activity. *Nature* **446**, 916–920
23. Urano, T., Saito, T., Tsukui, T., Fujita, M., Hosoi, T., Muramatsu, M., Ouchi, Y., and Inoue, S. (2002) Efp targets 14-3-3 sigma for proteolysis and promotes breast tumour growth. *Nature* **417**, 871–875
24. Gack, M.U., Kirchhofer, A., Shin, Y.C., Inn, K.S., Liang, C., Cui, S., Myong, S., Ha, T., Hopfner, K.P., and Jung, J.U. (2008) Roles of RIG-I N-terminal tandem CARD and splice variant in TRIM25-mediated antiviral signal transduction. *Proc. Natl. Acad. Sci. USA* **105**, 16743–16748
25. Sumpter, R. Jr, Loo, Y.M., Foy, E., Li, K., Yoneyama, M., Fujita, T., Lemon, S.M., and Gale, M. Jr (2005) Regulating intracellular antiviral defense and permissiveness to hepatitis C virus RNA replication through a cellular RNA helicase, RIG-I. *J. Virol.* **79**, 2689–2699
26. Zeng, W., Sun, L., Jiang, X., Chen, X., Hou, F., Adhikari, A., Xu, M., and Chen, Z.J. (2010) Reconstitution of the RIG-I pathway reveals a signaling role of unanchored polyubiquitin chains in innate immunity. *Cell* **141**, 315–330
27. Poeck, H., Bscheider, M., Gross, O., Finger, K., Roth, S., Rebsamen, M., Hannesschlager, N., Schlee, M., Rothenfusser, S., Barchet, W., Kato, H., Akira, S., Inoue, S., Endres, S., Peschel, C., Hartmann, G., Hornung, V., and Ruland, J. (2010) Recognition of RNA virus by RIG-I results in activation of CARD9 and inflammasome signaling for interleukin 1 beta production. *Nat. Immunol.* **11**, 63–69
28. Yu, H.B. and Finlay, B.B. (2008) The caspase-1 inflammasome: a pilot of innate immune responses. *Cell Host Microbe* **4**, 198–208
29. Oshiumi, H., Matsumoto, M., Hatakeyama, S., and Seya, T. (2009) Riplet/RNF135, a RING finger protein, ubiquitinates RIG-I to promote interferon-beta induction during the early phase of viral infection. *J. Biol. Chem.* **284**, 807–817
30. Oshiumi, H., Miyashita, M., Inoue, N., Okabe, M., Matsumoto, M., and Seya, T. (2010) The ubiquitin ligase Riplet is essential for RIG-I-dependent innate immune responses to RNA virus infection. *Cell Host Microbe* **8**, 496–509
31. Hu, J., Nistal-Villan, E., Voho, A., Ganee, A., Kumar, M., Ding, Y., Garcia-Sastre, A., and Wetmur, J.G. (2010) A common polymorphism in the caspase recruitment domain of RIG-I modifies the innate immune response of human dendritic cells. *J. Immunol.* **185**, 424–432
32. Gao, D., Yang, Y.K., Wang, R.P., Zhou, X., Diao, F.C., Li, M.D., Zhai, Z.H., Jiang, Z.F., and Chen, D.Y. (2009) REUL is a novel E3 ubiquitin ligase and stimulator of retinoic-acid-inducible gene-I. *PLoS One* **4**, e5760
33. Wang, Y., Zhang, H.X., Sun, Y.P., Liu, Z.X., Liu, X.S., Wang, L., Lu, S.Y., Kong, H., Liu, Q.L., Li, X.H., Lu, Z.Y., Chen, S.J., Chen, Z., Bao, S.S., Dai, W., and Wang, Z.G. (2007) Rig-I-/- mice develop colitis associated with downregulation of G alpha i2. *Cell Res* **17**, 858–868
34. Douglas, J., Cilliers, D., Coleman, K., Tatton-Brown, K., Barker, K., Bernhard, B., Burn, J., Huson, S., Josifova, D., Lacombe, D., Malik, M., Mansour, S., Reid, E., Cormier-Daire, V., Cole, T., and Rahman, N. (2007) Mutations in RNF135, a gene within the NF1 microdeletion region, cause phenotypic abnormalities including overgrowth. *Nat. Genet.* **39**, 963–965
35. Choi, M.K., Wang, Z., Ban, T., Yanai, H., Lu, Y., Koshiba, R., Nakaima, Y., Hangai, S., Savitsky, D., Nakasato, M., Negishi, H., Takeuchi, O., Honda, K., Akira, S., Tamura, T., and Taniguchi, T. (2009) A selective contribution of the RIG-I-like receptor pathway to type I interferon responses activated by cytosolic DNA. *Proc. Natl. Acad. Sci. USA* **106**, 17870–17875
36. Chiu, Y.H., Macmillan, J.B., and Chen, Z.J. (2009) RNA polymerase III detects cytosolic DNA and induces type I interferons through the RIG-I pathway. *Cell* **138**, 576–591
37. Ablasser, A., Bauernfeind, F., Hartmann, G., Latz, E., Fitzgerald, K.A., and Hornung, V. (2009) RIG-I-dependent sensing of poly(dA:dT) through the induction of an RNA polymerase III-transcribed RNA intermediate. *Nat. Immunol.* **10**, 1065–1072
38. Chase, A., Ernst, T., Fiebig, A., Collins, A., Grand, F., Erben, P., Reiter, A., Schreiber, S., and Cross, N.C. (2010) TFG, a target of chromosome translocations in lymphoma and soft tissue tumors, fuses to GPR128 in healthy individuals. *Haematologica* **95**, 20–26
39. Suzuki, H., Fukunishi, Y., Kagawa, I., Saito, R., Oda, H., Endo, T., Kondo, S., Bono, H., Okazaki, Y., and Hayashizaki, Y. (2001) Protein–protein interaction panel using mouse full-length cDNAs. *Genome Res.* **11**, 1758–1765
40. Hernandez, L., Pinyol, M., Hernandez, S., Bea, S., Pulford, K., Rosenwald, A., Lamant, L., Falini, B., Ott, G., Mason, D.Y., Delsol, G., and Campo, E. (1999) TRK-fused gene (TFG) is a new partner of ALK in anaplastic large cell lymphoma producing two structurally different TFG-ALK translocations. *Blood* **94**, 3265–3268
41. Pasmant, E., Masliah-Planchon, J., Levy, P., Laurendeau, I., Ortonne, N., Parfait, B., Valeyrie-Allanore, L., Leroy, K., Wolkenstein, P., Vidaud, M., Vidaud, D., and Bieche, I. (2011) Identification of genes potentially involved in the increased risk of malignancy in NF1-microdeleted patients. *Mol. Med.* **17**, 79–87
42. Zhao, H., Li, C.C., Pardo, J., Chu, P.C., Liao, C.X., Huang, J., Dong, J.G., Zhou, X., Huang, Q., Huang, B., Bennett, M. K., Molineaux, S.M., Lu, H., Daniel-Issakani, S., Payan, D.G., and Masuda, E.S. (2005) A novel E3 ubiquitin ligase TRAC-1 positively regulates T cell activation. *J. Immunol.* **174**, 5288–5297
43. Arimoto, K., Takahashi, H., Hishiki, T., Konishi, H., Fujita, T., and Shimotohno, K. (2007) Negative regulation of the RIG-I signaling by the ubiquitin ligase RNF125. *Proc. Natl. Acad. Sci. USA* **104**, 7500–7505
44. Arimoto, K., Konishi, H., and Shimotohno, K. (2008) UbcH8 regulates ubiquitin and ISG15 conjugation to RIG-I. *Mol. Immunol.* **45**, 1078–1084
45. Trompouki, E., Hatzivassiliou, E., Tsichritzis, T., Farmer, H., Ashworth, A., and Mosialos, G. (2003) CYLD is a deubiquitinating enzyme that negatively regulates NF-kappaB activation by TNFR family members. *Nature* **424**, 793–796
46. Kovalenko, A., Chable-Bessia, C., Cantarella, G., Israel, A., Wallach, D., and Courtois, G. (2003) The tumour suppressor CYLD negatively regulates NF-kappaB signalling by deubiquitination. *Nature* **424**, 801–805
47. Brummelkamp, T.R., Nijman, S.M., Dirac, A.M., and Bernards, R. (2003) Loss of the cylindromatosis tumour suppressor inhibits apoptosis by activating NF-kappaB. *Nature* **424**, 797–801
48. Massoumi, R., Chmielarska, K., Hennecke, K., Pfeifer, A., and Fassler, R. (2006) Cyld inhibits tumor cell proliferation by blocking Bcl-3-dependent NF-kappaB signaling. *Cell* **125**, 665–677
49. Friedman, C.S., O'Donnell, M.A., Legarda-Addison, D., Ng, A., Cardenas, W.B., Yount, J.S., Moran, T.M., Basler, C.F., Komuro, A., Horvath, C.M., Xavier, R., and Ting, A.T. (2008) The tumour suppressor CYLD is a negative regulator of RIG-I-mediated antiviral response. *EMBO Rep.* **9**, 930–936
50. Kirisako, T., Kamei, K., Murata, S., Kato, M., Fukumoto, H., Kanie, M., Sano, S., Tokunaga, F., Tanaka, K., and Iwai, K. (2006) A ubiquitin ligase complex assembles linear polyubiquitin chains. *EMBO J.* **25**, 4877–4887
51. Inn, K.S., Gack, M.U., Tokunaga, F., Shi, M., Wong, L.Y., Iwai, K., and Jung, J.U. (2011) Linear ubiquitin assembly complex negatively regulates RIG-I- and TRIM25-mediated type I interferon induction. *Mol. Cell* **41**, 354–365
52. Diebold, S.S., Montoya, M., Unger, H., Alexopoulou, L., Roy, P., Haswell, L.E., Al-Shamkhani, A., Flavell, R., Borrow, P., and Reis e Sousa, C. (2003) Viral infection switches non-plasmacytoid dendritic cells into high interferon producers. *Nature* **424**, 324–328
53. Garcia-Sastre, A., Egorov, A., Matassov, D., Brandt, S., Levy, D.E., Durbin, J.E., Palese, P., and Muster, T. (1998) Influenza A virus lacking the NS1 gene replicates in interferon-deficient systems. *Virology* **252**, 324–330
54. Gack, M.U., Albrecht, R.A., Urano, T., Inn, K.S., Huang, I.C., Carnero, E., Farzan, M., Inoue, S., Jung, J.U., and Garcia-Sastre, A. (2009) Influenza A virus NS1 targets the ubiquitin ligase TRIM25 to evade recognition by the host viral RNA sensor RIG-I. *Cell Host Microbe* **5**, 439–449
55. Zhao, C., Denison, C., Huibregtse, J.M., Gygi, S., and Krug, R.M. (2005) Human ISG15 conjugation targets both IFN-induced and constitutively expressed proteins functioning in diverse cellular pathways. *Proc. Natl. Acad. Sci. USA* **102**, 10200–10205
56. Knobeloch, K.P., Utermohlen, O., Kisser, A., Prinz, M., and Horak, I. (2005) Reexamination of the role of ubiquitin-like modifier ISG15 in the phenotype of UBP43-deficient mice. *Mol. Cell Biol.* **25**, 11030–11034
57. Sun, Z., Ren, H., Liu, Y., Teeling, J.L., and Gu, J. (2011) Phosphorylation of RIG-I by casein kinase II inhibits its antiviral response. *J. Virol.* **85**, 1036–1047
58. Yanai, H., Ban, T., Wang, Z., Choi, M.K., Kawamura, T., Negishi, H., Nakasato, M., Lu, Y., Hangai, S., Koshiba, R., Savitsky, D., Ronfani, L., Akira, S., Bianchi, M. E., Honda, K., Tamura, T., Kodama, T., and Taniguchi, T. (2009) HMGB proteins function as universal sentinels for nucleic-acid-mediated innate immune responses. *Nature* **462**, 99–103
59. Oshiumi, H., Sakai, K., Matsumoto, M., and Seya, T. (2010) DEAD/H BOX 3 (DDX3) helicase binds the RIG-I adaptor IPS-1 to up-regulate IFN-beta-inducing potential. *Eur. J. Immunol.* **40**, 940–948
60. Soulat, D., Burckstummer, T., Westermayer, S., Goncalves, A., Bauch, A., Stefanovic, A., Hantschel, O., Bennett, K.L., Decker, T., and Superti-Furga, G. (2008) The DEAD-box helicase DDX3X is a critical component of the TANK-binding kinase 1-dependent innate immune response. *EMBO J.* **27**, 2135–2146
61. Schroder, M., Baran, M., and Bowie, A. G. (2008) Viral targeting of DEAD box protein 3 reveals its role in TBK1/IKKepsilon-mediated IRF activation. *EMBO J.* **27**, 2147–2157
62. Miyashita, M., Oshiumi, H., Matsumoto, M., and Seya, T. (2011) DDX60, a DExD/H box helicase, is a novel antiviral factor promoting RIG-I-like receptor-mediated signaling. *Mol. Cell Biol.* **31**, 3802–3819

Self-Enhancement of Hepatitis C Virus Replication by Promotion of Specific Sphingolipid Biosynthesis

Yuichi Hirata[1], Kazutaka Ikeda[2,3], Masayuki Sudoh[4], Yuko Tokunaga[1], Akemi Suzuki[5], Leiyun Weng[6], Masatoshi Ohta[3], Yoshimi Tobita[1], Ken Okano[7], Kazuhisa Ozeki[7], Kenichi Kawasaki[4], Takuo Tsukuda[4], Asao Katsume[4], Yuko Aoki[4], Takuya Umehara[1], Satoshi Sekiguchi[1], Tetsuya Toyoda[6], Kunitada Shimotohno[8], Tomoyoshi Soga[3], Masahiro Nishijima[9,10], Ryo Taguchi[2,11], Michinori Kohara[1]*

1 Department of Microbiology and Cell Biology, Tokyo Metropolitan Institute of Medical Science, Setagaya-ku, Tokyo, Japan, **2** Department of Metabolome, Graduate School of Medicine, The University of Tokyo, Bunkyo-ku, Tokyo, Japan, **3** Institute for Advanced Biosciences, Keio University, Kakuganji, Tsuruoka, Yamagata, Japan, **4** Kamakura Research Laboratories, Chugai Pharmaceutical Co., Ltd., Kamakura, Kanagawa, Japan, **5** Institute of Glycoscience, Tokai University, Hiratsuka-shi, Kanagawa, Japan, **6** Unit of Viral Genome Regulation, Institut Pasteur of Shanghai, Key Laboratory of Molecular Virology & Immunology, Chinese Academy of Sciences, Shanghai, China, **7** Fuji-Gotemba Research Laboratories, Chugai Pharmaceutical Co., Ltd., Gotemba, Shizuoka, Japan, **8** Research Institute, Chiba Institute of Technology, Narashino, Chiba, Japan, **9** National Institute of Health Sciences, Setagaya-ku, Tokyo, Japan, **10** Showa Pharmaceutical University, Machidashi, Tokyo, Japan, **11** Department of Biomedical Sciences, College of Life and Health Sciences, Chubu University, Kasugai-shi, Aichi, Japan

Abstract

Lipids are key components in the viral life cycle that affect host-pathogen interactions. In this study, we investigated the effect of HCV infection on sphingolipid metabolism, especially on endogenous SM levels, and the relationship between HCV replication and endogenous SM molecular species. We demonstrated that HCV induces the expression of the genes (*SGMS1* and *2*) encoding human SM synthases 1 and 2. We observed associated increases of both total and individual sphingolipid molecular species, as assessed in human hepatocytes and in the detergent-resistant membrane (DRM) fraction in which HCV replicates. SGMS1 expression had a correlation with HCV replication. Inhibition of sphingolipid biosynthesis with a hepatotropic serine palmitoyltransferase (SPT) inhibitor, NA808, suppressed HCV-RNA production while also interfering with sphingolipid metabolism. Further, we identified the SM molecular species that comprise the DRM fraction and demonstrated that these endogenous SM species interacted with HCV nonstructural 5B polymerase to enhance viral replication. Our results reveal that HCV alters sphingolipid metabolism to promote viral replication, providing new insights into the formation of the HCV replication complex and the involvement of host lipids in the HCV life cycle.

Citation: Hirata Y, Ikeda K, Sudoh M, Tokunaga Y, Suzuki A, et al. (2012) Self-Enhancement of Hepatitis C Virus Replication by Promotion of Specific Sphingolipid Biosynthesis. PLoS Pathog 8(8): e1002860. doi:10.1371/journal.ppat.1002860

Editor: Aleem Siddiqui, University of California, San Diego, United States of America

Received January 4, 2012; **Accepted** June 27, 2012; **Published** August 16, 2012

Funding: This study was supported by grants from the Ministry of Education, Culture, Sports, Science, and Technology of Japan; the Program for Promotion of Fundamental Studies in Health Science of the National Institute of Biomedical Innovation of Japan; and the Ministry of Health, Labor, and Welfare of Japan. The funders had no role in study design, data collection and analysis, decision to publish, or preparation of the manuscript.

Competing Interests: M. Sudoh, A. Katsume, K. Okano, K. Ozeki, K. Kawasaki, T. Tsukuda, and Y. Aoki are employees of Chugai Pharmaceutical Co. Ltd. This does not alter our adherence to all PLoS Pathogens policies on sharing data and materials.

* E-mail: kohara-mc@igakuken.or.jp

Author Summary

One of the key components for hepatitis C virus (HCV) propagation is lipids, some of which comprise membranous replication complexes for HCV replication. Research on cofactors that are involved in the formation of the membranous replication complex has advanced steadily; on the other hand, the lipids constituting the membranous replication complex remain to be elucidated. Here, we report that HCV modulates sphingolipid metabolism by promoting sphingolipid biosynthesis, to enhance viral replication. Specifically a specific molecular species of sphingomyelin (SM), a type of sphingolipid interacts with HCV nonstructural 5B polymerase, enhancing HCV replication. This work highlights the relationship between specific molecular species of SMs and HCV replication, giving new insight into the formation of the HCV replication complex and the involvement of host lipids in the HCV life cycle.

Introduction

Lipids have long been known to play dual roles in biological systems, functioning in structural (in biological membranes) and energy storage (in cellular lipid droplets and plasma lipoproteins) capacities. Research over the past few decades has identified additional functions of lipids related to cellular signaling, microdomain organization, and membrane traffic. There are also strong indications of the important role of lipids in various stages of host-pathogen interactions [1].

Sphingomyelin (SM) is a sphingolipid that interacts with cholesterol and glycosphingolipid during formation of the raft domain, which can be extracted for study as a detergent-resistant membrane (DRM) fraction [2]. Recently, raft domains have drawn attention as potential platforms for signal transduction and pathogen infection processes [3,4]. For instance, raft domains may serve as sites for hepatitis C virus (HCV) replication [5,6]. Additionally, *in vitro* analysis indicates that synthetic SM binds to the nonstructural 5B polymerase (RdRp) of HCV [7]. This association allows RdRp to localize to the DRM fraction (known to be the site of HCV replication) and activates RdRp, although the degree of binding and activation differs among HCV genotypes [7,8]. Indeed, suppression of SM biosynthesis with a serine palmitoyltransferase (SPT) inhibitor disrupts the association between RdRp and SM in the DRM fraction, resulting in the suppression of HCV replication [7,9].

Multiple reports have indicated that HCV modulates lipid metabolism (e.g., cholesterol and fatty acid biosynthesis) to promote viral replication [10–12]. However, the effect of HCV infection on sphingolipid metabolism, especially on endogenous SM levels, and the relationship between HCV replication and endogenous SM molecular species remain to be elucidated as there are technical challenges in measuring SM levels (for both total and individual molecular species) in hepatocytes.

To address these questions, we first utilized mass spectrometry (MS)-based techniques and analyzed uninfected and HCV-infected chimeric mice harboring human hepatocytes. Second, we developed a hepatotropic SPT inhibitor, NA808, and used this tool to elucidate the effects of inhibition of sphingolipid biosynthesis on hepatocyte SM levels. Third, we tested the inhibitor's anti-HCV activity in humanized chimeric mice, and demonstrated the relationship between HCV and endogenous SM in human hepatocytes. Finally, we identified the endogenous SM molecular species carried by the DRM fraction, defining the association between these molecular species and HCV replication.

Results

HCV upregulates SM and ceramide levels in hepatocytes of humanized chimeric mice

First, we examined the effects of HCV infection on SM biosynthesis in hepatocytes using humanized chimeric mice. The study employed a previously described mouse model (SCID/uPA) into which human hepatocytes were transplanted (see Materials and Methods). The average substitution rate of the chimeric mouse livers used in this study was over 80% [13], and HCV selectively infected human hepatocytes. This model supports long-term HCV infections at clinically relevant titers [13,14]. Indeed, the HCV-RNA levels reached (at 4 weeks post-infection) 10^8–10^9 copies/mL in the genotype 1a group (**Figure 1A**) and 10^6–10^7 copies/mL in the genotype 2a group (**Figure 1B**).

Once serum HCV-RNA levels had plateaued, we observed elevated expression of the genes (*SGMS1* and *2*) encoding human SM synthases 1 and 2; this pattern was HCV-specific, as demonstrated by the fact that the increase was not seen in hepatitis B virus-infected mice (**Figure 1C and Figure S1**). SM synthases convert ceramide to SM, so we next examined SM and ceramide levels in hepatocytes of both HCV-infected and uninfected chimeric mice. SM and ceramide levels were assessed using MS spectrometry, which allows analysis of samples at the single lipid species level as well as at the whole lipidome level. MS analysis showed that the level of ceramide, the precursor to SM, was increased in hepatocytes obtained from chimeric mice infected with HCV of either genotype (**Figure 1D**). Further, MS analysis showed that infection of chimeric mice with HCG9 (genotype 1a) was associated with increased SM levels in hepatocytes (**Figure 1E**). Similarly, SM levels were elevated in the hepatocytes of HCR24 (genotype 2a)-infected chimeric mice. These results indicate that infection with HCV increases total SM and ceramide levels in human hepatocytes.

MS analysis was conducted to determine which of several molecular species of SM [15] are present in HCV-infected hepatocytes. SM molecular species were analyzed in extracts obtained from a human hepatocyte cell line (HuH-7 K4) and from hepatocytes derived from the humanized chimeric mice. We identified four major peaks as SM molecular species (*d*18:1-16:0, *d*18:1-22:0, *d*18:1-24:0, and *d*18:1-24:1), and other peaks as phosphatidylcholine (**Figure 1F**). Infection-associated increases were seen for all ceramide molecular species, with significant changes in three of four species (excepting *d*18:1-16:0; $p<0.05$) with genotype 1a, and in all four species with genotype 2a ($p<0.05$) (**Figure 1G**). Upon infection with HCV of either genotype, hepatocytes tended to show increased levels of all four identified SM molecular species, but the changes were significant only for one species (*d*18:1-24:1; $p<0.05$) in genotype 1a and for two species (*d*18:1-16:0 and *d*18:1-24:1; $p<0.01$) in genotype 2a (**Figure 1H**). In cell culture, negligible amount of SM was likely increased by HCV infection. With respect to each molecular species, d18:1-16:0 SM was likely increased by HCV infection (**Figure S2**). These results indicate that HCV infection increases the abundance of several SM and ceramide molecular species.

Relationship between the SGMS genes and HCV infection

To clarify the relationship between SGMS1/2 and HCV, we investigated the correlation between SGMS1/2 expression and liver HCV-RNA in humanized chimeric mice. We found that SGMS1, but not SGMS2, had a correlation with liver HCV-RNA in HCV-infected humanized chimeric mice (**Figures 2A and 2B**).

Next, to clarify whether HCV infection of human hepatocytes increases the expression of the genes (*SGMS1* and *SGMS2*), we examined the effect of silencing HCV genome RNA on the expression of these genes in HCV-infected cells (**Figures 2C and 2D**). We found that silencing the HCV genome RNA decreases the expression of *SGMS1* and *SGMS2*.

The above results motivated us to examine the relationship between SGMS1/2 and HCV replication. Therefore, we examined the effect of SGMS1/2 mRNA silencing on HCV replication using subgenomic replicon cells [7,16]. We observed that silencing SGMS1 mRNA suppressed HCV replication, whereas silencing SGMS2 mRNA had no such effect (**Figures 2E and 2F**). These results indicate that SGMS1 expression has a correlation with HCV replication.

Characterization of the hepatotropic SPT inhibitor NA808

Based on our data, we hypothesized that HCV might alter the metabolism of sphingolipids, providing a more conducive environment for progression of the viral life cycle. To explore the relationship between HCV and sphingolipids, we investigated the effect of sphingolipid biosynthesis inhibition on HCV and the lipid profiles of SM and ceramide using HCV-infected chimeric mice harboring human hepatocytes. To inhibit the biosynthesis of sphingolipids, we used NA808, a chemical derivative of NA255, which is an SPT inhibitor derived from natural compounds [7]. We found that NA808 (**Figure 3A**) suppressed both the activity of SPT (**Figure 3B**) and biosynthesis of sphingolipids (**Figure 3C**) in a dose-dependent manner.

The conventional SPT inhibitor myriocin is not clinically beneficial due to immunosuppression through restriction of T-cell proliferation [17,18]. However, NA808 showed little immunosuppressive effect at the concentration at which NA808 suppressed HCV replication (**Figures 3D and 3E**). Moreover, pharmacokinetic analysis using [^{14}C]-labeled NA808 in rat models showed

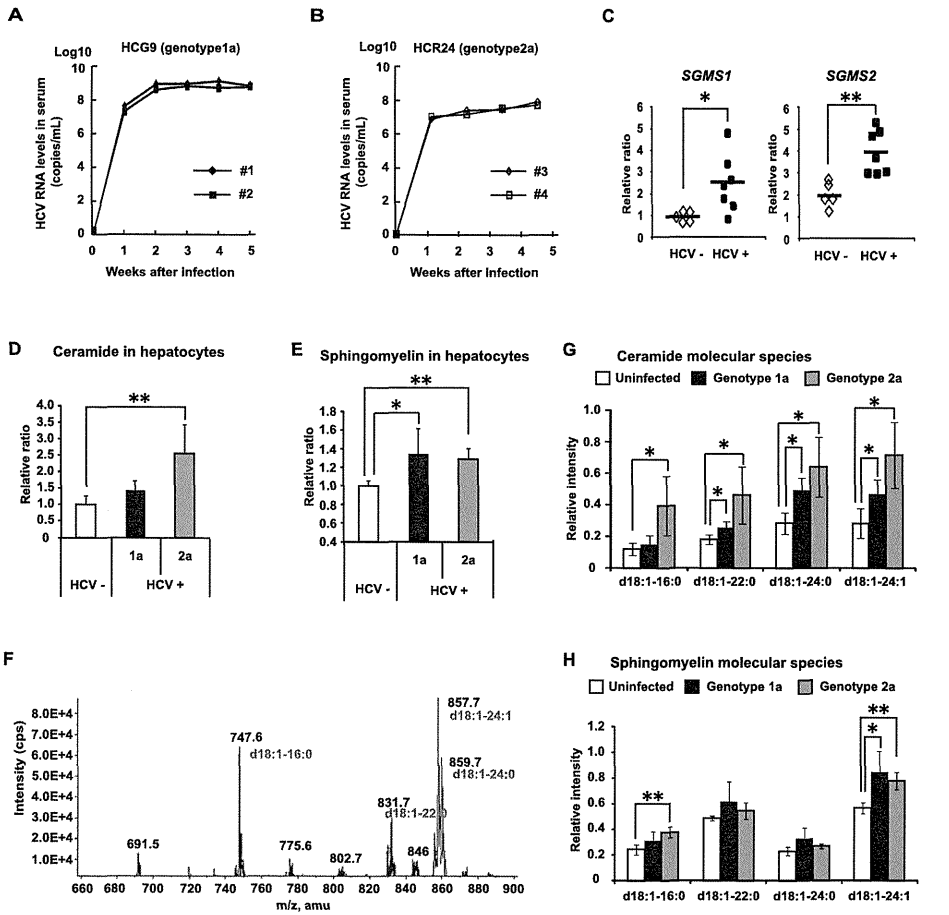

Figure 1. HCV alters sphingolipid metabolism. (**A, B**) Time-course studies of humanized chimeric mice inoculated with human serum samples positive for HCV genotype 1a (**A**) or 2a (**B**). (**C**) mRNA expression of *SGMS1* and *SGMS2* in uninfected (white, n = 5) and HCV genotype 1a-infected (black, n = 7) chimeric mice. (**D, E**) Effects of HCV infection on hepatocyte SM and ceramide levels in humanized chimeric mice. Relative intensity of total ceramide (**D**) and total shingomyelin (SM) (**E**) in uninfected mouse hepatocytes (white bar, n = 4), HCV genotype 1a-infected mouse hepatocytes (black bar, n = 5), and HCV genotype 2a-infected mouse hepatocytes (dark gray bar, n = 3). (**F**) Mass spectrum of SM in Bligh & Dyer extracts of a human hepatocyte cell line (HuH-7 K4). (**G, H**) Effects of HCV infection on hepatocyte SM and ceramide levels in humanized chimeric mice. Relative intensity of individual ceramide molecular species (**G**) and individual SM molecular species (**H**) in uninfected mouse hepatocytes (white bar, n = 3), HCV genotype 1a-infected mouse hepatocytes (black bar, n = 3), and HCV genotype 2a-infected mouse hepatocytes (dark gray bar, n = 3). In all cases, error bars indicate SDs. *$p<0.05$ and **$p<0.01$ compared with uninfected hepatocytes.
doi:10.1371/journal.ppat.1002860.g001

that NA808 mainly accumulated in the liver and small intestine (**Table S1**). These results indicate that NA808 suppressed SPT activity, with hepatotropic and low immunosuppressive properties.

Based on these results, we then examined the effects of inhibition of sphingolipid biosynthesis with NA808 on HCV replication using subgenomic replicon cells [7,16]. The luciferase activity of FLR3-1 showed that replication was suppressed by NA808 in a dose-dependent manner with no effect on cell viability, as measured by the WST-8 assay (**Figure 3E**). Similarly, western blot and immunofluorescence analysis showed that NA808 effectively suppressed HCV replication (**Figures 3F and 3G**).

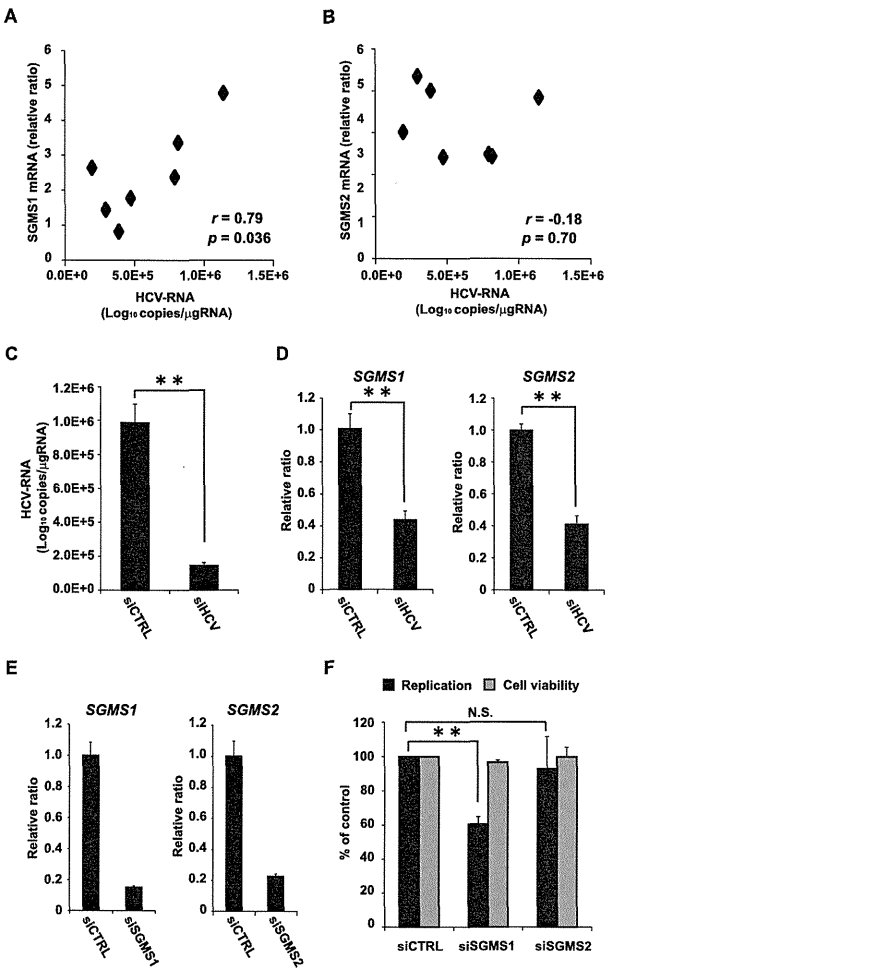

Figure 2. Relationship between the SGMS genes and HCV infection. (**A, B**) The correlation between SGMS1/2 and liver HCV-RNA of HCV infected humanized chimeric mice (n = 7). (**C**) The effect of silencing HCV genome RNA with siRNA (siE-R7: 1 nM) on HCV in HCV-infected cells. (**D**) The effect of silencing HCV genome RNA with siRNA (siE-R7: 1 nM) on the expression of SGMS1/2 mRNA measured by RTD-PCR. (**E**) The effect of silencing SGMS1/2 mRNA with siRNA (3 nM each) measured by RTD-PCR. (**F**) The effect of silencing SGMS1/2 mRNA with siRNA (3 nM) on HCV replication in FLR 3-1. In all cases, error bars indicate SDs. *$p<0.05$ and **$p<0.01$.
doi:10.1371/journal.ppat.1002860.g002

Inhibition of sphingolipid biosynthesis impedes HCV infection of chimeric mice

To evaluate the effects of inhibition of sphingolipid biosynthesis in an animal model, we administered NA808 or pegylated interferon-α (PegIFN-α) via intravenous or subcutaneous injection to HCV-infected chimeric mice harboring human hepatocytes (**Table S2**). In chimeric mice infected with HCV genotype 1a, NA808 treatment led to a rapid decline in serum HCV-RNA (approximately 2–3 log units within 14 days). On the other hand, PegIFN-α produced less than a 1 log unit reduction, despite being delivered at 20 times the typical clinical dose (**Figure 4A**). Furthermore, results of 21-day NA808 treatment (5 mg/kg) in individual mice indicated that serum HCV RNA continued to decrease in all chimeric mice without viral breakthrough

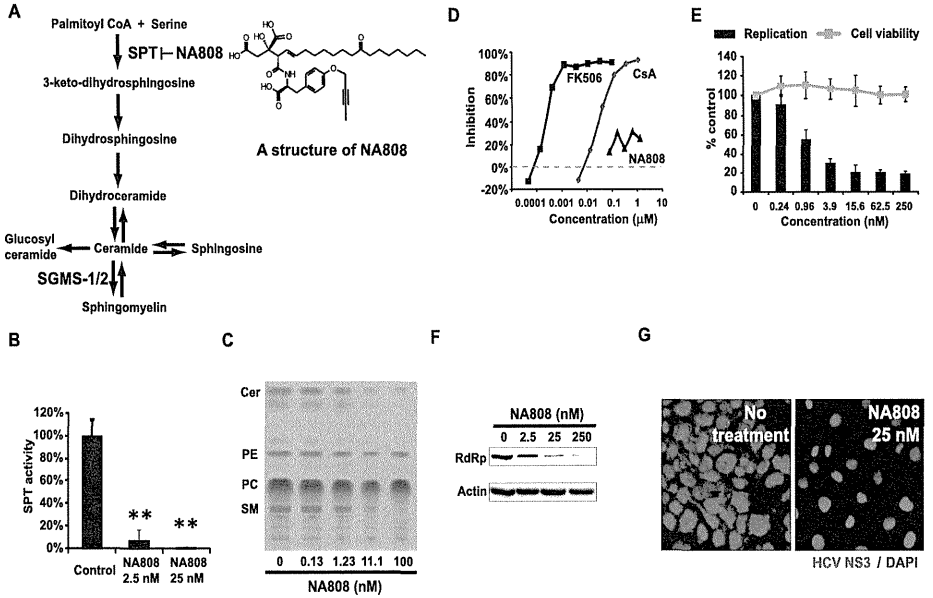

Figure 3. Characterization of the hepatotropic serine palmitoyltransferase inhibitor NA808. (**A**) Sphingolipid biosynthesis pathway and structure of NA808. (**B**) Activity of SPT in FLR3-1 cells after 72 h of NA808 treatment. $^{**}p<0.01$ compared with control. (**C**) Results of TLC showing *de novo* sphingolipid biosynthesis in the presence of NA808. Cer = ceramide, PE = phosphatidylethanolamine, PC = phosphatidylcholine, SM = sphingomyelin. (**D**) Immunosuppressive activity of NA808. Cyclosporin A (CsA) and tacrolimus (FK-506) were used as positive controls. (**E**) Effects of NA808 on HCV replication (black bars) and cell viability (gray symbols) in FLR 3-1 replicon-containing cells. Error bars indicate SDs. (**F**) Effects of NA808 on the level of the RdRp and β-actin, as assessed by Western blotting. (**G**) Effect of NA808 on the production of HCV NS3 protein (green) in FLR3-1 replicon-containing cells, as assessed by immunofluorescence analysis. Nuclear DNA was stained with DAPI (blue).
doi:10.1371/journal.ppat.1002860.g003

(**Figure 4B**). Notably, in 2 of 5 chimeric mice, serum HCV-RNA was not detectable at the end of the 21-day regimen. Consistent with this observation, the levels of both hepatic HCV-RNA and HCV core protein decreased significantly ($p<0.01$ and $p<0.05$, respectively) following NA808 treatment, these effects being dose dependent (**Figure 4C**). Immunofluorescence analysis and immunohistochemistry confirmed the reduced abundance of HCV core protein after 14 days of treatment (**Figure 4D and Figure S3**).

In genotype 2a-infected chimeric mice, NA808 decreased serum HCV-RNA by approximately 3 log units within 14 days (**Figure 4E**). NA808-treated mice displayed a corresponding reduction in hepatic HCV-RNA (**Figure 4F**). NA808 did not affect body weight or human serum albumin levels (**Figures S4A and S4B**). Furthermore, hematoxylin and eosin (H&E) staining revealed little morphological change in response to treatment with NA808. Immunofluorescence analysis also indicated that NA808 did not affect the production of human albumin (**Figure S4C**). Thus, inhibition of sphingolipid biosynthesis by an SPT inhibitor impeded HCV replication in an animal infection model, regardless of HCV genotype.

Inhibition of SPT decreases ceramide and SM levels in hepatocytes of humanized chimeric mice

We next investigated the effects of sphingolipid biosynthesis inhibition on SM and ceramide levels in hepatocytes of humanized chimeric mice. Pharmacokinetic analysis in a rat model indicated that NA808 has hepatotropic properties (**Table S1**). Consistent with this analysis, our study in chimeric mice also indicated that the NA808 concentration was much higher in the liver than in serum (**Figure S5**). Furthermore, we observed that serum SM content was not decreased by NA808 treatment (**Figure S6**), in contrast to the effects previously observed for myriocin, another SPT inhibitor [19].

In HCV-infected chimeric mouse hepatocytes, MS analysis indicated that HCV infection resulted in increased ceramide and SM levels. However, treatment of infected animals with NA808 (5 mg/kg) attenuated this increase in ceramide and SM levels in hepatocytes, and the change in SM was significant ($p<0.05$) compared to the level observed in HCV-infected chimeric mice with no treatment. This effect of NA808 on ceramide and SM levels was dose-dependent (**Figures 5A and 5B**). We also found that SM levels and hepatic HCV-RNA were correlated (**Figure 5C**).

Interestingly, treatment with NA808 effectively decreased two specific SM and ceramide molecular species (*d*18:1-22:0 and *d*18:1-24:0), slightly decreased one other species (*d*18:1-24:1), and hardly decreased another (*d*18:1-16:0). Further, we found that among SM and ceramide molecular species, *d*18:1-16:0 did not change (**Figures 5D and 5E**). These results indicate that the

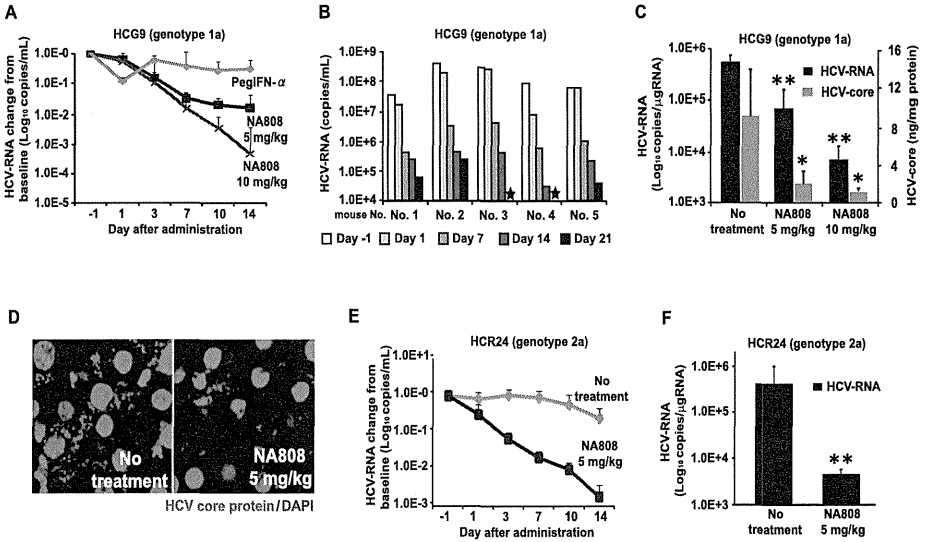

Figure 4. Inhibition of sphingolipid biosynthesis with hepatotropic serine palmitoyltransferase (SPT) inhibitor NA808 exerts anti-HCV effect. (**A**) Serum HCV-RNA levels in response to treatment with NA808 (blue, 5 mg/kg/day, purple, 10 mg/kg/day, n = 6 each), or PegIFN-α (pink, 30 μg/kg twice weekly, n = 4). (**B**) Effect of NA808 (5 mg/kg/day) on serum HCV-RNA levels. A star indicates that HCV-RNA was not detected. (**C**) Levels of liver HCV-RNA (black) and HCV core protein (gray) after the 14-day treatment. $^{*}p<0.05$ and $^{**}p<0.01$ compared with no treatment. (**D**) Histological analysis using immunofluorescent labeling of HCV core protein (green) and fluorescent staining of nuclei (blue). (**E**) Serum HCV-RNA levels in response to no treatment (pink, n = 3) or NA808 treatment (blue, 5 mg/kg/day, n = 4). (**F**) Liver HCV-RNA levels in genotype 2a-infected mice after the 14-day treatment. $^{*}p<0.05$ and $^{**}p<0.01$ compared with no treatment. In all cases, error bars indicate SDs.
doi:10.1371/journal.ppat.1002860.g004

effects of sphingolipid biosynthesis inhibition varied among the molecular species.

Considering these results, we found a discrepancy in SM molecular species which were considered to be important for HCV replication. To elucidate the relationship between SM molecular species and HCV replication, we attempted to identify endogenous SM molecular species comprising the DRM fraction and to evaluate the effects of HCV infection and inhibition of sphingolipid biosynthesis on SM levels of the DRM.

Relationship between endogenous SM molecular species constituting the DRM and HCV replication

We previously reported that SM interacts with RdRp, allowing it to localize to the DRM fraction where HCV replicates and activates RdRp [7,8], and that suppression of SM biosynthesis disrupts the association between RdRp and SM in the DRM fraction, resulting in suppression of HCV replication [7,8]. In the present study, treatment with NA808 decreased SM levels in the DRM fraction; the decreased presence of SM correlated with decreased RdRp abundance, but the same effect was not seen for HCV nonstructural protein 3 (**Figures S7A–C**). Given these results, we investigated whether HCV replication was induced by elevated SM levels. Specifically, we compared SM levels in the DRM fraction between HCV-infected hepatocytes and uninfected hepatocytes. MS analysis showed that HCV increased SM levels in the DRM fraction more remarkably than in whole cells (**Figure 6A**). Next, we identified SM molecular species composing the DRM fraction and found that the composition ratio of SM molecular species was distinct between whole cells and DRM fractions in both HCV-infected and uninfected hepatocytes (**Figure 6B and Figure S8**). The DRM was composed primarily (69%) of *d*18:1-16:0, followed (in decreasing order) by *d*18:1-24:0, *d*18:1-22:0, and *d*18:1-24:1; the abundance of all SM molecular species increased upon HCV infection (**Figure 6C**). Further, NA808 treatment decreased all SM molecular species in the DRM fraction. Consistently, NS3 protease inhibitor decreased all SM molecular species in the DRM fraction of subgenomic replicon cells (**Figure S9**).

To address the association between RdRp and the endogenous SM molecular species composing the DRM, we used high-performance liquid chromatography (HPLC) to separate each SM molecular species from bulk SM derived from bovine milk and brain. We evaluated the relationship between RdRp and these endogenous SM molecular species using *in vitro* analysis. Enzyme-linked immunosorbent assay (ELISA) indicated that these endogenous SM molecular species bound to RdRp more readily than the bulk SM derived from milk as a positive control (**Figure 6D**). Further, *in vitro* HCV transcription analysis showed that three SM species (*d*18:1-16:0, *d*18:1-22:0, and *d*18:1-24:1) increased *in vitro* RdRp activation by approximately 5-fold, whereas the *d*18:1-24:0 species increased activation by 2-fold (**Figure 6E**). In a previous study, the soluble RdRp without its C-terminal hydrophobic 21-amino-acid sequence was used in *in vitro* analysis [8], and whether the relationship between RdRp and SM proved in this analysis

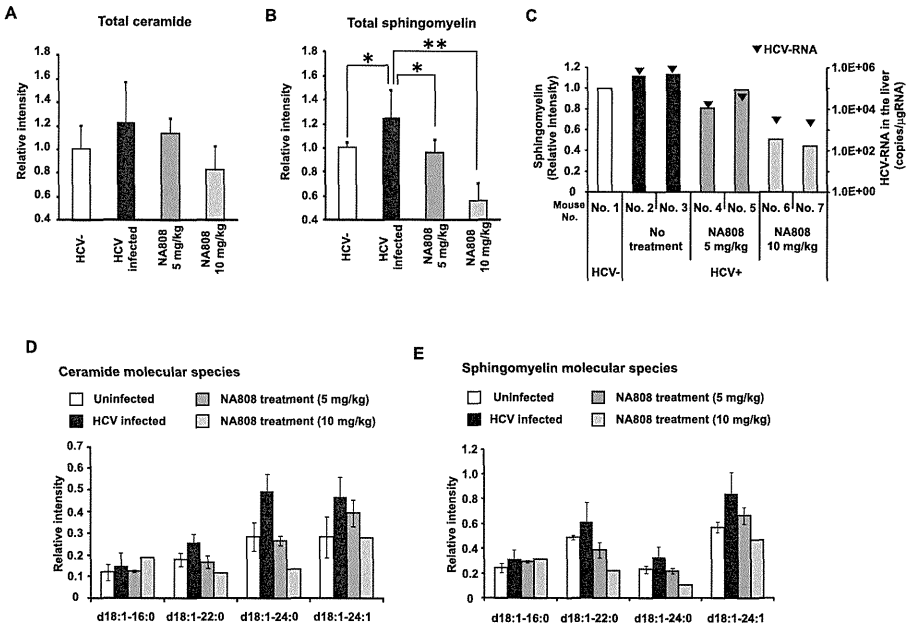

Figure 5. Effects of NA808 treatment on sphingomyelin (SM) and ceramide (total and individual molecular species). (**A, B**) Relative ratio of total ceramide (**A**) and SM (**B**) in uninfected mice (white, n = 4), HCV genotype 1a-infected mice (black, n = 5), and HCV-infected mice treated with NA808 for 14 days (dark gray, 5 mg/kg, n = 4; light gray, 10 mg/kg, n = 3). *$p<0.05$ and **$p<0.01$ compared with HCV-infected mice. (**C**) SM levels (bars) and HCV RNA levels (black arrowhead) in the livers of mice treated for 14 days with NA808 (5 or 10 mg/kg/day) and untreated chimeric mice. (**D, E**) Relative intensities of individual ceramide molecular species (**D**) and individual SM molecular species (**E**) in uninfected mice (white, n = 3), HCV-infected mice (black, n = 3), and HCV-infected mice treated with NA808 for 14 days (dark gray, 5 mg/kg, n = 2; light gray, 10 mg/kg, n = 1). In all cases, error bars indicate SDs.
doi:10.1371/journal.ppat.1002860.g005

reflected the state in the membranous replication complex remains to be elucidated. Therefore, we attempted to examine the effect of endogenous SM molecular species on HCV replicase activity *in vivo* using digitonin-permeabilized semi-intact replicon cells, which permit monitoring of the function of the active HCV replication complex (**Figure 6F**) [20]. This *in vivo* analysis also enabled us to deliver the extrinsically added SM molecular species directly to the cytosol. This RNA replication assay indicated that the endogenous SM molecular species (*d*18:1-16:0 and *d*18:1-24:0) enhanced HCV-RNA replication, these species being consistent with the two SM molecular species that primarily constitute the DRM and are decreased significantly by NA808 treatment (**Figures 6G and 6H**). These results suggest that HCV infection modifies the levels of specific endogenous SM molecular species, which in turn enhance HCV-RNA replication by interacting with RdRp.

Discussion

In this study, we showed that HCV alters sphingolipid metabolism, resulting in a better environment for viral replication. Specifically, HCV increased SM content in the DRM fraction; this step is essential for viral replication since SM is a key component of the membranous replication complex and interacts with RdRp. Employing MS analysis, we identified endogenous SM molecular species (located in the DRM fraction) that increased upon HCV infection, and demonstrated that these endogenous SM molecular species interact directly with RdRp, enhancing HCV replication. Thus, we concluded that HCV modulates sphingolipid metabolism to promote viral replication.

We found that the expression levels of SGMS1/2 and the content of SM and ceramide in HCV-infected humanized chimeric mouse livers was increased (Figure 1). Our measurement revealed that chronic HCV infection promoted sphingolipid biosynthesis. HCV is known to induce cellular stress [21,22]. A variety of cell stressors increase intracellular ceramide content during the execution phase of apoptosis [23,24], indicating that ceramide is a proapoptotic lipid mediator. Furthermore, activation of ceramide-metabolizing enzymes such as glucosylceramide synthase and SM synthase can attenuate apoptosis by decreasing the intracellular ceramide content [25,26]. We found that HCV infection correlated with increased mRNA levels of the genes that encode human SM synthases (*SGMS1/2*) and glucosylceramide synthase (*UGCG*) (data not shown). Thus, the increase in ceramide levels observed in our study was likely to activate enzymes that transfer ceramide to other sphingolipids. On the other hand, Diamond et al. reported on lipidomic profiling performed over the

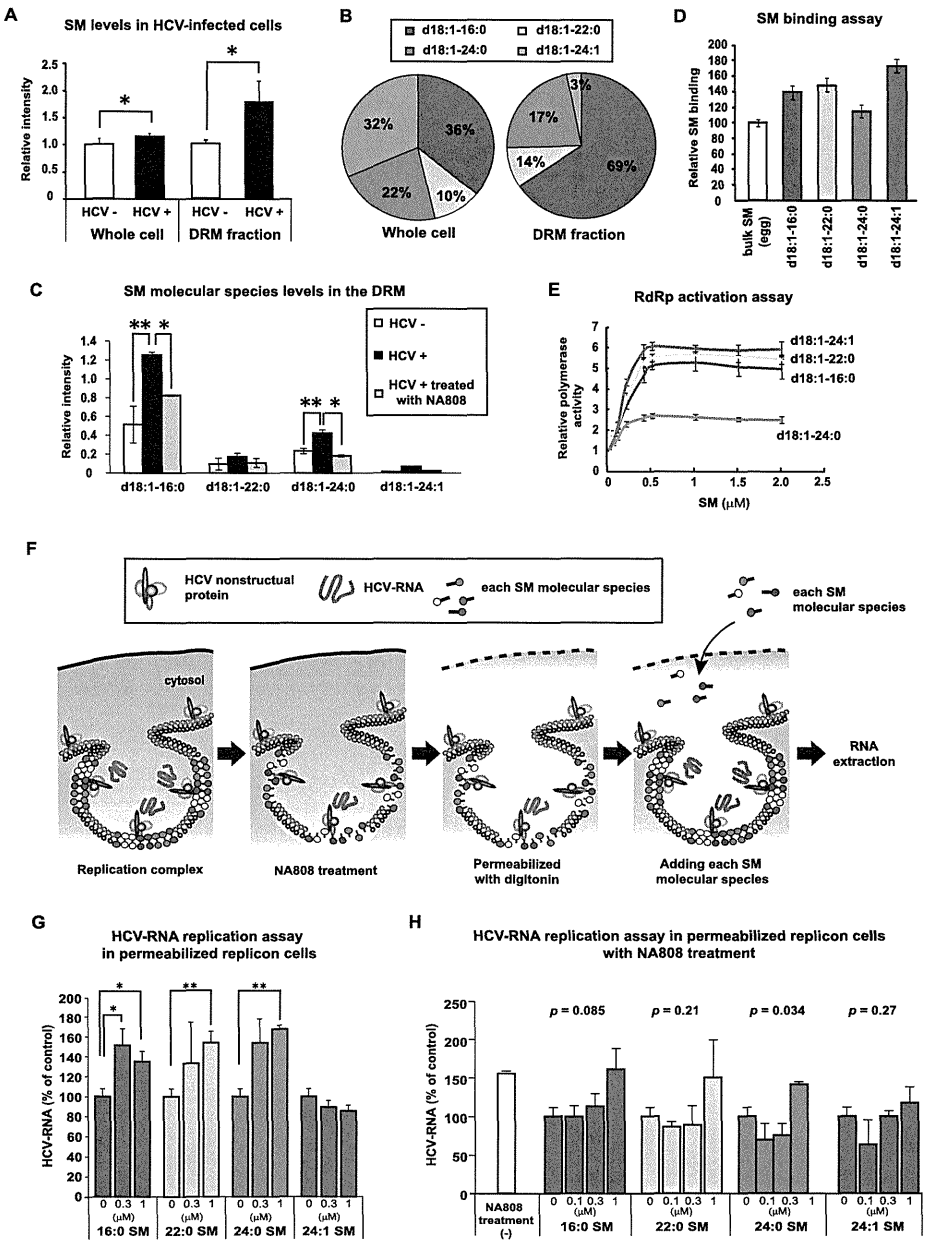

Figure 6. Specific sphingomyelin molecular species upregulated by HCV promote HCV replication on the detergent-resistant membrane fraction. (**A**) Comparison of the relative amounts of SM, as measured by MS analysis, in whole cells and the DRM fraction of mock-infected (HuH-7 K4 cells) (white, n = 6; whole cells, n = 3; DRM fraction) and HCV (JFH-1)-infected cells (JFH/K4 cells) (black, n = 6; whole cells, n = 3; DRM fraction). (**B**) Composition ratio of SM molecular species in whole cells and DRM fraction of HCV-infected cells. (**C**) Relative intensities of each SM molecular species in the DRM fraction of mock-infected cells (white, n = 2) and HCV-producing cells without (black, n = 2) or with NA808 treatment (gray, n = 2). (**D**) Results of the ELISA SM binding assay (n = 3 each). (**E**) Average activation kinetics of each SM molecular species on HCR6 (genotype 1b) RdRp (n = 3 each). (**F**) Scheme of HCV-RNA replicase assay using digitonin-permeabilized cells. (**G, H**) Effect of each SM molecular species on HCV-RNA in digitonin-permeabilized replicon cells treated without (G) or with 10 nM NA808 (H) (n = 3 each). In all cases, error bars indicate SDs. *$p<0.05$ and **$p<0.01$.
doi:10.1371/journal.ppat.1002860.g006

time course of acute HCV infection in cultured Huh-7.5 cells and observed that specific SM molecular species were decreased 72 h after HCV infection [27]. Given that their study focused on acute HCV infection, the reason for this discrepancy may be due to the severity of infection, suggesting that the influence of HCV infection on sphingolipid metabolism differs between acute and chronic infections. We also demonstrated that HCV infection correlates with increased abundance of specific SM and ceramide molecular species, with the profiles of individual lipids differing for infection by HCG9 (genotype 1a) and HCR24 (genotype 2a). The precise mechanism and meaning of these differences remain to be elucidated.

Our results indicated that SGMS1 expression had a correlation with HCV replication. This indicates that SM synthesized by SGMS1 contributes to HCV replication. A previous report revealed that in cultured cell lines, SGMS1 localizes in Golgi apparatus while SGMS2 localizes in the plasma membrane [28]. Thus, the results of this previous report suggest that SMs synthesized by SGMS1 can be easily incorporated into membranous replication complexes. As for SGMS2, we found that HCV infection significantly increased the expression of SGMS2, although the relationship between SGMS2 and HCV replication was hardly seen in this study. The relationship between SGMS2 and HCV propagation, thus, is an issue that should be elucidated in future studies.

We also demonstrated in this study that reduction of SM molecular species by NA808, a hepatotropic SPT inhibitor with little immunosuppressive activity, inhibits HCV replication in humanized chimeric mice regardless of viral genotype (Figure 4). Notably, treatment with NA808 (5 mg/kg) restored SM and ceramide levels in the liver to the levels observed in uninfected chimeric mice (Figure 5). Apparently, a slight reduction in SM had a significant influence on HCV, indicating that SM plays an important role in the HCV life cycle. SM is required for many viral processes in host-pathogen interactions [29–31]. For instance, viral envelopes of human immunodeficiency virus type 1 (HIV-1) and herpes simplex virus (HSV) are enriched with SM, which is necessary for efficient virus infectivity [32,33]. With regard to HCV, in addition to efficient virus infectivity [34], SM is present in the raft domain, which serves as a site of virus replication, together with other sphingolipids and cholesterol [6]. Moreover, SM is a component of VLDL whose assembly component and pathway is required for HCV morphogenesis and secretion [34,35]. The above-mentioned observations suggest that SM plays a multifaceted role in the HCV life cycle; therefore, SM is likely to be a good therapeutic target.

HCV is thought to replicate in a specialized compartment characterized as a DRM (designated as the membranous replication complex) [6]. SM, cholesterol, and phosphatidylinositol (PI) are thought to be the lipids that make up the membranous replication complex. With regard to PI, several siRNA screening have recently identified type III phosphatidylinositol 4-kinases (PI4K) as crucial host factors for HCV replication [36–39]. In HCV replicon containing cells, PI4P distribution is altered and enriched in the membranous replication complex by PI4KIIIα synthesis. Although the ability of PI to influence membrane bending and regulate intracellular processes (e.g. vesicle fusion, budding, and sorting) has been reported, the role of PI4P in the formation of the membranous replication complex remains to be elucidated. SM and cholesterol organize the solid membrane characterized as the DRM, where HCV replicates [6]. In fact, we and other groups demonstrated that reduction of SM and cholesterol suppressed HCV replication [7,9,12,40]. We performed the immunofluorescent analysis using lysenin. However, lysenin did not co-localize with NS4B protein. To date, it has been reported that lysenin-binding to SM is increased in the form of SM clusters, and that glycosphingolipids hinder lysein-binding to SM [41] Lipid rafts form of HCV replication complex do not have the characters of lysenin-binding to SM.

Further, the role of SM is not only to act as a constituent of the membranous replication complex, but also to bind and activate RdRp [7,8]. In this study, to gain further insight into the HCV membranous replication complex, we attempted to analyze which SM molecular species comprise the membranous replication complex, given that the diversity of molecular species is believed to be responsible for the physiochemical properties of the biomembrane [42] (Figure 6). We found that the composition ratio of SM molecular species observed in this study was quite different between the whole cell and DRM fractions. Further, to identify whether these SM molecular species contribute to HCV replication, we conducted rescue experiments using HCV replicon-containing cells (carrying intact RdRp and active membranous replication complexes) in which each SM molecular species was extrinsically added to replicon cells treated with NA808. However, in this experiment, addition of SM caused cell death. Therefore, we used digitonin-permeabilized semi-intact replicon cells, which enabled us to deliver the extrinsically added SM molecular species directly to the cytosol without catalytic effect and permitted monitoring of intact RdRp and replication complexes. We demonstrated that the specific endogenous SM molecular species (*d*18:1-16:0 and *d*18:1-24:0) enhance HCV-RNA replication, these species being consistent with the two SM molecular species which mainly constitute the DRM. Collectively, these results suggest that the HCV replication complex characterized as DRM is the specialized compartment that is composed of SM molecular species. These findings will provide new insights into the formation of the HCV replication complex and the involvement of host lipids in the HCV life cycle.

Materials and Methods

Ethics statement

This study was carried out in strict accordance with both the Guidelines for Animal Experimentation of the Japanese Association for Laboratory Animal Science and the recommendations in the Guide for the Care and Use of Laboratory Animals of the National Institutes of Health. All protocols were approved by the ethics committee of Tokyo Metropolitan Institute of Medical Science. The patient with HCV infection who provided the serum samples gave written informed consent before blood collection.

Cells

The HCV subgenomic replicon cells FLR3-1 (genotype 1b, Con-1) was cultured at 37°C in Dulbecco's modified Eagle's medium GlutaMax-I (Invitrogen, Carlsbad, CA, USA) supplemented with 10% fetal bovine serum (FBS) and 0.5 mg/mL G418. HuH-7 K4 cells (cured of HCV by IFN treatment) and the JFH/K4 cells persistently infected with the HCV JFH-1 strain were maintained in DMEM containing 10% FCS and 0.1 mg/mL penicillin and streptomycin sulfate. MH-14 cells were grown in Dulbecco's modified Eagle's medium supplemented with 10% fetal bovine serum, 100 U/mL nonessential amino acids, 0.1 mg/mL penicillin and streptomycin sulfate, and 0.5 mg/mL G418.

siRNA assay

siCONTROL, siSGMS1, and siSGMS2 were purchased from Dharmacon RNA Technologies (Lafayette, CO, USA). The siCONTROL Non-Targeting siRNA #3 was used as the negative control siRNA. We used siRNAs against the HCV genome (siE-R7) [16]. The chemically synthesized siRNAs were transfected into cells using Lipofectamine RNAiMAX (Invitrogen) and Opti-MEM (Invitrogen) by reverse-transfection. Cells were characterized at 96 h after transfection.

Serine palmitoyltransferase activity

We assessed SPT activity in the liver as previously described, with minor modifications [43]. Briefly, frozen cells were homogenized in HEPES buffer (10 mM HEPES, 2 mM sucrose monolaurate, and 0.25 M sucrose, pH 7.4), and homogenates were centrifuged at 10,000×*g* for 20 min. From the resulting supernatant, samples containing 200 μg protein were assayed for SPT activity using [^{14}C]-serine and palmitoyl-CoA (Sigma-Aldrich, St. Louis, MO, USA) as substrates.

Proliferation assay

Human peripheral blood cells (AllCells, Emeryville, CA, USA) were plated onto 96-well plates and treated with phytohemagglutinin with or without immunosuppressant reagents. After 2 days of stimulation, [^{3}H]-thymidine-containing growth medium was added, and the cultures were incubated for another 18 h. T-cell proliferation was assessed by comparing the level of thymidine incorporation to that in the stimulated control.

Anti-hepatitis C virus assay in Huh-7 cells harboring subgenomic replicons

Replication was determined after 72 h with a Bright-Glo luciferase assay kit (Promega, Madison, WI, USA). The viability of replicon cells was determined using a cell counting kit (Dojindo, Kumamoto, Japan) according to the manufacturer's instructions.

Western blot analysis

Cells were resuspended in lysis buffer (10 mM Tris, pH 7.4 containing 1% SDS, 0.5% Nonidet P-40, 150 mM NaCl, 0.5 mM EDTA, and 1 mM dithiothreitol). Ten micrograms of the resulting protein sample were electrophoresed on a 10% sodium dodecyl sulfate-polyacrylamide gel and subsequently transferred to a polyvinylidene difluoride membrane (Immobilon-P; Millipore, Billerica, MA, USA). HCV nonstructural protein 3 (NS3) and nonstructural 5B polymerase (RdRp) were detected with rabbit anti-NS3 polyclonal antibody (R212) and mouse anti-RdRp monoclonal antibody (5B-14) prepared in our laboratory. β-Actin was detected with anti-β-actin monoclonal antibody (Sigma-Aldrich).

Immunofluorescent staining of hepatitis C virus replicon cells

After treatment with 25 nM NA808 for 96 h, FLR3-1 cells were probed with anti-NS3 polyclonal antibody (R212; the primary antibody). Next, an anti-rabbit IgG-Alexa 488 conjugate (Invitrogen) was applied as the secondary antibody.

Thin-layer chromatography analysis

Thin-layer chromatography (TLC) analysis was performed as described previously [9]. Briefly, cells were incubated with [^{14}C]-serine in Opti-MEM (Invitrogen). Cells extracts were obtained using the Bligh & Dyer method [44] and were spotted onto Silica Gel 60 TLC plates (Merck, Darmstadt, Germany) for separation. Radioactive spots were detected using a BAS 2000 system (Fuji Film, Kanagawa, Japan).

Membrane flotation assay

Cells were lysed in TNE buffer (25 mM Tris-HCl, 150 mM NaCl, 1 mM EDTA) and passed 20 times through a 25-gauge needle. Nuclei and unbroken cells were removed by centrifugation at 1,000×*g* for 5 min. After ensuring that the amount of total protein was equivalent across all samples, cell lysates were treated with 1% Triton on ice for 30 min and then subjected to a sucrose gradient (10%, 30%, and 40%). The sucrose gradient was centrifuged at 247,220×*g* in a Beckman SW41 Ti rotor (Beckman Coulter Inc., Brea, CA, USA) for 14 h at 4°C. Fractions (1 mL) were collected from the top of the gradient.

Infection of mice with hepatitis C virus genotypes 1a and 2a

Chimeric mice infected with HCV were prepared as previously described [45]. Briefly, approximately 40 days after the transplantation procedure, mice were intravenously injected with 5×10^5 copies/mouse of HCG9 (genotype 1a) or HCR24 (genotype 2a) that had been collected from patient serum.

Quantification of HCV RNA by real-time polymerase chain reaction

Total RNA was purified from 1 μL of chimeric mouse serum using SepaGene RV-R (Sanko Junyaku Co. Ltd., Tokyo, Japan) and from liver tissue using Isogene (Nippon Gene Co. Ltd., Tokyo, Japan). HCV RNA was quantified by quantitative real-time polymerase chain reaction (PCR) using previously reported techniques [9]. For serum, this technique has a lower limit of detection of 4000 copies/mL. Therefore, samples in which HCV RNA was undetectable were assigned this minimum value.

Quantification of HCV core protein by ELISA

Liver specimens were homogenized in TNE buffer. Aliquots of 5 μg of total protein were assayed for core protein levels with an Ortho HCV core protein ELISA kit (Eiken Chemical, Tokyo, Japan).

Indirect immunofluorescence analysis

The primary antibody for immunofluorescence analysis of liver sections was anti-HCV core protein monoclonal antibody (5E3) [46]. Monoclonal antibody labeling was followed by staining with anti-mouse IgG Alexa-488. The nuclei were stained using 4′,6-diamidino-2-phenylindole (DAPI).

Gene expression analysis

To measure mRNA levels, total RNA samples were extracted from the mouse livers and cDNA was synthesized using a High-Capacity cDNA Reverse Transcription Kit (Applied Biosystems, Foster City, CA, USA). The cDNA solution was assessed by quantitative PCR performed with TaqMan Gene Expression Assays (Applied Biosystems) and an ABI 7700 Sequence Detection System (Applied Biosystems).

Quantification of SM and ceramide in liver

We quantified liver SM and ceramide levels using a mass spectrometer (MS). Electrospray ionization (ESI)-MS analysis was performed using a 4000Q TRAP quadrupole-linear ion trap hybrid MS (AB SCIEX, Foster City, CA, USA) with an UltiMate 3000 nano/cap/micro-liquid chromatography system (Dionex Corporation, Sunnyvale, CA, USA) combined with an HTS PAL autosampler (CTC Analytics AG, Zwingen, Switzerland). The total lipid fractions expected to contain SM and ceramide, were subjected directly to flow injection and were selectively analyzed by neutral loss scanning of 60 Da (HCO_2+CH_3) from SM $[M+HCOO]^-$ in the negative ion mode, and multiple-reaction monitoring using a combination of ceramide $[Cer-H_2O+H]^+$ and the product (long-chain base) $[LCB-H_2O+H]^+$ in the positive ion mode [47,48]. The mobile phase composition was acetonitrile:methanol:water at 6:7:2 (0.1% ammonium formate, pH 6.8) and a flow rate of 10 µL/min. The typical injection volume was 3 µL of total lipids, normalized by protein content.

LC/ESI-MS analysis was performed using quadrupole/time of flight (Q-TOF) micro with an ACQUITY UPLC system (Waters Corporation, Milford, MA, USA) in the negative ion mode and an Agilent 6230 with an Agilent 1290 Infinity LC system (Agilent Technologies, Inc., Loveland, CO, USA) in the positive ion mode. Reversed-phase LC separation was achieved using an ACQUITY UPLC BEH column (150 mm×1.0 mm i.d., Waters Corporation) at 45°C. The mobile phase was acetonitrile:methanol:water at 19:19:2 (0.1% formic acid+0.028% ammonia) (A) and isopropanol (0.1% formic acid+0.028% ammonia) (B), and the composition was produced by mixing these solvents. The gradient consisted of holding A:B at 90:10 for 7.5 min, then linearly converting to A:B at 70:30 for 32.5 min, and then linearly converting to A:B at 40:60 for 50 min. The detailed procedure for LC/ESI-MS was described previously [49,50].

Separation of SM molecular species by HPLC

Bovine milk or brain SM (Avanti Polar Lipids. Inc., Alabaster, AL, USA) was dissolved in chloroform:methanol (2:1), then separated according to molecular species by reversed-phase HPLC. The *d*18:1-16:0, 22:0, and 24:0 molecular species of SM were isolated from bovine milk SM, while the *d*18:1-24:0 and 24:1 molecular species were isolated from brain SM. Bovine milk and brain SM were then separated on Senshu PAK ODS (C18) columns (Senshu Scientific Co., Ltd., Tokyo, Japan) using methanol as the eluting solvent at a flow rate of 1 mL/min. The fatty acid compositions of the purified fractions were analyzed by LC/ESI-MS. The amount of SM in each fraction was quantified using an SM assay kit (Cayman Chemical, Ann Arbor, MI, USA). We confirmed that the purity of each molecular species was approximately 90% without *d*18:1-24:1 (about 70%) (data not shown).

In vitro HCV transcription

In vitro HCV transcription was performed as previously described [8].

SM binding assay using ELISA

An SM binding assay was performed as previously described [8] using rabbit anti-HCV RdRp sera (1:5000) and an HRP-conjugated anti-rabbit IgG antibody (1:5000). Optical density at 450 nm (OD_{450}) was measured on a Spectra Max 190 spectrophotometer (Molecular Devices, Sunnyvale, CA, USA) using the TMB Liquid Substrate System (Sigma).

RNA replication assays in permeabilized replicon cells

The analysis using digitonin-permeabilized replicon cells was performed as previously described [20] with minor modifications. Briefly, MH-14 cells of about 80% confluency were pre-cultured for 2 h in complete Dulbecco's modified Eagle's medium containing 5 µg/mL actinomycin D (Nacalai Tesque, Kyoto, Japan), then washed with cold buffer B (20 mM HEPES-KOH (pH 7.7 at 27°C), 110 mM potassium acetate, 2 mM magnesium acetate, 1 mM EGTA, and 2 mM dithiothreitol). The cells were permeabilized by incubation in buffer B containing 50 µg/mL digitonin for 5 min at 27°C, and the reaction was stopped by washing twice with cold buffer B. The permeabilized cells were then incubated for 4 h at 27°C in the reaction mixture with or without each lipid. The reaction mixture consisted of 2 mM manganese(II) chloride, 1 mg/mL acetylated bovine serum albumin (Nacalai Tesque), 5 mM phosphocreatine (Sigma), 20 units/mL creatine phosphokinase (Sigma), 50 µg/mL actinomycin D, and 500 µM each of ATP, CTP, GTP, and UTP (Roche Diagnostics, Basel, Switzerland) in buffer B (pH 7.7). Total RNA was purified by the acid guanidinium-phenol-chloroform method. In this assay, considering that the estimated SM content in human hepatocytes is 3–4 nmol/mg protein, as demonstrated by MS analysis (**Figure S10**), the amount of SM we added in the replicase assay was 0.3–1 µM. (i.e. 0.03–0.3 nmol/0.3 mL/0.1 mg protein/12 well; the reaction volume in the replicase assay was 0.3 mL/12 wells and each well of the 12 well cell culture plates contained approximately 0.1 mg protein.)

Statistical analysis

Statistical analysis was performed using the Student's *t*-test equipped with Excel 2008 (Microsoft, Redmond, WA, USA). To measure the strength of the association, Pearson correlation coefficient was calculated using Excel 2008. A p-value<0.05 was considered statistically significant.

Supporting Information

Figure S1 Impacts of HBV infection on expression of sphingomyelin (SM) biosynthesis genes. mRNA expression of *SGMS1* and *SGMS2* genes (encoding SM synthases 1 and 2, respectively) in uninfected (white) and infected (black) chimeric mice (n = 5 per group).
(JPG)

Figure S2 Effect of HCV infection in cultured cells. Comparison of the relative amounts of SM, as measured by MS analysis, in mock-infected (HuH-7 K4 cells) (white) and HCV (JFH-1)-infected cells (JFH/K4 cells) (black) (n = 1 per group).
(JPG)

Figure S3 The expression of HCV core protein in HCV-infected chimeric mice. Histological analysis using immunohistochemical labeling of HCV core protein.
(JPG)

Figure S4 Effects of NA808 on HCV-infected chimeric mice. (**A**) Average body weight of mice during treatment. (**B**) Average human albumin concentrations in the sera of mice during treatment. (**C**) Histological analysis using H&E staining and immunofluorescent labeling of human albumin (red). In all cases, error bars indicate SDs.
(JPG)

Figure S5 Concentrations of NA808 in chimeric mice receiving NA808 treatment. Concentration of NA808 in the liver (gray) and serum (black) of chimeric mice treated with 5 mg/kg or 10 mg/kg NA808. Stars indicate that NA808 level was not detected.
(JPG)

Figure S6 Sphingomyelin (SM) levels in the serum of chimeric mice receiving NA808 treatment. SM levels in the serum of chimeric mice (n = 3 per group) that were uninfected (HCV−), or infected (HCV+) but untreated or treated with 5 or 10 mg/kg NA808. Error bars indicate SDs.
(JPG)

Figure S7 Effects of NA808 on associations between the HCV nonstructural 5B polymerase (RdRp) and sphingomyelin (SM). (**A**) Comparison of SDS-PAGE and TLC results for replicon cells receiving no treatment (Control) or NA808 treatment (NA808). NA808 dosage was 2.5 nM (for TLC) or 25 nM (for SDS-PAGE). (**B**) Relative band intensities of RdRp and NS3 in detergent-resistant membrane (DRM) fractions from cells receiving no treatment (Control) or 25 nM NA808 treatment (NA808). (**C**) Relative band intensities of SM in DRM fractions from cells receiving no treatment (Control) or 2.5 nM NA808 treatment (NA808).
(JPG)

Figure S8 Composition ratio of SM molecular species in whole cells and DRM fraction of uninfected cells.
(JPG)

Figure S9 Effect of NS3 protease inhibitor on SM molecular species in the DRM fractions of subgenomic replicon cells. (A) Effect of NS3 protease inhibitor (VX950) on HCV replication (dark grey bars) and cell viability (light grey bars) in FLR3-1 replicon-containing cells. Error bars indicate SD. (B) Effect of NS3 protease inhibitor (VX950; 3 µM) on SM molecular species of DRM fractions of FLR 3-1 replicon-containing cells. Error bars indicate SDs.
(JPG)

Figure S10 The estimated SM content in human hepatocytes. Left bar (white) indicates the intensity of SM internal standard (SM d18:0-12:0; 1 nmol) by mass spectrometer. Right bar indicates the intensity of 1 mg protein of human hepatocyte (HuH-7 K4).
(JPG)

Table S1 Distribution of radioactivity in tissues after a single intravenous administration of [^{14}C] NA808 at 2 mg/kg to non-fasting male rats.
(PDF)

Table S2 Treatment administration for HCV-infected chimeric mice. Administration of reagents was started at day 0. The amount of NA808 was adjusted according to the body weight of the mice. Dose began at 5 mg/kg or 10 mg/kg and was reduced by half at each 10% reduction in body weight (half circle). At 20% reduction, administration was discontinued. Open circle indicates each manipulation was performed as required.
(PDF)

Text S1 Materials and methods for supporting information. Methods for "Infection of chimeric mice with hepatitis B virus", "Quantification of human albumin", "Histological staining and indirect immunofluorescence analysis", and "Quantification of sphingomyelin (SM) in serum" are described.
(DOCX)

Acknowledgments

We are very grateful to Dr. Makoto Hijikata of the Department of Viral Oncology, Institute for Virus Research, Kyoto University for his technical support. We thank Isao Maruyama and Hiroshi Yokomichi of PhoenixBio Co., Ltd. for maintenance of and technical assistance with the chimeric mice.

Author Contributions

Conceived and designed the experiments: M. Kohara. Wrote the paper: Y. Hirata. Y. Hirata performed the experiment of chimeric mice and HCV-infected cells. K. Ikeda, M. Ohta, T. Soga, and R. Taguchi performed lipid analysis by MS spectrometry. M. Sudoh, A. Katsume, and Y. Aoki evaluated the antiviral effects of NA808, K. Okano and K. Ozeki examined the tissue distribution of NA808. K. Kawasaki and T. Tsukuda synthesized derivatives from natural compounds. Y. Tokunaga, Y. Tobita, T. Umehara, and S. Sekiguchi performed some experiments on the chimeric mice. L. Weng and T. Toyoda conducted the experiments on the interaction between RdRp and SM. M. Kohara and Y. Hirata performed data analysis on the chimeric mice and cells. K. Ikeda, M. Ohta, T. Soga, and R. Taguchi performed data analysis on the result of MS spectrometry. A. Suzuki, K. Shimotohno, and M. Nishijima provided tools and expert information.

References

1. Wenk MR (2006) Lipidomics of host-pathogen interactions. FEBS Lett 580: 5541–5551.
2. Brown DA, Rose JK (1992) Sorting of GPI-anchored proteins to glycolipid-enriched membrane subdomains during transport to the apical cell surface. Cell 68: 533–544.
3. Simons K, Toomre D (2000) Lipid rafts and signal transduction. Nat Rev Mol Cell Biol 1: 31–39.
4. van der Meer-Janssen YP, van Galen J, Batenburg JJ, Helms JB (2010) Lipids in host-pathogen interactions: pathogens exploit the complexity of the host cell lipidome. Prog Lipid Res 49: 1–26.
5. Aizaki H, Lee KJ, Sung VM, Ishiko H, Lai MM (2004) Characterization of the hepatitis C virus RNA replication complex associated with lipid rafts. Virology 324: 450–461.
6. Shi ST, Lee KJ, Aizaki H, Hwang SB, Lai MM (2003) Hepatitis C virus RNA replication occurs on a detergent-resistant membrane that cofractionates with caveolin-2. J Virol 77: 4160–4168.
7. Sakamoto H, Okamoto K, Aoki M, Kato H, Katsume A, et al. (2005) Host sphingolipid biosynthesis as a target for hepatitis C virus therapy. Nat Chem Biol 1: 333–337.
8. Weng L, Hirata Y, Arai M, Kohara M, Wakita T, et al. (2010) Sphingomyelin activates hepatitis C virus RNA polymerase in a genotype-specific manner. J Virol 84: 11761–11770.
9. Umehara T, Sudoh M, Yasui F, Matsuda C, Hayashi Y, et al. (2006) Serine palmitoyltransferase inhibitor suppresses HCV replication in a mouse model. Biochem Biophys Res Commun 346: 67–73.
10. Kapadia SB, Chisari FV (2005) Hepatitis C virus RNA replication is regulated by host geranylgeranylation and fatty acids. Proc Natl Acad Sci U S A 102: 2561–2566.
11. Su AI, Pezacki JP, Wodicka L, Brideau AD, Supekova L, et al. (2002) Genomic analysis of the host response to hepatitis C virus infection. Proc Natl Acad Sci U S A 99: 15669–15674.
12. Takano T, Tsukiyama-Kohara K, Hayashi M, Hirata Y, Satoh M, et al. (2011) Augmentation of DHCR24 expression by hepatitis C virus infection facilitates viral replication in hepatocytes. J Hepatol 55: 512–521.
13. Tateno C, Yoshizane Y, Saito N, Kataoka M, Utoh R, et al. (2004) Near completely humanized liver in mice shows human-type metabolic responses to drugs. Am J Pathol 165: 901–912.
14. Mercer DF, Schiller DE, Elliott JF, Douglas DN, Hao C, et al. (2001) Hepatitis C virus replication in mice with chimeric human livers. Nat Med 7: 927–933.